https://doi.org/10.5194/egusphere-2025-3250
Preprint. Discussion started: 13 October 2025

Short-Lived Halogen Sources and Chemistry in the Community Earth System Model v2 (CESM2-SLH)

Rafael P. Fernandez[1,2,*], Carlos A. Cuevas[1], Julián Villamayor[1], Aryeh Feinberg[1], Douglas E. Kinnison[3], Francis Vitt[3], Adriana Bossolasco[1,4], Javier A. Barrera[1,5], Amelia Reynoso[2], Orlando G. Tomazzeli[2], Qinyi Li[6] and Alfonso Saiz-Lopez[1,*]

[1] Department of Atmospheric Chemistry and Climate, Institute of Physical Chemistry Blas Cabrera, CSIC, Madrid, 28006, Spain
[2] Institute for Interdisciplinary Science, National Research Council (ICB-CONICET/UNCUYO). School of Natural Sciences, National University of Cuyo (FCEN/UNCUYO), Mendoza, 5501, Argentina
[3] Atmospheric Chemistry, Observations & Modeling Laboratory (ACOM), NSF National Center for Atmospheric Research (NCAR), Boulder, CO 80301, USA
[4] Physics Institute of Northwest Argentina (INFINOA-CONICET/UNT), Tucumán, Argentina.
[5] Research Institute for Physical Chemistry of Córdoba, National Research Council (INFIQC-CONICET/UNC). Department of Physical Chemistry, School of Chemical Sciences, National University of Córdoba (FCQ/UNC), Córdoba, Argentina
[6] Environment Research Institute, Shandong University, Qingdao, China.

Correspondence to: Alfonso Saiz-Lopez (a.saiz@csic.es) and Rafael P. Fernandez (rpfernandez@mendoza-conicet.gob.ar)

Abstract. The implementation of short-lived halogen (SLH) sources and atmospheric chemistry in the Community Earth System Model v1 (CESM1), has extended the capabilities of this state-of-the-art model to study how SLH chemistry alters the oxidative capacity of the atmosphere and, consequently, the Earth's climate. In this manuscript, we summarize 15 years of research and developments of SLH chemistry in CESM1 and present a complete revision of the porting of the original SLH implementation into the latest released version of CESM (v2), hereafter CESM2-SLH. This includes a detailed description of all offline and online sources of organic and inorganic SLH, as well as the gas-phase and heterogeneous recycling of chlorine, bromine and iodine in the troposphere and stratosphere, including their species-independent atmospheric sinks. In doing so, we provide a comprehensive evaluation of how changes in model parameters and coupled dynamics within the Community Atmosphere Model v6 (CAM6) affect SLH abundances and their implications. The new CESM2-SLH implementation offers various component sets (compsets) and resolutions, all of which result in equivalent global budgets and zonal distributions of organic and inorganic chlorine, bromine and iodine, which in turn, lead to SLH impacts on atmospheric composition that are consistent with previous CESM1 results. The released CESM2-SLH version includes specific namelist options, input files and technical notes detailing the most important SLH updates implemented over the CESM2/CAM6 routines. Our results show that the global tropospheric burden and tropical stratospheric injection of organic and inorganic chlorine, bromine and iodine species in CESM2-SLH are in agreement with observational assessments and previous modelling studies using CESM1, resulting in significant reductions in global ozone abundance (−21-28% at the surface, −17-22% in the troposphere and −2-3% in the stratosphere) as well as in OH and NO_2 (ranging between −2-9% and −1-10%, respectively), depending on the specific model configuration and resolution. Based on this, we encourage the wider CESM community to consider the released CESM2-SLH scheme to obtain a more realistic representation of the background influence of natural and anthropogenic short-lived halogen sources and chemistry in air quality and Earth's climate studies.

Keywords. CESM2-SLH, Natural and Anthropogenic Halogens, Atmospheric Chemistry, Chemistry-Climate coupling.

https://doi.org/10.5194/egusphere-2025-3250
Preprint. Discussion started: 13 October 2025

1 Introduction

Over the past few decades, both observational and modelling studies have shown that Short-Lived Halogens (SLH) are widespread and ubiquitously distributed throughout the troposphere and stratosphere (Chance, 1998; Alicke et al., 1999; Saiz-Lopez et al., 2007; Read et al., 2008; Thornton et al., 2010; Prados-Roman et al., 2015a; Koenig et al., 2020). This SLH definition (Saiz-Lopez et al., 2023) includes the contribution from organic (i.e., carbon-bonded) very short-lived (VSL) halocarbons with a chemical lifetime smaller than 6 months plus the contribution of inorganic halogen species (collectively called Cl_y, Br_y and I_y for chlorine, bromine and iodine, respectively) that, through chemical cycling, partition between reactive and reservoir fractions within the gas-phase. Due to their short lifetime, reactive halogens affect atmospheric chemical composition including the depletion of tropospheric ozone (O_3), and consequently, the production of the hydroxyl radical (OH) and the partitioning between both hydrogen (HO_2/OH) and nitrogen (NO_2/NO) oxides (Saiz-Lopez and von Glasow, 2012). In addition, SLH compounds contribute to stratospheric ozone depletion (Salawitch et al., 2005; Sinnhuber et al., 2009), particularly over Antarctica where reactive bromine and iodine enhance de depth and size of the springtime ozone hole (Fernandez et al., 2017; Cuevas et al., 2022). Recently, SLH has been shown to influence the Earth radiative balance through direct and indirect chemical coupling with methane (CH_4) (Li et al., 2022), O_3 (Saiz-Lopez et al., 2023) and OH (Bossolasco et al., 2025), as well as the oxidation of dimethyl sulphide (DMS) and other sulphate sources which, in turn, can alter the formation of cloud condensation nuclei (Wohl et al., 2024).

VSL consist of organic halogenated source gases (SGs) such as chloro-, bromo-, iodo-carbons which are present in the atmosphere in the form they were emitted. Bromine and iodine SGs are predominantly natural and emitted from the oceans (e.g., $CHBr_3$, CH_2Br_2 and CH_3I), whereas chlorine species such as CH_2Cl_2 and C_2Cl_4 have an important contribution from anthropogenic sources (WMO, 2022). The oceans are also the source of abiotic emission of hypoiodous acid (HOI) and molecular iodine (I_2) following the deposition of tropospheric ozone to the ocean surface and the reaction with iodide ions (Carpenter et al., 2013; MacDonald et al., 2014). This oceanic source of inorganic iodine is estimated to account for ~75% of the total source of atmospheric iodine, with the rest coming from VSL iodocarbons (Prados-Roman et al., 2015b). Similarly, very efficient heterogeneous reactions occurring at the surface of sea-salt aerosols (SSA) can result in the initial uptake and subsequent release of different halogen species within the Marine Boundary Layer (MBL), constituting a significant source of inorganic chlorine and bromine to the lower atmosphere, which is currently considered to be the dominant natural halogen source (WMO, 2018; Saiz-Lopez et al., 2023).

Once in the atmosphere, VSL SGs photo-decompose to release inorganic halogen product gases (PGs) that cycle back and forth between reactive (ClO_x, BrO_x and IO_x) and reservoir species, the whole group of which constitute SLH species. In contrast, long-lived Ozone Depleting Substances (ODSs), such as chloro-fluoro-carbons (CFCs) and brominated halons, remain unreactive throughout the troposphere until they are photodecomposed in the stratosphere (WMO, 2018, 2022) . The photochemical cycling of SLH involves chemical reactions with other hydrogen, nitrogen, carbon and sulphur species, modifying the chemical composition of the atmosphere and therefore affecting its oxidative capacity and consequently, the Earth's climate (Li et al., 2022; Saiz-Lopez et al., 2023; Bossolasco et al., 2025). While detailed descriptions of the overall processes and reactions occurring in the atmosphere have been widely described in the literature (e-g-. see the reviews of (Saiz-Lopez and von Glasow, 2012; Simpson et al., 2015) and supplementary information of previous studies (Saiz-Lopez et al., 2014, 2023; Badia et al., 2021)), here we only provide a general description of the most relevant chemical cycles in which SLH participate, which can certainly be expanded and complemented following the comprehensive SLH literature referenced herein.

The first step in the long reactive chain of SLH is the photochemical breakdown of either organic VSL halocarbons and/or photo-labile inorganic halogen species that results in the release of chlorine, bromine and iodine atoms, typically represented by X,Y = Cl, Br, I (R1a–R1c). Once in the atmosphere, these highly reactive halogen atoms (particularly I and Br) can catalytically destroy ozone (O_3), which in turn, controls the tropospheric formation of the hydroxyl radical OH through

https://doi.org/10.5194/egusphere-2025-3250
Preprint. Discussion started: 13 October 2025

the reaction of O^1D with water vapour (R2−R4). Here, note that OH is typically referred to as the "atmospheric detergent" because it dominates the photodecomposition of different volatile organic compounds (VOCs), and therefore controls the oxidative capacity of the troposphere (R5a). Similarly, direct reactions of halogen radicals (particularly Cl atoms) with several VOCs also contribute to the photochemical degradation of biogenic compounds and anthropogenic pollutants emitted to the atmosphere (R5b−R7), including CH_4. As a result, halogen chemistry alters the overall partitioning between nitrogen (NO_x = NO + NO_2) and hydrogen (HO_x = OH + HO_2) cycling (R8−R10), which has important implications for determining the chemical composition not only for halogens, but also for several reactive and reservoir species in the global atmosphere. Therefore, SLH chemistry can either increase the photochemical degradation rate of VOCs as well as the formation of aerosols (Saiz-Lopez and von Glasow, 2012; Simpson et al., 2015), while at the same time it can decrease the OH-driven chemical destruction and/or production rates due to their direct influence on O_3 abundance (Iglesias-Suarez et al., 2020; Badia et al., 2021; Saiz-Lopez et al., 2023), which in turn controls OH (Benavent et al., 2022; Bossolasco et al., 2025). Finally, it is worth noting that depending on the background environment, reactive halogen chemistry can also result in ozone production under polluted environments due to the formation of nitryl chloride ($ClNO_2$) that, through photolysis (R11), represents an additional source of NO_x (R12-R13).

$$CHX_3 + h\nu \rightarrow 3X \quad \text{(R1a)}$$

$$CH_2XY + OH \rightarrow X + Y \quad \text{(R1b)}$$

$$X_2/XY + h\nu/OH \rightarrow (2)X + Y \quad \text{(R1c)}$$

$$X + O_3 \rightarrow XO \quad \text{(R2)}$$

$$O_3 + h\nu \rightarrow O^1D + O_2 \quad \text{(R3)}$$

$$O^1D + H_2O \rightarrow 2\,OH \quad \text{(R4)}$$

$$OH + VOCs \rightarrow RO_2 + HO_2 \quad \text{(R5a)}$$

$$X/Y + VOCs \rightarrow RO_2 + HX \quad \text{(R5b)}$$

$$RO_2 + NO \rightarrow NO_2 + RO \quad \text{(R6)}$$

$$RO + O_2 \rightarrow HO_2 + products \quad \text{(R7)}$$

$$HO_2 + NO \rightarrow NO_2 + OH \quad \text{(R8)}$$

$$XO + HO_2 \rightarrow HOX \quad \text{(R9)}$$

$$HOX + h\nu \rightarrow X + OH \quad \text{(R10)}$$

$$ClNO_2 + h\nu \rightarrow Cl + NO_2 \quad \text{(R11)}$$

$$NO_2 + h\nu \rightarrow NO + O^3P \quad \text{(R12)}$$

$$O^3P + O_2 + M \rightarrow O_3 \quad \text{(R13)}$$

https://doi.org/10.5194/egusphere-2025-3250
Preprint. Discussion started: 13 October 2025

In this work, we describe the implementation of SLH chemistry into the Community Earth System Model, version 2 (CESM2) (Danabasoglu et al., 2020), which include version 6 of the Community Atmospheric Model (CAM6) physics (Gettelman et al., 2019a), as well as the tropospheric and stratospheric (TS1) chemistry scheme within CAM6-Chem (Emmons et al., 2020). The corresponding SLH implementation in the Whole Atmosphere Community Climate Model v6 (WACCM6) troposphere, stratosphere, mesosphere, and lower thermosphere (TSMLT1) chemical scheme (Gettelman et al., 2019b) has also been performed. The implementation is based on most of the previous SLH developments implemented in CESM1 (Ordóñez et al., 2012; Saiz-Lopez et al., 2012). Due to the changes between the base CESM1 and CESM2 models in several atmospheric fields such as sea surface temperature (SST), SSA and the corresponding aerosols surface area density (SAD) computation, as well as the different prescribed pollutant emissions, meteorological fields and/or atmospheric dynamics (Gettelman et al., 2019a; Danabasoglu et al., 2020; Emmons et al., 2020; Simpson et al., 2023), all of which affect SLH chemical cycling, transport and washout in the atmosphere, we have included a new user-defined namelist section including a set of scaling-factors that allows CESM2-SLH performance to be consistent with the previous version of the model.

The paper is organized as follows: Section 2 reviews the historical developments of SLH chemistry in CESM1, and describes the implementation and porting to the different CESM2-SLH compsets available. Then, in Section 3 we present a comprehensive description of SLH global abundances and distributions obtained with the new CESM2-SLH model and how they compare with previous CESM1 results as well as with observations. Finally, section 4 provides several remarks, suggestions and notes of caution for new CESM2-SLH users, emphasising the need and types of model validation checks that must be performed in case other configurations beyond the ones described here are used.

2 Model Description

The implementation of SLH sources and chemistry in CESM described in this work has been performed in version 2.2.0 (branch *cesm2.2-asdbranch*), whose atmospheric component is based on CAM6 (branch *cam_cesm2_2_rel_09*). To simplify the validation of SLH chemistry amongst all the available model configurations in CESM2, we focused on the widely used *FCnudged* and *FCHIST* compsets (https://docs.cesm.ucar.edu/models/cesm2/config/2.2/compsets.html), expanding their default namelists and configuration files to include SLH sources and chemistry. These *FCASE* compsets are forced with prescribed SSTs, while an additional fully-coupled model compset for WACCM has also been developed based on *BWHIST* (Gettelman et al., 2019b). In particular, and given that the following model inputs are of relevance for the computation of SLH sources and sinks, we highlight that the current CESM2-SLH configuration includes a climatological SST configuration from (Huang et al., 2017) and an explicit representation of SSA lifting, transport and removal based on 3 (three) individual bins as described in (Tilmes et al., 2023). This differs from the original SSA representation available in the CAM4-Chem version used for the initial implementation of SLH in CESM1. In addition, note that most of the previous CAM4-Chem configurations were performed using the old Specified Dynamics (SD) approach forced with high-frequency meteorological fields from a previous CAM-Chem simulation (e.g., (Saiz-Lopez et al., 2023) and references therein), while the *FCnudged* and *FWnudged* compset in CESM2-SLH are based on the new nudging approach (Davis et al., 2022) that considers air temperature (T), zonal and meridional wind velocity (respectively, u and v) from MERRA2 (Modern-Era Retrospective analysis for Research and Applications v2) reanalysis (Rienecker et al., 2011). Given that most of the initial SLH developments were performed on top of a discontinued CESM1 version that is no longer available to the community, the current CESM2-SLH implementation is presented and sustained with a double purpose: *i)* to be easily configured by users that are not initially familiarized with SLH chemistry; and *ii)* to allow the whole scientific community to evaluate the global mean influence of SLH in atmospheric chemistry and their implications for the Earth's climate system.

https://doi.org/10.5194/egusphere-2025-3250
Preprint. Discussion started: 13 October 2025

Below we provide a brief review of the historical implementation of SLH in CAM4-Chem (Section 2.1), and then present a comprehensive description of the main sources (Section 2.2), gas-phase and multi-phase SLH chemistry (Section 2.3) and removal processes (Section 2.4) ported into CESM2-SLH. The final Section 2.5 describes the complete list of SLH compsets available with their corresponding namelist updates and scaling factors, which are required for a proper SLH model setup within the different resolutions and configurations existing in CESM2.

2.1 Historical Developments of SLH in CAM-Chem

Below we provide a brief description of the most important SLH developments originally implemented in CESM1 (CAM4-Chem). Although not strictly chronological, we begin with the initial descriptive papers that presented the main sources, reactions and halogen species, then continue with the subsequent updates and improvements, and finalize with the latest modelling studies that have demonstrated the importance of considering SLH chemistry to improve our understanding of atmospheric chemistry, air quality and climate evolution from past, to present and future. All these developments, have been led by the Atmospheric Chemistry and Climate group (AC2, IQF-CSIC, Madrid, Spain), in close cooperation with the Atmospheric Chemistry Observations & Modeling Department (ACOM-NCAR, Boulder, Colorado) and the Institute for Interdisciplinary Science (ICB-CONICET/UNCUYO, Mendoza, Argentina), as well as with fundamental contributions from other research groups around the world. Although most of previous research used the term VSL or VSLs to refer to organic halogenated very short-lived substances, in this work and following the most recent and complete representation of short-lived halogens in CESM (Saiz-Lopez et al., 2023), we expanded the terminology to SLH, which includes, in addition to VSL, those inorganic halogen species (Cl_y, Br_y and I_y) that rapidly interconvert between each other and are responsible for the halogen impacts in the atmosphere (Saiz-Lopez et al., 2023).

The initial description of SLH halogen chemistry in CAM-Chem was published in (Ordóñez et al., 2012), who presented a complete set of tables with all photochemical processes considered and also developed the VSL halocarbon emission inventory that was used in all subsequent studies. The companion work of (Saiz-Lopez et al., 2012) performed the first estimation of the impacts of combined SLH (chlorine, bromine and iodine) on tropospheric ozone and radiative balance. Here we acknowledge that these initial works considered offline inorganic iodine emissions. Afterwards, (Prados-Roman et al., 2015b, 2015a) implemented the online computation of oceanic iodine emissions and determined the negative geophysical feedback with tropospheric ozone that led to the hypothesis that atmospheric iodine levels would have tripled since the onset of the Industrial Era, later confirmed by ice-core observations (Cuevas et al., 2018). Further updates related mostly to heterogeneous recycling processes occurring in the MBL, Free Troposphere (FT) and Upper Troposphere (UT), relevant for properly quantifying the contribution of SLH to the stratospheric halogen loading of bromine (Fernandez et al., 2014) and iodine (Saiz-Lopez et al., 2014, 2015), led to quantification of the overall impact of natural bromine and iodine over the Antarctic ozone hole (Fernandez et al., 2017; Cuevas et al., 2022), as well as the seasonal variability within the mid-latitudes (Barrera et al., 2020). These updates included the online implementation of SSA-dehalogenation sources which are of particular importance for improving BrO observations in the MBL (Koenig et al., 2017), as well as the inclusion of higher order iodine oxides (I_xO_y), whose effective photolysis was found to be necessary to reproduce iodine observations in the upper troposphere and lower stratosphere (Saiz-Lopez et al., 2014, 2015; Koenig et al., 2020). For the particular case of chlorine, the contribution of anthropogenic VSL was implemented based on the emissions inventories from (Hossaini et al., 2019) and (Claxton et al., 2020), with further updates related to the inorganic chlorine emissions resulting from the heterogeneous recycling of nitrogen oxides and nitric acid over chloride-rich aerosols, the so called acid-displacement reactions (Li et al., 2022). These allowed to evaluate for the first time the combined impact of halogens (chlorine, bromine and iodine) over tropospheric ozone during the 21st century (Iglesias-Suarez et al., 2020; Badia et al., 2021) in comparison with pristine pre-industrial conditions (Barrera et al., 2023); as well as the enhanced chemical coupling (in concert) of natural and anthropogenic

https://doi.org/10.5194/egusphere-2025-3250
Preprint. Discussion started: 13 October 2025

SLH on the lowermost tropical stratosphere ozone trends (Villamayor et al., 2023). Based on these works, and thanks to the implementation of CH_4 emission-driven simulations (Li et al., 2022) and polar halogen emissions from the sea-ice (Fernandez et al., 2019, 2024), SLH were demonstrated to induce an overall cooling effect on the climate system arising from the direct and indirect (and sometimes opposite) influence of reactive halogens over ozone, methane, aerosols and stratospheric water vapour (Saiz-Lopez et al., 2023). CESM1 simulations including SLH also enabled quantification of the radiative influence of DMS and methanethiol (MeSH) oceanic emissions on the direct sulphate aerosol radiative effect over the Southern Ocean (Veres et al., 2020; Wohl et al., 2024), while the overall influence of SLH on all tropospheric oxidants has recently been described in (Bossolasco et al., 2025). The role of anthropogenic SLH emissions from biomass burning and other sources on long-term atmospheric chemistry and mercury contamination over continental Asia has also been evaluated using CESM1-SLH (Chang et al., 2024; Fu et al., 2024). The model has been also employed to evaluate the potential of chlorine based interventions in climate mitigation through methane reduction (Li et al., 2023; Meidan et al., 2024), as well as to quantify for the first time the role of the stratosphere on the global mercury cycle and surface deposition (Saiz-Lopez et al., 2025).

It is important to note that not all processes, reactions and implications summarized in previous studies have been implemented in the current release of CESM2-SLH described in this work. Please refer to Section 2.5.2 below for further details. Finally, it is worth noting that following the pioneering implementation of combined SLH emissions and chemistry into CAM4-Chem, other research groups implemented SLH schemes in different models, which in many cases followed the original implementation of SLH in CESM, particularly for iodine. These include global and regional models such as GEOS-Chem (Sherwen et al., 2016b, 2016a), CMAQ (Sarwar et al., 2015), WRF-Chem (Badia et al., 2019), SOCOL (Karagodin-Doyennel et al., 2021) and LMDZ-INCA (Caram et al., 2023).

2.2 Short-Lived Halogen Emissions

The starting point of SLH implementation in CESM was the development of an oceanic emission inventory of VSL halocarbons (Ordóñez et al., 2012), which not only represents an important tropospheric halogen source, but was also needed to reproduce total stratospheric bromine loading observations (WMO, 2018, 2022). To achieve this goal, many global models -including CESM- initially assumed a constant surface abundance of the two main bromocarbons (i.e., bromoform ($CHBr_3$) and dibromomethane (CH_2Br_2)) and imposed a Lower Boundary Condition (LBC) of 1.2 pptv each (adding up to 6 pptv of total bromine at the model surface), which resulted in an additional bromine stratospheric injection of approximately 5 pptv (Eyring et al., 2013; Hegglin et al., 2014). However, motivated by the rapid photochemical-degradation of VSLs in the troposphere, spatially- and temporally-resolved emission inventories were implemented to account for oceanic halocarbon emission sources of bromine and iodine (which include mostly natural sources), and was later extended to chlorocarbons, for which the anthropogenic emissions dominate. These original VSL oceanic sources, which represent the initial step releasing highly reactive Cl, Br and I atoms in the lower troposphere, were further extended by computing the on-line recycling of inorganic halogen sources occurring at the ocean surface as well as over sea-salt aerosols. Sections 2.2.1 and 2.2.2 describe, respectively, the natural and anthropogenic sources of VSLs halocarbons implemented in CESM2-SLH, while Section 2.2.3 describes the online recycling of halogen reservoirs that represent a net source of SLH to the atmosphere.

2.2.1 Natural Offline Halocarbon Emissions

The implementation of VSL halocarbons emitted from the ocean in CESM has been extensively described in the original work of (Ordóñez et al., 2012). The methodology follows a top-down approach based on chlorophyll-a monthly climatology from the SeaWIFS project for the 1998-2003 period (Melin, 2013), and the iterative adjustment of emission flux strength by comparing modelled distributions and vertical profiles of VSL halocarbons with both available surface and aircraft

https://doi.org/10.5194/egusphere-2025-3250
Preprint. Discussion started: 13 October 2025

observations. Nine halogenated VSL species are included in the (Ordóñez et al., 2012) emission inventory, including individual emissions of two bromocarbons ($CHBr_3$ and CH_2Br_2), three bromo-chlorocarbons (CH_2BrCl, $CHBrCl_2$ and $CHBr_2Cl$), two iodocarbons (CH_3I and CH_2I_2), one iodo-chloro (CH_2ICl) and another iodo-bromo (CH_2IBr) carbon, respectively. All of these species are well known to be emitted from biologically active oceans as side products of the metabolite of different micro- and macro-algae and phytoplankton colonies (Carpenter and Liss, 2000; Carpenter et al., 2003). In the (Ordóñez et al., 2012) inventory, the oceanic emission shows a seasonal and latitudinal distribution, with most of the emission (~70%) occurring over the tropics (20°N-20°S), approximately 25% arising from the north and south mid-latitudes (20º-50º on both hemispheres) and the remaining 5% released from ice-free oceanic regions from the high-latitudes and polar regions. The net oceanic emission flux of each halocarbon species (E_{spec}) is given by Eq. (1);

$$E_{spec} = 1.127 \times 10^5 \times f_{spec} \times r_{coast} \times chl\_a \ , \quad (1)$$

where f_{spec} is a species-dependent scaling factor iteratively adjusted to improve model-observation agreement, r_{coast} is a constant enhancement factor applied only to coastal areas outside the tropics (20°N-20°S), and *chl_a* is the SeaWIFS monthly climatology chlorophyll-a distribution (Ordóñez et al., 2012). Note that, differing from previous VSL inventories that considered only latitudinal bands (Warwick et al., 2006b, 2006a; Butler et al., 2007; Jones et al., 2010), the (Ordóñez et al., 2012) inventory introduces a tropical geographically-heterogeneous and seasonally dependent variability, which allows for an improved spatio-temporal representation of VSL halocarbon distribution in the global troposphere. Despite the emission flux is read offline with a monthly mean resolution, routine *mo_srf_emissions.F90* was modified to apply an hourly dependent profile to the flux strength of all halocarbons due to their photosynthetic dependence on radiation intensity: i.e., emissions follow either a Gaussian or top-hat diurnal profile, with minimal (or zero) night-time emissions and peak emissions at local solar noon (Ordóñez et al., 2012). Given that no long-term trend has been established for natural oceanic organic halogen emissions, the emission strength of oceanic halocarbons is assumed to follow a constant climatology. To include the offline VSL halocarbon emissions from the (Ordóñez et al., 2012) inventory, users just need to include the name of the species within the *srf_emiss_specifier* namelist option, and point at the specific file for each individual species (see Section 2.5). All changes related to the implementation of offline oceanic VSLs sources have been performed in routines *mo_srf_emissions.F90* and *mo_usrrxt.F90* within the *chemistry/mozart* folder.

Finally, it is important to mention that the original (Ordóñez et al., 2012) inventory was developed almost 15 years ago and initially implemented in CAM4-Chem. Since then, several improvements in the representation of large-scale ascent and transport across the MBL have been included in CESM2 (Simpson et al., 2020). In addition, updated in the emission strength and distribution of air pollutants have modified the oxidative capacity of the troposphere (Emmons et al., 2020). Therefore, an equivalent top-down iterative process to reproduce VSL observations was performed in the current CESM2-SLH version, focused on replicating the CESM1 representation of the VSL SGs vertical profiles as well as the stratospheric bromine and iodine injection obtained with the different model configurations (i.e., free-running or nudged versions). As a result, the original bromine emission fluxes from (Ordóñez et al., 2012) were increased by a constant factor of 1.15 (i.e., 15%) in all locations, which leads to consistency with previous CESM1 results (Fernandez et al., 2014, 2021); see Section 3.2.2). The rationale for increasing the offline emission fluxes is that the reduction of transport across the MBL and the increase near-surface oxidative capacity (dominated by the larger surface OH abundance in CAM6-Chem relative to CAM4-Chem) results in more efficient conversion from SGs to PGs at lower model levels in the current CESM2- SLH version. Note that due to the much shorter lifetime, no scaling was applied to VSL iodocarbons.

https://doi.org/10.5194/egusphere-2025-3250
Preprint. Discussion started: 13 October 2025

2.2.2 Anthropogenic Offline Halocarbon Emissions

For the particular case of chlorine, anthropogenic SLH sources are included following the (Hossaini et al., 2019) and (Claxton et al., 2020) emission inventory, which considers time-dependent emissions of two of the dominant organic chlorine species observed in the atmosphere (CH_2Cl_2 and C_2Cl_4). Based on these works, an increasing trend from 2000 to 2020 is imposed to the emission files for the recent past. In addition, the contribution of $CHCl_3$ and $C_2H_4Cl_2$ to the total tropospheric VSL chlorine loading is considered by imposing surface LBCs for each species (i.e., following the initial approach applied to $CHBr_3$ and CH_2Br_2, see Section 2.2.1). Given that the dominant VSL chlorine sources are anthropogenic (between 90-100% for CH_2Cl_2, C_2Cl_4 and $C_2H_4Cl_2$, with only a significant natural fraction for $CHCl_3$) and presents a pronounced hemispheric asymmetry (WMO, 2022), hereafter we assume all of these offline emissions to have only an anthropogenic origin. Consistent with the scaling factor applied to the (Ordóñez et al., 2012) inventory, both VSLs chlorocarbon surface emissions and LBCs were globally scaled by a constant factor of 1.15 (15% enhancement) globally. The resulting global trend of anthropogenic chlorocarbon emissions implemented in CESM2-SLH is in agreement with current estimates and observations (Hossaini et al., 2019; Claxton et al., 2020; WMO, 2022) (see Section 3.2.2). It should be noted that some additional anthropogenic halocarbon sources, as those arising from the waste treatment of power-plants as well as oceanic aquaculture have been described in the literature (Carpenter et al., 2000; Leedham et al., 2013; Jia et al., 2023) but not yet implemented neither in CESM1 nor in CESM2-SLH. To include the offline anthropogenic VSL halocarbon emissions for chlorine, in addition to increasing the *srf_emiss_specifier* namelist option with CH_2Cl_2 and C_2Cl_4, users should expand the *flbc_list* to include $CHCl_3$ and $C_2H_4Cl_2$ (see Section 2.5). Differing from natural VSL sources, anthropogenic VSL emissions included in *mo_srf_emissions.F90* present a flat hourly profile (i.e., no diurnal variation is applied).

2.2.3 Online Emissions of Inorganic Halogens

In addition to the VSL halocarbon emissions, abiotic sources of inorganic halogens are implemented in the model. Here it is worth noting that these ocean-related sources have different routes for iodine compared to bromine and chlorine, and therefore are described separately. Inorganic iodine (HOI and I_2) emissions from the ocean surface are computed online following the ozone-driven oxidation of aqueous iodide occurring at the seawater surface (Carpenter et al., 2013). To include this emission in CESM2-SLH, variables HOI and I_2 must be included altogether with the standard *srf_emiss_specifier* used for VSL halocarbons, although the imposed offline file represents just a place-holder as the input values are forced to zero after being read within *mo_srf_emissions.F90* routine and replaced by the online computation. The implementation of this source, which in CESM2-SLH is now performed in a new routine called *iodine_emissions.F90*, has been described in detail in (Prados-Roman et al., 2015b), and is based on the parameterized expressions from (MacDonald et al., 2014). The online emission fluxes for HOI and I_2 are computed by Eq. (2a) and (2b), respectively,

$$F_{HOI} = [O_3] \times \left(4.15 \times 10^5 \times \sqrt{\frac{[I^-_{aq}]}{w}} - \left(\frac{20.6}{w}\right) - 23600 \times \sqrt{[I^-_{aq}]}\right), \quad (2a)$$

$$F_{I2} = [O_3] \times \left[I^-_{aq}\right]^{1.3} \times \left(1.74 \times 10^9 - (6.54 \times 10^8 \times ln(w))\right), \quad (2b)$$

where $[O_3]$ and w are the surface ozone abundance (ppbv) and wind speed, respectively, computed over the ocean at the lowest model level. $[I^-_{aq}]$ is the aqueous iodide seawater concentration computed by Eq. (2c), which in turn depends on the model SST,

https://doi.org/10.5194/egusphere-2025-3250
Preprint. Discussion started: 13 October 2025

$$[I^-_{aq}] = 1.46 \times 10^6 \times exp\left(\frac{-9134}{SST}\right) \quad (2c)$$

Note that the fitting approach applied to the laboratory observations resulted in an unrealistic iodine emission flux for low wind conditions. Therefore, a wind speed mask imposing w = 3 m/s is applied to Eqs. 2a and 2b for all model gridpoints where w < 3 m/s. Not doing so could result in an overestimation of iodine fluxes from the ocean during calm periods (Inamdar et al., 2020). Finally, we highlight the first order dependence of F_{HOI} and F_{I2} with ozone abundance, which has important consequences for the long-term trend of iodine emissions during the historical period (see Section 3).

For bromine and chlorine, additional abiotic inorganic source emissions arise from the so-called SSA-dehalogenation reactions. In this case, the online computation of inorganic halogen emissions assumes an oxidized gas-phase species to be deposited on the sea-salt aerosol surface, followed by an heterogeneous reaction that captures a reduced halide reservoir within the substrate that is oxidized before being released to the gas-phase (Fernandez et al., 2014). This complex redox process is parameterized to proceed in a single-step heterogeneous reaction dependent on the collisional frequency of the gas-phase species and the substrate, as well as on the degassing efficiency of the halogenated product released to the atmosphere. Differing from iodine, this recycling process is not included as a typical emission species within *srf_emiss_specifier*, but instead has been implemented as non-stoichiometric halogen reactions within the *chem_mech.in* based on the Free-Regime Approximation (FRA) approach (McFiggans et al., 2000) following Eq. (3),

$$F^{XY}_{SSA} = \frac{1}{4} \times \gamma^{ox} \times \left(100 \times \sqrt{\frac{8 \times R \times T}{\pi \times M^{ox}_w}}\right) \times SAD_{SSA} \times [Spec_{ox}] \times DF \times mask_{SSA}\ , \quad (3)$$

Here, F^{XY}_{SSA} is the flux of inorganic halogens (in the form of X_2 or XY, with X,Y = Cl, Br or I) in molec. cm^{-3} s^{-1}, γ^{ox} represents the accommodation coefficient of the gas-phase halogenated oxidized reservoir colliding with the SSA, M_w^{ox} is the molecular weight (g mol^{-1}) of the oxidized species used to compute the mean-root square molecular speed, which in turn depends on the modelled temperature at each gridpoint (R is the universal gas constant and T units are in K). Furthermore, the surface area density of SSA (SAD_{SSA} in cm^{-2} cm^{-3}) is computed considering the 3 (three) SSA bins represented in the model, while [$Spec_{ox}$] is the atmospheric molecular concentration (molec. cm^{-3}) of the gas-phase oxidized halogen species ($XONO_2$, XNO_2 and/or HOX, with X = Cl, Br and I) colliding with SSA. Finally, DF is a seasonal-dependent normalized depletion factor that represents the efficiency of the recycling reaction for any given atmospheric condition, while $mask_{SSA}$ is a logical mask that limits the occurrence of the SSA-dehalogenation processes above a pressure threshold of 300 hPa. Here it should be noted that the photochemical degradation of offline VSLs sources described in previous sections constitute the initial step releasing the halogen atoms that partition between different gas-phase reservoirs that, on a subsequent step, can be deposited over the sea-salt substrates and being recycled back to the gas phase. Further details on the SSA-dehalogenation implementation in CESM can be found elsewhere (Ordóñez et al., 2012; Fernandez et al., 2014, 2021).

The FRA for several halogen and nitrogen reservoirs has been implemented in routine *mo_usrrxt.F90* and assumes that the bromide and chloride content of SSA is sufficiently large to act as an effectively infinite halide reservoir capable of sustaining the surface heterogeneous-redox reaction. This implies that the bromide and/or chloride content in the SSA bulk is always in excess compared to the abundance of the gas-phase halogen reservoir that deposits over the aerosol surface, which is valid for fresh SSA typically found close to the ocean surface. Table 1 summarizes all 9 independent reactions releasing either gas phase X_2 or XY, where the non-stoichiometric coefficients between reactants and products for each gas-phase halogen species determines the net inorganic halogen flux. For example, when brominated reservoirs are oxidized (*het_ss_0-het_ss_2*), each cycle represents the additional release of 0.65 Br + 0.35 Cl to the gas-phase (in the form of Br_2 and BrCl),

https://doi.org/10.5194/egusphere-2025-3250
Preprint. Discussion started: 13 October 2025

while for the case of chlorinated reservoirs, only chloride is captured and released to the gas-phase as Cl_2. It should be noted that for the particular case of iodine reservoirs (*het_ss_6-het_ss_8*), the SSA-dehalogenation process represents a net source of chlorine and bromine (0.5 Br and 0.5 Cl in the form of IBr and ICl), but only a shift in partitioning among different iodine species without constituting a net source of inorganic iodine to the atmosphere (i.e., the reaction is stoichiometric for iodine). Given the large changes in SSA abundance and distribution between CESM1 and CESM2 (see Fig. S1), and with the objective of reproducing previously estimated SSA-dehalogenation fluxes and burdens obtained in CESM1, the accommodation coefficients (γ^{ox}) originally provided by (Ordóñez et al., 2012) have been readjusted within reasonable ranges in CESM2-SLH. In doing so, we acknowledge that most of the reported γ^{ox} values for halogenated reservoirs have very large uncertainties and are strongly dependent on the composition of the aerosols (Sander, 2015) and therefore the final value considered is largely based on adjusting the model output with atmospheric observations of individual chlorine, bromine and iodine species (see Section 3.2.2).

Table 1: Heterogeneous recycling processes representing a net source of inorganic halogens in CESM2-SLH.

Reaction tag	non-stoichiometric reaction	Molecular Weight [$]	Gamma (γ^{ox})	net halogen release
Halogenated-reservoirs				
het_ss_0	$BrONO_2$ -> 0.65*Br_2 + 0.35*BrCl	1.22E+03	0.01	0.65 Br + 0.35 Cl
het_ss_1	$BrNO_2$ -> 0.65* Br_2 + 0.35* BrCl	1.29E+03	0.005	0.65 Br + 0.35 Cl
het_ss_2	HOBr -> 0.65* Br_2 + 0.35* BrCl	1.47E+03	0.0125	0.65 Br + 0.35 Cl
het_ss_3	$ClONO_2$ -> CL_2	1.47E+03	0.006	1.00 Cl
het_ss_4	$ClNO_2$ -> CL_2	1.61E+03	0.006	1.00 Cl
het_ss_5	HOCl -> CL_2	2.01E+03	0.03	1.00 Cl
het_ss_6	$IONO_2$ -> 0.5*IBr + 0.5*ICl	1.05E+03	0.003	0.50 Br + 0.50 Cl
het_ss_7	INO_2 -> 0.5*IBr + 0.5*ICl	1.10E+03	0.006	0.50 Br + 0.50 Cl
het_ss_8	HOI -> 0.5*IBr + 0.5*ICl	1.21E+03	0.0018	0.50 Br + 0.50 Cl
Oxidized nitrogen-compounds				
het_ss_9	HNO_3 -> HCl	1.83E+03	0.01	1.00 Cl
het_ss_11	N_2O_5 -> 2*HNO_3	1.40E+03	0.0143	(1.00 – $yield^{ClNO2}$)
het_ss_12	N_2O_5 -> $ClNO_2$ + HNO_3	1.40E+03	0.0143	$yield^{ClNO2}$

[$] Values for the molecular weight actually correspond to the following term from Eq. (3), $\left(\sqrt{\frac{8\times R}{\pi\times M_w^{ox}}}\right)$, where temperature has been excluded from the square-root and is later multiplied by an independent $\left(\sqrt{T}\right)$ term.

Careful consideration of SSA and other aerosols representation is key across CESM versions. In particular, any change in the representation of both the abundance and distribution of SSA in the model (e.g. (Danabasoglu et al., 2020) for CESM2) will have a direct impact on halogen production via SSA dehalogenation, consequently altering the SLH tropospheric budget and burden. This was indeed the case when shifting from CAM4-Chem to CESM2-CAM6, where the SSA representation changed from a continuous (bulk) representation considering 4 different bin sizes to a modal aerosol representation considering only 3 (three) bins, and in addition, the vertical extent of sea-salt in the free-troposphere was largely reduced to improve the model agreement with observations (Lamarque et al., 2012; Tilmes et al., 2023). Therefore, to easily adjust the online efficiency of the SSA-dehalogenation flux and avoid changes in the atmospheric burden of inorganic halogens in the troposphere, the released CESM2-SLH configuration now includes a group of SLH scaling factors (*&slh_nl,*) within the user-defined namelist (*user_nl_cam*) to allow individual users to adjust the SSA-dehalogenation source in the different model

https://doi.org/10.5194/egusphere-2025-3250
Preprint. Discussion started: 13 October 2025

resolutions and configurations in order to assure a consistent halogen atmospheric loading that are consistent with those shown in this work (see Section 2.5).

For chlorine, additional inorganic halogen sources arise from the heterogeneous recycling of nitrogen species (N_2O_5 and HNO_3) on halide-rich SSA (see Eq. 3 and Table 1). In the first case, the SSA uptake and recycling of N_2O_5 drives two key processes: *i)* the well-documented hydrolysis to produce HNO_3 (*het_ss_11*, (Lamarque et al., 2012)); and *ii)* the production of nitryl chloride ($ClNO_2$), which constitutes a net chlorine source (*het_ss_12*). The latter is of importance as $ClNO_2$ photolysis in polluted environments lead to ozone production (Knipping and Dabdub, 2003; Thornton et al., 2010). Within CESM2-SLH, the $ClNO_2$ yield is computed online based on a cubic expression dependent on the total sea-salt aerosol mass within each of the sea-salt aerosol bins (Li et al., 2022). In the second case (*het_ss_9* in Table 1), the acid-displacement reaction HNO_3 → HCl represent the acid-uptake of chloride content from the sea-salt bulk, which in turn depends on a fixed HNO_3 accommodation coefficient (Sander, 2015), as implemented in other models including chlorine chemistry (Hossaini et al., 2016). The CESM2-SLH implementation of both chlorine sources follows the FRA-approach described above for the oxidized halogen reservoirs (Eq. 3), although in this case the gas-phase species that deposit over the sea-salt aerosol and drives the heterogeneous recycling does not contain an oxidized halogen, but is the oxidized nitrogen species the one that captures the sea-salt chloride from the aerosol bulk. To allow a direct adjustment of the source-strength for different representations of sea-salt aerosol loadings, we also include individual *&slh_nl* scaling factors for N_2O_5 and HNO_3 recycling (see Section 2.5). We note that stoichiometric N_2O_5 recycling over halide-poor tropospheric aerosols is also considered in the model, although for these reactions the halogen uptake and recycling only constitute a partitioning shift between different halogen and nitrogen species (see Section 2.3.3 for details).

Finally, we highlight the importance of adjusting the strong model dependence of online SLH sources and burdens depending on the sea-salt abundances and distributions represented in different model configurations (see Fig. S1). Note that the accommodation coefficients (γ) and depletion factors (DF) altering the reactive efficiency for the different species reported in the literature possess a wide range of values and large uncertainties that depend on variables that are unconstrained in the simplified parameterization implemented in CESM2-SLH (e.g., pH dependence, halide content, etc; (Sander, 2015; Burkholder et al., 2019). Consequently, variations in SSA fields, pollutant emissions, and atmospheric composition (e.g., HO_x/NO_x partitioning), combined with non-linear heterogeneous recycling (Table 1), may cause regional over-/under-estimations of halogen content in localized regions in comparison with previous CESM1 studies (see Section 3.2.3).

2.3 Short-Lived Halogen Chemistry

In the following subsections, we provide an independent description of the main photochemical (Section 2.3.1), gas-phase (Section 2.3.2) and heterogeneous-phase (Section 2.3.3) reactions implemented in the default CESM2-SLH chemical scheme. This scheme builds upon the TS1.2 benchmark chemical mechanism used in CESM2 (Emmons et al., 2020), which explicitly includes the volatility basis set (VBS) parameterization for secondary organic aerosol formation (Tilmes et al., 2019, 2023). The complete set of SLH reactions added to the TS1-simpleVBS branch within the precompiled *trop_strat_mam4_slh* chemical pre-processor (chem_mech.in) is included in the Supplementary Information (Tables S1, S2 and S3). Overall, the final SLH chemical mechanism implemented in CAM-Chem introduces 12 additional chlorine SLH species, resulting in a total of 34 chlorinated compounds that participate in 67 new reactions. These new reactions are categorized as: photolysis (11), odd-halogen reactions (6), organic-halogen reactions (20), sulfur-halogen reactions (2), heterogeneous recycling on tropospheric aerosols (7), sea-salt recycling source (11), and stratospheric mapped reactions (10), where 11+6+20+2+7+11+10=67. Similarly, for bromine we incorporated 9 species on top of 19 brominated compounds to reach a total of 53 new reactions (respectively distributed as 10+9+8+1+6+6+13=53 to the same categories), while for the case of iodine, 19 new species and a total of 17+39+2+1+10+6+18=93 reactions were implemented. Note that some of the reactions

https://doi.org/10.5194/egusphere-2025-3250
Preprint. Discussion started: 13 October 2025

involve inter-halogen interactions (e.g., ClO + BrO), and therefore are double-counted within each family. Therefore, considering all chlorine, bromine and iodine, a total of 31+46+24+4+17+16+25=163 new SLH reactions were implemented. Finally, we highlight that the same SLH chemical scheme has also been merged into the TSMLT1 mechanism for WACCM (tag MZ197, *waccm_tsmlt_mam4_slh*).

2.3.1 Photochemical Reactions

A comprehensive list of all photochemical halogen reactions included in the SLH scheme is shown in Supplementary Table S1, based on the original publication compiled in (Ordóñez et al., 2012) and (Saiz-Lopez et al., 2014), with further updates from (Badia et al., 2021; Saiz-Lopez et al., 2023). This includes 11, 10 and 17 new photolysis reactions for chlorine, bromine and iodine, respectively, which adds up to previously defined photolysis reactions of long-lived halocarbons as well as odd-chlorine and odd-bromine reactions that are required for properly representing stratospheric ozone depletion in CESM2 (Gettelman et al., 2019b). The absorption cross sections and quantum yields are taken from the latest JPL (Burkholder et al., 2019) and IUPAC (Atkinson et al., 2007, 2008) handbooks, and are included within the *xs_long* and *xs_short* file typically used in CAM-Chem and WACCM. Wavelength integrated *J-values* are computed as a function of temperature and height considering the model actinic flux and a Look-Up-Table (LUT) approach (Kinnison et al., 2007; Lamarque et al., 2012; Emmons et al., 2020).

Note that the photodegradation of anthropogenic VSLs ($CHCl_3$, CH_2Cl_2 and C_2Cl_4) results in the formation of phosgene ($COCl_2$), which constitutes a halogen intermediate that accumulates in the upper troposphere until it photo-decomposes in the lower stratosphere (see Fig. S3) (Hossaini et al., 2016). Therefore, phosgene does not participate in direct ozone destruction in the lower-stratosphere until it releases the Cl atoms through photolysis. However, and given that the only source of phosgene in the model is the degradation of VSL, we consider the contribution of $COCl_2$ within the PGs chlorine fraction, in line with the latest (WMO, 2022) report. In addition, some laboratory measurements show that the absorption tail for the C_2Cl_4 cross-section can extend beyond $\lambda > 270$ nm (Keller-Rudek et al., 2013). However, the JPL19-5 handbook (Burkholder et al., 2019) recommends neglecting the photochemical breakdown above this threshold. Within CESM2-SLH, forcing to zero the absorption above 270 nm was required to reproduce observations of this particular anthropogenic halocarbon in the upper troposphere. Not doing so resulted in a complete decomposition of this compound driven by a too efficient photodissociation all the way down to the surface (Roozitalab et al., 2024). Finally, note that Table S1 considers the photodissociation of higher order iodine oxides (I_xO_y, with x = 2 and y = 2, 3, 4). The absorption cross sections of these species were derived from solution spectrum measured at the University of Leeds (Lewis et al., 2020), which were subsequently scaled to estimate absolute absorption cross-sections (Gómez Martín et al., 2005). Therefore, and supported by experimental measurements (Saiz-Lopez et al., 2014) as well as on several follow-up papers demonstrating that considering I_xO_y photolysis was required to reproduce gas-phase and particulate iodine observations (Saiz-Lopez et al., 2015; Koenig et al., 2020), the released CESM2-SLH chemical mechanism is based on the J_{IxOy} scheme for iodine proposed in (Saiz-Lopez et al., 2014).

2.3.2 Gas-Phase Reactions

A complete description of all bimolecular Arrhenius type reactions of halogen species are shown in Supplementary Table S2, where for the sake of simplicity we have ordered reactions in the following groups: Odd-Oxygen, Odd-Chlorine, Odd-Bromine, Odd-Iodine, VSL halocarbon degradation and reactions with sulphur and carbon compounds. All these developments have been initially described in (Ordóñez et al., 2012), with additional updates for iodine described in (Saiz-Lopez et al., 2014). In addition, all termolecular reactions considered in the default SLH chemical mechanism are shown in Table S3. Note that for the final implementation of SLH chemistry in CESM2, all expressions, reaction-rate coefficients and

https://doi.org/10.5194/egusphere-2025-3250
Preprint. Discussion started: 13 October 2025

temperature dependence factors have been updated to the reported values in the last JPL 19-5 handbook (Burkholder et al., 2019).

Oxidation of DMS to produce sulphur dioxide (SO_2) by BrO, Cl and IO are also included in the updated SLH chemical scheme. Here, we highlight that improvements in sulphur chemistry representation in CESM, including SO_2 and tropospheric sulphate formation and washout, are a major source of uncertainty for radiative forcing estimations (Ge et al., 2022) and are currently under development. Therefore we decided to maintain in the updated SLH mechanism the benchmark sulphur scheme implemented in TS1.2 (Emmons et al., 2020). Similarly, CESM2-SLH uses the Modal Aerosol Model with 4 modes (MAM4) scheme, which computes the formation and growth of sulphate, black carbon and organic matter, secondary organic aerosols, sea salt, and dust (Liu et al., 2016). MAM4 is the default aerosol scheme in CESM2 and has not been updated within the SLH scheme, although the perturbations of reactive halogens on OH abundance can indirectly influence the aerosol burden (Saiz-Lopez et al., 2023). In the following section, we describe the direct heterogeneous processes involving inorganic halogens.

2.3.3 Heterogeneous Reactions

Heterogeneous SLH reactions occurring over different types of atmospheric substrates have also been implemented (see Table 2). It is worth noting that unlike the SSA-dehalogenation source described in Section 2.2.3, all of these reactions are stoichiometric and therefore do not represent a net halogen source from the aerosol to the gas-phase, but instead, result in a change in individual species partitioning between gaseous reactants and products. Indeed, in all cases, the substrate surface (e.g., ice-crystals, cloud droplets and/or other anthropogenic aerosols typically considered in CAM6 like black-carbon, organic carbon, sulphate, nitrate, etc.) acts like a catalyst and does not contribute with any halogen content. For heterogeneous reactions occurring over ice-crystals, we compute the reaction rate constant ($rate_{ICE}$), using an equivalent FRA approach. This method accounts for the total number of gas-phase species that are assumed to be uptake by the aerosol surface, resulting in the following expressions for uni-molecular

$$rate_{ICE}^{uni} = \frac{1}{4} \times \gamma^X \times \left(100 \times \sqrt{\frac{8 \times R \times T}{\pi \times M_w^X}}\right) \times SAD_{ICE} \times mask_{ICE-strat} \,, \quad (4a)$$

and bimolecular

$$rate_{ICE}^{bi} = \frac{1}{4} \times \gamma^X \times \left(100 \times \sqrt{\frac{8 \times R \times T}{\pi \times M_w^X}}\right) \times SAD_{ICE} \times mask_{ICE-strat} \times \frac{1}{[Y]} \,, \quad (4b)$$

reactions shown in Table 2. Here, γ^x and M_w^X are, respectively, the accommodation coefficient and the molecular weight of the gas-phase halogenated reservoir species (X) that is initially taken up by the ice-crystal, SAD_{ICE} represents the surface area density of ice crystals and is computed online based on the ice-water content in clouds (CLDICE) from the CAM6 model, and $mask_{ICE\text{-}strat}$ is a logical mask imposed to limit the computation below the model tropopause and avoid double-counting recycling reactions historically implemented to occur in the stratosphere (Kinnison et al., 2007; Fernandez et al., 2014). All these developments are included in the original *mo_usrrxt.F90* routine. For bimolecular reactions, note that the reaction rate is normalized by the atmospheric concentration of the most abundant halogenated species (either X or Y) involved in the reaction. The original implementation of these reactions has been described in detail in (Fernandez et al., 2014) for bromine and chlorine and in (Saiz-Lopez et al., 2015) for the case of iodine.

https://doi.org/10.5194/egusphere-2025-3250
Preprint. Discussion started: 13 October 2025

The heterogeneous recycling reaction of N_2O_5 shown in Table 2 takes place on tropospheric aerosols in continental regions. In contrast to reaction *het_ss_12* in Table 1 that occurs only over sea-salt aerosols, the tagged reaction *usr_N2O5_aer2* in Table 2 can also occur over tropospheric aerosols over continental domains, which produces $ClNO_2$ that can further photolyze to release NO_2 and consequently result in additional ozone production within polluted environments (i.e., high-NO_x regimes). However, and given that the model aerosol components within MAM4 (i.e., black-carbon, organic-carbon, sulphate and/or nitrate) do not represent a halide reservoir, reaction *usr_N2O5_aer2* assumes that the reduced chlorine atom that is oxidized over the substrate surface must be initially captured by the aerosol in the form of HCl, which further react at the aerosol surface to produce $ClNO_2$ that is released back to the gas phase (reactive uptake). For this particular process, the heterogeneous rate constant is computed following the standard *hetrxtrate* function in *mo_usrrxt.F90* (Lamarque et al., 2012), which considers the accommodation coefficients and production yields from (McDuffie et al., 2018, 2019). The implementation of the photochemical recycling of nitrogen oxides is based on (Li et al., 2022) following the HNO_3 acid-displacement developments from (Hossaini et al., 2016).

Table 2: Heterogeneous recycling processes representing a change in partitioning of inorganic halogens in CESM2-SLH.

tag	stoichiometric reaction	Molecular Weight [$]	Gamma (γ^{ox})
ice-crystals			
ice_trp_br_1	$BrONO_2$ -> $HOBr + HNO_3$	1.22E+03	0.3
ice_trp_cl_1	$ClONO_2$ -> $HOCl + HNO_3$	1.47E+03	0.1
ice_trp_hbr_5	$HOCl + HBr$ -> $BrCl + H_2O$	2.01E+03	0.2
ice_trp_hbr_6	$HOBr + HBr$ -> $Br_2 + H_2O$	1.47E+03	0.12
ice_trp_hcl_5	$HOCl + HCl$ -> $Cl_2 + H_2O$	2.01E+03	0.2
ice_trp_hcl_6	$HOBr + HCl$ -> $BrCl + H_2O$	1.47E+03	0.3
ice_trp_hi_5	$HOCl + HI$ -> $ICl + H_2O$	2.01E+03	0.12
ice_trp_hi_6	$HOBr + HI$ -> $IBr + H_2O$	1.47E+03	0.12
ice_trp_i_1	$IONO_2$ -> $HOI + HNO_3$	1.06E+03	0.1
ice_trp_i_2	$HOI + HCl$ -> $ICl + H_2O$	1.21E+03	0.12
ice_trp_i_3	$HOI + HBr$ -> $IBr + H_2O$	1.21E+03	0.12
ice_trp_i_4	$HOI + HI$ -> $I_2 + H_2O$	1.21E+03	0.12
tropospheric aerosols			
usr_N2O5_aer2[&]	$N_2O_5 + HCl$ -> $ClNO_2 + HNO_3$	1.40E+03	0.02

[$] Values for the molecular weight correspond to the following term from Eq. (3), $\left(\sqrt{\frac{8\times R}{\pi\times M_w^{ox}}}\right)$, where temperature has been excluded from the square-root and is later multiplied by an independent $\left(\sqrt{T}\right)$ term.

[&] A reaction yield of 0.138 is considered for $ClNO_2$ production (Li et al., 2022).

Regarding stratospheric heterogeneous reactions involving halogenated reservoirs that are important for the ozone layer, we complemented a full set of SLH reactions mapping the historical implementation performed in *mo_strato_rates.F90* for WACCM (Marsh et al., 2013; Fernandez et al., 2017; Cuevas et al., 2022). This includes re-activation reactions occurring over stratospheric sulphate (SAD_{SULFC}), ice-crystals (SAD_{ICE}) and nitric acid trihydrate (SAD_{NAT}) surfaces (Kinnison et al., 2007), for which independent accommodation coefficients (γ) have been computed for the main reactions involving the major chlorinated and brominated reservoirs, many of them including a logical condition of humidity and/or temperature-dependence updates (Solomon et al., 2015). Based on (Cuevas et al., 2022), we extended the same approach to consider equivalent heterogeneous reactions in the stratosphere for the minor halogenated reservoirs (mainly HOCl and HOBr), as well as the

https://doi.org/10.5194/egusphere-2025-3250
Preprint. Discussion started: 13 October 2025

previously neglected iodine species (see Table 3). In doing so, and despite laboratory measurements suggesting that the reactive efficiencies of iodine species are larger than those for bromine and chlorine (Solomon et al., 1994; Koenig et al., 2020), we assumed identical accommodation coefficients and reaction yields for chlorine and bromine as those originally computed in the default WACCM scheme. Based on the original implementation in CESM1 (Fernandez et al., 2017; Saiz-Lopez et al., 2023), for FC compsets we imposed prescribed stratospheric sulphate aerosols above the tropopause (Mills et al., 2016), which results in smaller SAD_{SULFC} fields compared to those computed with MAM4 (see Fig. S2). Therefore, the modelled impact of these reactions in the lower stratosphere should represent a lower limit compared to WACCM (Cuevas et al., 2022). Note that equivalent logical conditions based on $mask_{ICE\text{-}strat}$ have also been applied to all equivalent tropospheric iodine reactions occurring over tropospheric ice-crystals to avoid double counting.

Table 3: Update of stratospheric heterogeneous reactions for minor bromine and iodine species in CESM2-SLH.

het-recycling reaction	Substrate/ tag	gamma	Substrate/ tag	gamma	Substrate/ tag	gamma
mapped to chlorine	sulphate		NAT		Water-ice	
HOCl + HCl -> Cl_2 + H_2O	het5	f(T,P,HCl,HOCl,H2O,r)	het10	0.1	het16	0.2
HOCl + HBr -> BrCl + H_2O	**het5_hbr**	**f(T,P,HCl,HOCl,H2O,r)**	**het10_hbr**	**0.1**	**het16_hbr**	**0.2**
HOCl + HI -> ICl + H_2O	**het5_hi**	**f(T,P,HCl,HOCl,H2O,r)**	**het10_hi**	**0.1**	**het16_hi**	**0.2**
mapped to bromine						
HOBr + HCl -> BrCl + H_2O[$]	het6	f(T,P,HCl,HOBr,H2O,r)	**het10b**	**0.1**	het17	0.3
HOBr + HBr -> Br_2 + H_2O	**het6_hbr**	**f(T,P,HCl,HOBr,H2O,r)**	**het10bhbr**	**0.1**	**het17_hbr**	**0.3**
HOBr + HI -> IBr + H_2O	**het6_hi**	**f(T,P,HCl,HOBr,H2O,r)**	**het10bhi**	**0.1**	**het17_hi**	**0.3**
new iodine (mapped to bromine)						
$BrONO_2$ -> HOBr + HNO_3	het3	f(T,P,H2O,r)	het11	0.006	het14	0.3
$IONO_2$ -> HOI + HNO_3	**slf_str_i_1**	**f(T,P,H2O,r)**	**nat_str_i_1**	**0.006**	**ice_str_i_1**	**0.3**
HOI + HCl -> ICl + H_2O	**slf_str_i_2**	**f(T,P,HCl,HOBr,H2O,r)**	**nat_str_i_2**	**0.1**	**ice_str_i_2**	**0.3**
HOI + HBr -> IBr + H_2O	**slf_str_i_3**	**f(T,P,HCl,HOBr,H2O,r)**	**nat_str_i_3**	**0.1**	**ice_str_i_3**	**0.3**
HOI + HI -> I_2 + H_2O	**slf_str_i_4**	**f(T,P,HCl,HOBr,H2O,r)**	**nat_str_i_4**	**0.1**	**ice_str_i_4**	**0.3**

Bold font style highlights the mapped reactions and gammas applied to the corresponding regular font expression originally implemented in (Marsh et al., 2013). For chlorine and bromine reactions we extended the original reaction tag-name, while for iodine expressions we adopted an independent tag-convention indicative of the substrate where each reaction occurs.

[$] For the case of HOBr + HCl -> BrCl + H_2O reaction only tag het10b was updated on top of the original scheme.

2.4 Species-specific dry and wet deposition

The implementation of species-independent dry and wet deposition processes in CESM1 CAM4-Chem has been previously described in the literature (Ordóñez et al., 2012; Fernandez et al., 2014; Saiz-Lopez et al., 2014). Here we briefly summarize the main approaches used to compute the removal or sink of SLH from the atmosphere, focusing on the few cases where a different approach was implemented in CESM2-SLH. Note that the model only considers the removal of inorganic halogen species, and therefore the sinks of VSL halocarbons are only chemical while for inorganic PGs deposition represents the major sink.

https://doi.org/10.5194/egusphere-2025-3250
Preprint. Discussion started: 13 October 2025

Table 4: Independent halogen species considered for dry and wet deposition in CESM2-SLH.

species	Dry deposition velocity ($m\ s^{-1}$)	Wet deposition solubility (K_H, $M\ atm^{-1}$)	Ice_uptake[&]
Chlorine			
HCl	2.00E-02	1.54E+00	YES
HOCl	1.00E-02	9.30E+02	YES
$ClONO_2$	1.00E-02	1.00E+06	YES
$ClNO_2$	5.00E-03	3.50E-02	YES
$COCl_2$	1.00E-02	5.90E-04	
$CHCl_2O_2$	1.00E-02	1.70E-03	
Bromine			
HBr	2.00E-02	7.20E-01	
HOBr	1.60E-02	1.90E+03	
$BrONO_2$	5.00E-03	1.00E+06	FRA
$BrNO_2$	5.00E-03	3.00E-01	YES
Br_2	1.00E-02	7.60E-01	
BrCl		9.40E-01	
Iodine			
IBr	1.00E-02	2.40E+01	
ICl	1.00E-02	1.10E+02	
HI	1.00E-02	7.80E-01	FRA
HOI	7.50E-03	FRA	FRA
$IONO_2$	7.50E-03	1.00E+06	FRA
INO_2	7.50E-03	3.00E-01	
IO		4.50E+02	
OIO		1.00E+04	
I_2O_2	1.00E-02	1.00E+04	YES
I_2O_3	1.00E-02	1.00E+04	YES
I_2O_4	1.00E-02	1.00E+04	YES

[&] FRA indicate that for that particular case, the Free Regime Approximation was applied, see Table 5.

The depositional flux of gas-phase halogenated inorganic species due to dry deposition is calculated as the product of the deposition velocity of each individual species times its concentration at the lowest model surface (Ordóñez et al., 2012), following the original implementation within *mo_drydep.F90* in CAM-Chem (Lamarque et al., 2012). Table 4 summarises the complete list of gas-phase species that are considered in the *drydep_list*, and shows the individual deposition velocity for each species. In addition, inorganic halogens are also removed by wet-deposition, following the default NEU scheme (Neu and Prather, 2012). Both nucleation scavenging (rainout) and impaction scavenging (below-cloud washout) are implemented in the wet-removal schemes based on (Lamarque et al., 2012), although it is worth noting that we updated the *mo_neu_wetdep.F90* routine to avoid mapping the ice-uptake of halogen species to that of HNO_3, as this resulted in too efficient washout of bromine and iodine in the upper troposphere (Fernandez et al., 2014). This was achieved by including the additional variable *gas_wetdep_ice_uptake_list* within the *&wetdep_inparm* namelist group (see Section 2.5). The individual

https://doi.org/10.5194/egusphere-2025-3250
Preprint. Discussion started: 13 October 2025

Henry law coefficients (k_H) for all chlorine, bromine and iodine species shown in Table 4 are mostly based on the compilation of Henry Laws constants from (Sander, 2015) and IUPAC (Atkinson et al., 2007, 2008).

Table 5: Free Regime Approximation reactions representing a net sink of inorganic halogens in CESM2-SLH.

tag	het-recycling washout	Molecular Weight [$]	Gamma (γ^{ox})	type of surface
	Iodine			
ice_fr_hi	HI ->	1.29E+03	0.02	SAD_{ICE}
ice_fr_hoi	HOI ->	1.21E+03	3.00E-04	SAD_{ICE}
ice_fr_iono2	$IONO_2$ ->	1.06E+03	0.02	SAD_{ICE}
liq_fr_hoi	HOI ->	1.21E+03	3.00E-04	SAD_{LIQ}
ss_ixoy_2	I_2O_2 ->	8.61E+02	0.0025	SAD_{SSA}
ss_ixoy_3	I_2O_3 ->	8.38E+02	0.0025	SAD_{SSA}
ss_ixoy_4	I_2O_4 ->	8.16E+02	0.0025	SAD_{SSA}
	Bromine			
ice_fr_brono2	$BrONO_2$ ->	1.22E+03	1.00E-02	SAD_{ICE}

[$] Values for the molecular weight actually correspond to the following term from Eq. (3), $\left(\sqrt{\frac{8\times R}{\pi\times M_w^{ox}}}\right)$, where temperature has been excluded from the square-root and is later multiplied by an independent $\left(\sqrt{T}\right)$ term.

Halogenated reservoir species are assumed to be adsorbed by liquid droplets and ice-crystals, where they can undergo either: *i)* reactive uptake (chemical recycling and re-emission back to the atmosphere) or ii) permanent removal from the gas phase through washout (substrate capture/adsorption). Consequently, the modelled total inorganic halogen loading (Cl_y, Br_y and I_y), particularly in the Tropical Tropopause Layer (TTL), is determined by the competition between the wet deposition efficiency relative to the heterogeneous recycling (Aschmann et al., 2011; Aschmann and Sinnhuber, 2013). For iodine, (Saiz-Lopez et al., 2014, 2015) determined that it was not possible to reproduce IO observations in the free troposphere because the NEU scheme washout of major iodine reservoirs was too efficient and iodine was completely removed within the lower troposphere. Therefore, for the particular case of HOI, HI and $IONO_2$, we calculate wet deposition with the FRA unimolecular approach for the dominant I_y species, considering Eq. (4a) to determine the collisional frequency. These ice-uptake processes are assumed to lead to deposition of iodine from the atmosphere (see non-stoichiometric removal reactions in Table 5). For HOI, which is the dominant iodine species in the lower troposphere, the FRA was implemented for both liquid-droplets and ice-crystals, where the former considers the surface area density of liquid clouds (SAD_{LIQ}) and the latter considers SAD_{ICE} (Saiz-Lopez et al., 2014). Note that the non-reactive uptake or substrate capture of higher-order iodine oxides is also assumed to proceed efficiently on sea-salt aerosols following the FRA approach (Saiz-Lopez et al., 2015), although due to the efficient I_xO_y photolysis this additional sink of atmospheric iodine is a minor contributor compared to scavenging of major I_y species. Finally, we note that the ice-uptake for $BrONO_2$, one of the most abundant brominated reservoirs in the TTL and lower stratosphere, followed the NEU scheme and was assumed to be infinitely efficient in CESM1 (Fernandez et al., 2014). Following the FRA approach implemented for $IONO_2$, we have now implemented the FRA for $BrONO_2$ over ice-crystals in CESM2-SLH, which led to better agreement of the contribution of inorganic bromine to the total stratospheric bromine budget within tropical regions (see Section 3.2.2).

https://doi.org/10.5194/egusphere-2025-3250
Preprint. Discussion started: 13 October 2025

2.5 CESM2-SLH release

The implementation of short-lived halogen sources and chemistry was performed on top of version 2.2.0 of CESM2 (Danabasoglu et al., 2020), particularly over branch *cesm2.2-asdbranch*, which includes CAM6 tagged version *cam_cesm2_2_rel_09*. Based on this, we created additional forks, respectively called *cesm2.2-asdbranch_slh* and *cam_cesm2_2_rel_09_slh*, respectively, which incorporate SLH updates within the main FORTRAN routines of each CESM2 component, as well as necessary modifications to configuration files (e.g., *cime* and *cime_config*) and default namelist variables (see Chart S1 in the Supplementary Material). These changes enable the direct building and/or cloning of different SLH compsets. In particular, the updates in the CESM2-SLH release include: *i)* increasing the total number of halogenated species considered in the chemical mechanism, for some of which various species independent deposition velocity and Henry coefficients were required; *ii)* extending the number of species for which off-line and on-line emissions are considered, as well as those that are included as LBCs; *iii)* replacing the absorption cross-section files to include new SLH species that are not available in the default CESM2 files; *iv)* incorporating a new namelist group section for SLH (*&slh_nl*) along with additional namelist variables to consider independent ice-uptake efficiencies for some halogen species; *v)* expanding the total number of default namelist files that provide individual namelist values for the different SLH configurations and user's cases; *vi)* including pre-compiled chemical mechanism with all SLH updates for CAM-Chem and WACCM; and *vii)* mapping and updating the original compsets available in the benchmark CESM2.2.0 version to directly create and compile the different CESM2-SLH model cases. Section 2.5.1 describes the main changes implemented on each of the SLH compsets as well as the most important namelist updates and setup options that are required to properly configure a CESM2-SLH run. Finally, Section 2.5.2 summarizes the few SLH developments that have not been included in the present release, and highlights the associated limitations.

2.5.1 Available Compsets and Resolutions

Two main CESM2-SLH compsets have been developed based on the original CESM2 configurations: the *FCHIST_slh* and *FCnudged_slh* compsets. The default and suggested configurations that have been scientifically validated considers the coarse *f19_f19_mg17* (1.9º latitude × 2.5º longitude, hereafter 2°×2°) resolution and 32 vertical levels from the surface to approximately 40 km (4 hPa) during the 1980-2020 period. Unless stated otherwise, all external forcings and namelist options, including prescribed ocean SST and ice-coverage fields as well as solar radiation, cloud microphysics, gravity-wave dragging and dust emission factors are maintained identical to the default *FCHIST* and *FCnudged* parent's configuration (Danabasoglu et al., 2020; Emmons et al., 2020). To allow performing model simulations beyond the historical period, prescribed emission and LBC files based on the Climate Model Intercomparison Project – Phase 6 (CMIP6) data until year 2015, followed by the CMIP6 Shared Socio-economic Pathway 3.70 (SSP-370) scenario during the period 2016-2100 (Meinshausen et al., 2017; IPCC, 2022) were concatenated. Despite none of them have been used in this work, we note that additional emission and LBC files for other configurations using different SSP scenarios are available and can be easily changed using user-defined namelist options (see below). In addition, equivalent model configurations using a finer resolution *f09_f09_mg17* grid (0.9º latitude × 1.25º longitude, hereafter 1°×1°) have also been tested and adjusted to reproduce results in comparison with the (2º×2º) grids, although we recommend new users to select the coarse resolution setup as many of the online photochemical sources and recycling reactions described in Sections 2.2 and 2.3 depends on highly variable and resolution-dependent atmospheric fields, such as SAD_{SSA} and SAD_{ICE}. Similarly, we highlight that the existent resolution-related variability in lightning-NOx production within CESM2 (Emmons et al., 2020; Wild et al., 2020) significantly impact on the chemical partitioning and washout efficiency of SLH. Therefore, caution should be taken when shifting any SLH compset from a coarse to a fine resolution, as the resulting halogen abundances can significantly vary between them. Finally,

https://doi.org/10.5194/egusphere-2025-3250
Preprint. Discussion started: 13 October 2025

a fully-coupled *f19_g16 BWHIST_slh* as well as a whole atmosphere *f19_f19_mg17 FWnudged_slh* setups, both of them at (2º×2º) resolution and with 70 vertical levels, were also mapped to their corresponding WACCM compsets. Table 6 summarizes the names and configuration of the main CESM2-SLH compsets described in this work, as well as the time periods and conditions in which they have been tested and validated.

It is worth highlighting that most of the previous SLH studies based on CESM1 focused on a direct quantification of the changes in atmospheric composition by comparing a sensitivity including (*compset_slh*) and neglecting (*compset_noh*) short-lived halogen chemistry. However, the current CESM2-SLH release includes only the complete SLH configuration (e.g., *compset_slh*), and therefore, any study willing to perform an SLH vs. noSLH inter-comparison must configure the corresponding *compset_noh* setup. For example, note that the default CESM2 compset *FCHIST* considers LBCs for the two main bromocarbons ($CHBr_3$ and CH_2Br_2) in order to achieve a consistent stratospheric bromine loading, but the corresponding CESM2-SLH *FCHIST_slh* compset has replaced those LBCs by offline emissions files (see Section 2.2.1). Consequently, comparing *FCHIST_slh* vs. its parent *FCHIST* compset will not allow to address the impact of including (or not) $CHBr_3$ and CH_2Br_2, as both species are included in both configurations although with a different approach. Thus, new CESM2-SLH users willing to run a *FCHIST_noh* sensitivity, must start from the *FCHIST_slh* configuration, and then disable SLH sources, sinks, and /or chemical reactions involved according to their needs and the particular case and/or halogen family they are studying.

Table 6: Summary of the different model compsets and configurations implemented in CESM2-SLH.

Simulation name	SLH compset	parent's compset	resolution (lat × lon)	Vertical levels	chem_mech.in (chem_proc)	Period of time evaluated
suggested						
FCnudged_slh	Fcnudged_slh	FCnudged	(1.9º × 2.5º)	32L	trop_strat_mam4_slh	1980 - 2020
FCHIST_slh	FCHIST_slh	FCHIST	(1.9º × 2.5º)	32L	trop_strat_mam4_slh	1950 - 2020
available						
FCnudged_slh	Fcnudged_slh	FCnudged	(0.9º × 1.25º)	32L	trop_strat_mam4_slh	2000-2005
FCHIST_slh	FCHIST_slh	FCHIST	(0.9º × 1.25º)	32L	trop_strat_mam4_slh	2000-2005
FWnudged_slh	FWnudged_slh	FWSD	(1.9º × 2.5º)	70L	waccm_tsmlt_mam4_slh	2000-2005
BWHIST_slh	BWHIST_slh	BWHIST_BCG	(1.9º × 2.5º)	70L	waccm_tsmlt_mam4_slh	2000-2005

The main changes that must be applied to the default namelist variables are listed below (a default SLH *user_nl_cam* highlighting the required modifications is provided in Chart S2 in the Supplementary Material):

- **Initialization file:** The initial condition (*ncdata*) data has been replaced to ensure the stabilization of all SLH species and atmospheric compounds. Note that while 3 years of spin-up are sufficient to achieve tropospheric stabilization of SLH SGs and PGs, we recommend performing at least 7-10 years of spin-up for complete stratospheric stabilization when starting from an initial condition that neglects SLH.
- **Offline emissions:** The *srf_emis_specifier* within the *&chem_inparm* group has been expanded to include the offline emissions of $CHBr_3$, CH_2Br_2, CH_2BrCl, $CHBr_2Cl$, $CHBrCl_2$, CH_3I, CH_2I_2, CH_2IBr, CH_2ICl, CH_2Cl_2, C_2Cl_4, I_2, and HOI. Note that although HOI and I2 are included in this list, this serves just as a placeholder as their emissions are forced to zero after being read and are subsequently computed online within the *iodine_emissions.F90* routine.
- **Boundary conditions:** CH_3Cl and $C_2H_4Cl_2$ have been included in the *flbc_list* within the *&chem_surfvals_nl* group, as these species contribute to the atmospheric SLH chlorine loading. An updated *flbc_file* including the projected trend of these anthropogenic VSLs for the different SSPs has also been developed.

https://doi.org/10.5194/egusphere-2025-3250
Preprint. Discussion started: 13 October 2025

- **Absorption cross-sections:** To compute the photolysis of gas-phase organic and inorganic halogen species, wavelength-dependent absorption data of several SLH have been added to the default short-wave (*xs_short_file*) and temperature-dependent long-wave (*xs_long_file*) cross-section files within *&chem_inparm*.
- **Dry deposition:** The following species have been included in the *drydep_list* within *&drydep_inparm*: $ClONO_2$, HCl, HOCl, $ClNO_2$, $BrONO_2$, HBr, HOBr, $BrNO_2$, Br_2, $IONO_2$, HI, HOI, INO_2, I_2O_2, I_2O_3, I_2O_4, $CHCl_2O_2$, and $COCl_2$. The underlined species were already included in the default CESM2 setup.
- **Wet deposition:** The *gas_wetdep_list* within *&wetdep_inparm* has also been extended with the following species: $ClONO_2$, HCl, HOCl, COFCl, $BrONO_2$, HBr, HOBr, $ClNO_2$, $BrNO_2$, Br_2, BrCl, $IONO_2$, INO_2, HI, IO, OIO, ICl, IBr, I_2O_2, I_2O_3, I_2O_4, $CHCl_2O_2$, and $COCl_2$. Additionally, the new namelist variable *gas_wetdep_ice_uptake_list* was included with the following halogen variables: HNO_3, $ClONO_2$, HCl, HOCl, $BrNO_2$, $ClNO_2$, I_2O_2, I_2O_3 and I_2O_4,. Note that *ice_uptake = .true.* is always imposed for HNO_3 within *mo_neu_wetdep.F90* by default.
- **SLH scaling factors:** The new *&slh_nl* namelist section was incorporated, providing a set of scaling factors intended to adjust the recycling efficiency of the main processes affecting SLH sources and sinks when shifting between configurations.

Table 7: Adjusted values of *&slh_nl* scaling factors for each of the main CESM2-SLH compsets and resolutions.

compset resolution	FCnudged_slh (1.9º × 2.5º)	FCHIST_slh (1.9º × 2.5º)	FCnudged_slh (0.9º × 1.25º)	FCHIST_slh (0.9º × 1.25º)	Fwnudged_slh (1.9º × 2.5º)	BWHIST_slh (1.9º × 2.5º)
SSA-Sources						
SSAdehal_ScalingFactor	1.4	1.7	1.5	1.5	1.7	1.7
SSAhno3_ScalingFactor	1	1	1	1	1	1
SSAn2o5_ScalingFactor	1	1	1	1	1	1
FRA-Sinks						
LIQfraprx_ScalingFactor_I	1.5	1	1.5	1	1	1
ICEfraprx_ScalingFactor_I	1.3	1.7	0.9	0.9	1.9	2.8
ICEfraprx_ScalingFactor_Br	1	2	1	1	3	3

The calibrated *&slh_nl* scaling factors for the main CESM2-SLH compsets and resolutions are provided in Table 7. In case other model compsets and/or resolutions are used, it is the user´s responsibility to evaluate the global halogen loading in comparison with the validated *FCHIST_slh* and *FCnudged_slh* (2º×2º) results. A comparison of the SLH changes within the main configurations and resolutions considered in this work are shown in Section 3.4 below.

2.5.2 SLH Developments not Implemented in CESM2

As described in Section 2.1, the initial implementation and the subsequent updates of SLH sources and chemistry in CESM1 were performed in consecutive studies focused on different regions of the atmosphere and/or different processes affecting each of the individual halogen families within the complete SLH scheme. Simultaneously, non-SLH related model developments in different versions of CESM were also implemented, which have introduced variations in the distribution and impacts of SLH compared to the initial studies. Therefore, with the intention of: *i)* including the most scientifically-validated version of the SLH influence on atmospheric composition within the latest released version of CESM; and *ii)* keeping the closest model setup to the current CESM2 configurations typically used for climate and air quality studies on the global scale; the following SLH developments from CESM1 have not been included in the released CESM2-SLH version. The rationale

https://doi.org/10.5194/egusphere-2025-3250
Preprint. Discussion started: 13 October 2025

behind these exclusions and their potential implications for understanding SLH impacts on atmospheric composition are detailed below:

- **Emission-driven Methane simulations:** Despite (Li et al., 2022) highlighted the importance of performing emission-driven CH_4 simulations to properly evaluate the SLH influence on methane burden and radiative forcing, all default CESM2 configurations consider CH_4 LBCs altogether with other long-lived halogenated ODS and greenhouse gases (N_2O and CO_2). Consequently, current CESM2-SLH configuration does not allow to evaluate the direct (Cl-driven) and indirect (OH-driven) impacts of SLH chemistry on methane lifetime and radiative balance as those described in (Li et al., 2022) and (Saiz-Lopez et al., 2023).
- **Continental Inorganic Halogen emissions:** In addition to the anthropogenic halocarbon emissions of VSL chlorine, an anthropogenic emission inventory of continental inorganic halogens arising mostly from coal-burning and other sectors was developed in (Saiz-Lopez et al., 2023). Despite this inventory may be of significant relevance for regional or global air quality studies (Chang et al., 2024; Fu et al., 2024), they do not contribute to the stratospheric halogen loading while in addition it has been found that the SLH influence on global atmospheric composition is dominated by natural SLH (the so called AANE sensitivity in (Saiz-Lopez et al., 2023).
- **Polar sea-ice halogen sources and chemistry:** Given the significant architectural code changes in many model components between CESM1 and CESM2 (Danabasoglu et al., 2020) the inclusion of sea-ice halogen emissions and chemistry from the polar regions (Fernandez et al., 2019, 2024) have not been completely tested and evaluated, particularly for the southern hemisphere, and therefore are not considered in current CESM2-SLH. This omission includes other sea-ice related halocarbon emissions as those described in (Abrahamsson et al., 2018).
- **Halogen sources from dust:** The photocatalytic chlorine production (van Herpen et al., 2023) and iodine release (Koenig et al., 2021) from dust have also not been implemented in the released CESM2-SLH version. We believe that further research is required before a complete representation of these complex heterogeneous redox processes is parameterized and included alongside the rest of the widely validated SLH developments.
- **Expanded sulphur chemistry scheme:** This include MeSH emissions and chemical processing reported in (Wohl et al., 2024), as well as the hydroperoxymethyl thioformate (HPMTF) updated chemical scheme of DMS oxidation reported in (Veres et al., 2020). Despite the important role played by SLH in the atmospheric sulfur cycle, these CESM1 additions are not directly related to SLH chemistry. Therefore, we have decided not to include them in the final CESM2-SLH release, maintaining the default CESM2 sulphur chemistry.

3 Results

This section presents a comprehensive description of the main SLH effects on atmospheric composition resulting from the new CESM2-SLH model setup, and is oriented to provide a general view for new users not familiarized with SLH chemistry. We focus on mean tropical, global, zonal and surface quantities, as well as their integrated values within the troposphere and stratosphere. Results presented here show the net changes due to the SLH implementation, and, unless stated otherwise, are based on the *FCnudged_slh* and *FCHIST_slh* comparison with their corresponding *FCnudged_noh* and *FCHIST_noh* sensitivities for the coarse ($2^o \times 2^o$) horizontal resolution.

Section 3 is organized as follows: first, the individual emissions of organic and inorganic halogens are quantified in Section 3.1, altogether with the mean SLH surface and tropospheric burden changes across the historical (1980-2020) period. Section 3.2 evaluates the modelled spatio-temporal distribution of organic VSLs and inorganic halogens (reactive and reservoir species) during present-day conditions, defined as the mean 2015-2020 period. Section 3.3 assesses the impacts of SLH chemistry on the main atmospheric components during present-day, including O_3 and OH destruction, as well as the main changes in the chemical loss and production channels induced by SLH. For the particular case of ozone, the distinctive

https://doi.org/10.5194/egusphere-2025-3250
Preprint. Discussion started: 13 October 2025

influence over the troposphere and stratosphere is evaluated separately. Finally, Section 3.4 presents a model inter-comparison between the different CESM2-SLH resolutions and configurations. We highlight that in this work we do not attempt to provide a complete/exhaustive comparison with all previously published results as it would imply to replicate a large number of simulations with different configurations and periods of time (see Section 2.1). Instead, we provide a general description of the global levels and distributions of chlorine, bromine and iodine in CESM2-SLH as well as their global implications on atmospheric composition, and demonstrate that they are in line with previous CESM1 results. Nevertheless, we note that some discrepancies remain due to CESM2 updates in some features and parameters that directly or indirectly affect SLH abundance and chemistry. Therefore, we highlight that the current CESM2-SLH release has been optimized to obtain a good agreement for global emissions, budgets and distribution of SLH in comparison with previous studies, which in turn result in consistent halogen impacts on atmospheric composition (e.g. O_3, OH and NO_2).

3.1 Evolution of SLH Emissions and Burdens during the Historical Period

Figure 1 shows the global mean evolution of SLH emissions from 1980 to 2020, as well as the hemispheric distribution of the total halogen sources discriminated for each individual halogen family. Note that the emission flux of natural oceanic VSL halocarbons is read offline and remains constant throughout the entire period. This constitutes the only source of natural bromo- and iodo-carbons (Ordóñez et al., 2012). However, additional CH_2Cl_2 and C_2Cl_4 emissions from anthropogenic sources dominate the VSL chloro-carbon source (Hossaini et al., 2019; Claxton et al., 2020). In all cases, we highlight that all emitted VSLs halocarbons remain unreactive until they photolyze and/or are photochemically degraded by OH, where they release Cl, Br and I atoms that, due to their very high reactivity, react with other atmospheric components and partition among the different species within the Cl_y, Br_y and I_y halogen families. Although VSL are not the primary source of halogens in the MBL, their photodecomposition constitutes the critical first step in releasing inorganic chlorine and bromine to the atmosphere. These initially released halogens can subsequently be amplified through non-stoichiometric heterogeneous recycling processes, particularly via sea-salt aerosol dehalogenation (SSA-dehalogenation).

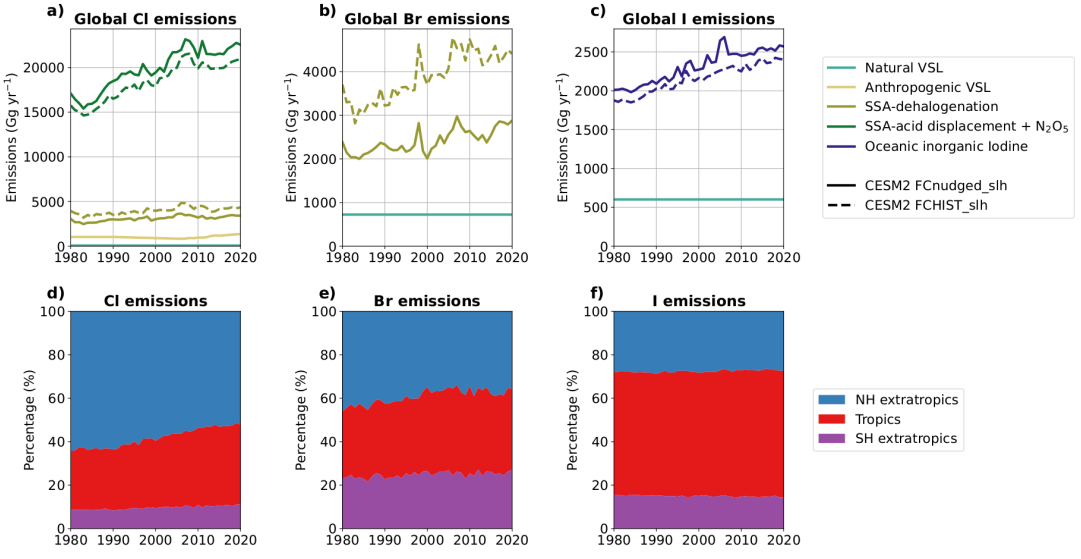

Figure 1: Historical evolution of global annual mean SLH emissions during 1980-2020. Top-row shows the individual contribution from offline and online sources for a) chlorine, b) bromine and c) iodine, while bottom-row shows the percentage distribution within the Tropical (20°N – 20°S) as well as Northern Hemisphere (NH = 20°N - 90°N) and Southern Hemisphere (SH = 20°S - 90°S) extra-tropical regions. Online emissions for the *FCnudged_slh* (solid) and *FCHIST_slh* (dashed) configurations are distinguished, while the contribution from offline sources are equivalent for both compsets.

https://doi.org/10.5194/egusphere-2025-3250
Preprint. Discussion started: 13 October 2025

In addition to offline VSL halocarbon emissions, inorganic halogen sources for chlorine, bromine and iodine are also computed online (see Section 2.2.3), which in all cases represent the dominant source of halogens to the atmosphere (Figure 1 and Table 8). Here we highlight that despite the main drivers of these parameterized expressions are significantly different for chlorine and bromine with respect to iodine, all of them show an increasing emission trend between 1980 and 2020 (Fig. 1). Indeed, (Prados-Roman et al., 2015b) suggested that this on-line ocean–atmosphere coupling represents a negative geochemical feedback loop by which current ocean emissions of iodine (HOI + I_2) would be 2-3 times higher than in pre-industrial times and act as a natural buffer for ozone pollution in the global marine environment, which was later demonstrated by ice-core iodine observations (Cuevas et al., 2018). Results for both *FCnudged_slh* and *FCHIST_slh* compsets show a global oceanic inorganic iodine flux increasing from 1.9-2.0 Tg I yr^{-1} in 1980 to 2.4-2.5 Tg I yr^{-1} in 2020 (Fig. 1c), with a dominant contribution from the tropical regions (Fig. 1f). In absolute terms, this values are larger than previously reported results obtained in CESM1, which ranged from 1.7-2.1 Tg I yr^{-1} depending on the period of time and model configuration (Prados-Roman et al., 2015b; Iglesias-Suarez et al., 2020; Barrera et al., 2023; Saiz-Lopez et al., 2023). The larger iodine flux in CESM2-SLH is coherent with the higher CESM2 surface ozone abundances compared to CESM1 (Fig. 2d) (Emmons et al., 2020), which is the main driver of the oceanic iodine flux enhancement (see Section 2.2.3). However, we note that current CESM2-SLH oceanic iodine flux remain below other models that implemented iodine emissions based on CESM1 (~2.7 Tg yr^{-1} in GEOS-Chem and ~2.9 Tg yr^{-1} in SOCOL; (Sherwen et al., 2016b; Karagodin-Doyennel et al., 2021)).

Regarding chlorine and bromine, the online recycling emissions are driven by, respectively, the acid-displacement reaction occurring over sea-salt aerosols and the SSA-dehalogenation source (Fig. 1a,b and Table 8). Similar to the oceanic inorganic iodine source, the modelled chlorine and bromine sources also increase from 1980 to 2020, although in this case the main driver is the positive trend in anthropogenic NO_x surface abundances (Fig. 2f). The net chlorine and bromine emissions respectively increase from approximately 15-16 Tg Cl yr^{-1} and 2.0-3.0 Tg Br yr^{-1} in 1980-1985 to 21-23 Tg Cl yr^{-1} and 2.8-4.4 Tg Br yr^{-1} during 2015-2020. Here, we note that chlorine sources present a larger inter-hemispheric difference due to the dominant contribution of NO_x emissions in the NH extratropical bands, which in turn increase the N_2O_5 and HNO_3 recycling (Fig. 1d). Following the larger SSA abundance within the *FCHIST_slh* setup (Fig. S1), the SAA-debromination source for this compset is larger than that for *FCnudged_slh*, although the corresponding bromine sinks for the former is also larger than for the latter, resulting in equivalent bromine tropospheric burdens (see Table 8). Further details on the contributions of individual emissions processes during present-day are provided in Section 3.2.

Figure 2 shows the inorganic halogen surface abundance during the 1980-2020 period for the *FCnudged_slh* and *FCHIST_slh* configurations. In order to compare the current CESM2-SLH inorganic halogen abundances with previous studies, Fig. 2 also shows the corresponding CESM1 *Serial_slh* and *Cyclical_slh* sensitivities corresponding to (Li et al., 2022) and (Saiz-Lopez et al., 2023), respectively. Despite not strictly identical, these CESM1 configurations were selected as they allow: *i)* to provide a quantitative visualization of the absolute abundances of each halogen family and their reactive to inorganic halogen ratios (XO_x/X_y, with XO_x = X + XO and X = Cl, Br and I); and *ii)* to show a qualitative comparison of the main atmospheric components driving the trends in the inorganic halogen budget within the different CESM versions. For example, given that the dominant halogen sources in the troposphere are computed online depending on the background concentration of O_3 and NO_2 (Figure 2d,f), the surface abundance of Cl_y, Br_y and I_y (Figure 2a-c) follows the temporal evolution of the former species within each model version. Here it is worth noting that driven by the different trend in surface ozone between CESM1 (cyan lines for *Serial_slh*) and CESM2 (blue for *FCHIST_slh* and pink for *FCnudged_slh*), surface I_y abundance for CESM2-SLH during the 1980-2020 period presents a larger increment than in CESM1, particularly after year 2000 (Fig. 2c), while I_y abundances in CESM1 remained approximately constant after year 2000 following the stable O_3 trend. A similar behaviour is also observed for Cl_y and Br_y, as their main sources depends mostly on the HNO_3 and N_2O_5 abundance as well as on the extent of partitioning of halogen reservoirs to $ClONO_2$ and $BrONO_2$, all of which increase for larger NO_x

https://doi.org/10.5194/egusphere-2025-3250
Preprint. Discussion started: 13 October 2025

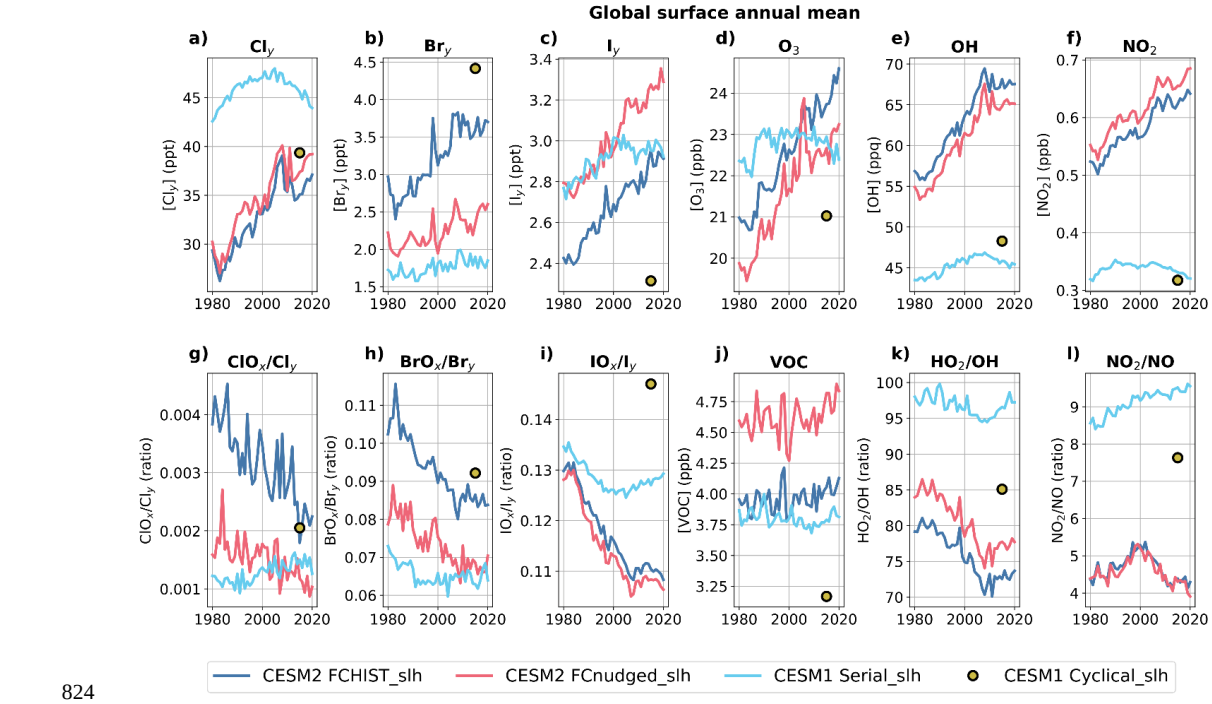

Figure 2: Historical evolution of global annual mean surface abundance and partitioning of main atmospheric components during 1980-2020. Top-row shows the total inorganic halogen surface abundance for a) Cl$_y$, b) Br$_y$ and c) I$_y$, as well as the surface mixing ratio for d) O$_3$, e) OH and f) NO$_2$. Panel j) shows the corresponding surface mixing ratio of major VOCs (sum of species: ISOP, MTERP, CH$_3$OH, C$_2$H$_5$OH, CH$_2$O, CH$_3$CHO, CH$_3$COOH, CH$_3$COCH$_3$, HCOOH, C$_2$H$_2$, C$_2$H$_4$, C$_2$H$_6$, C$_3$H$_8$, C$_3$H$_6$, BIGALK, BIGENE, MEK, TOLUENE, BENZENE, XYLENES). Bottom row shows the reactive (XOx) to reservoir (X$_y$) surface ratio (i.e., XO$_x$ / X$_y$) for g) chlorine, h) bromine and i) iodine, as well as the k) HO$_2$ / OH and l) NO$_2$ / NO mean ratio at the model surface. Results for the main *FCnudged_slh* (pink) and *FCHIST_slh* (blue) compsets obtained with the CESM2-SLH release are compared with those obtained in previous CESM1 studies: *Serial_slh* (cyan line) setup from (Li et al., 2022) **as well as *Cyclical_slh* (yellow circle) configuration from** (Saiz-Lopez et al., 2023)**.**

Figure 3 shows the tropospheric, stratospheric and total halogen burden across the 1980-2020 period resulting from the CESM2-SLH *FCnudged_slh* and *FCHIST_slh* (solid lines) configurations along with the corresponding *FCnudged_noh* and *FCHIST_noh* (dashed lines) sensitivities. Equivalent comparisons between the CESM1 *Serial_slh* and *Serial_noh* configurations are also shown. Several distinctive features are of major relevance to support the final CESM2-SLH configuration, as described below:

First, the temporal evolution of the stratospheric burden follows the expected trend with a maximum peak just before and after year 2000 for chlorine and bromine, respectively, which is in line with the temporal variation of the dominant long-lived ODSs that dominate the inorganic halogen burden in the stratosphere (WMO, 2018, 2022). In both cases, the increase in stratospheric Cl$_y$ and Br$_y$ burden due to SLH are equivalent between CESM1 and CESM2 configurations. For stratospheric iodine, all configurations show an equivalent stratospheric burden that remains constant with time (see Section 3.2.2). Reaching an equivalent stratospheric halogen enhancement for all configurations provides confidence that the modelled influence of SLH in the lower stratosphere within CESM2-SLH are in line with previous studies (see Section 3.3.4).

https://doi.org/10.5194/egusphere-2025-3250
Preprint. Discussion started: 13 October 2025

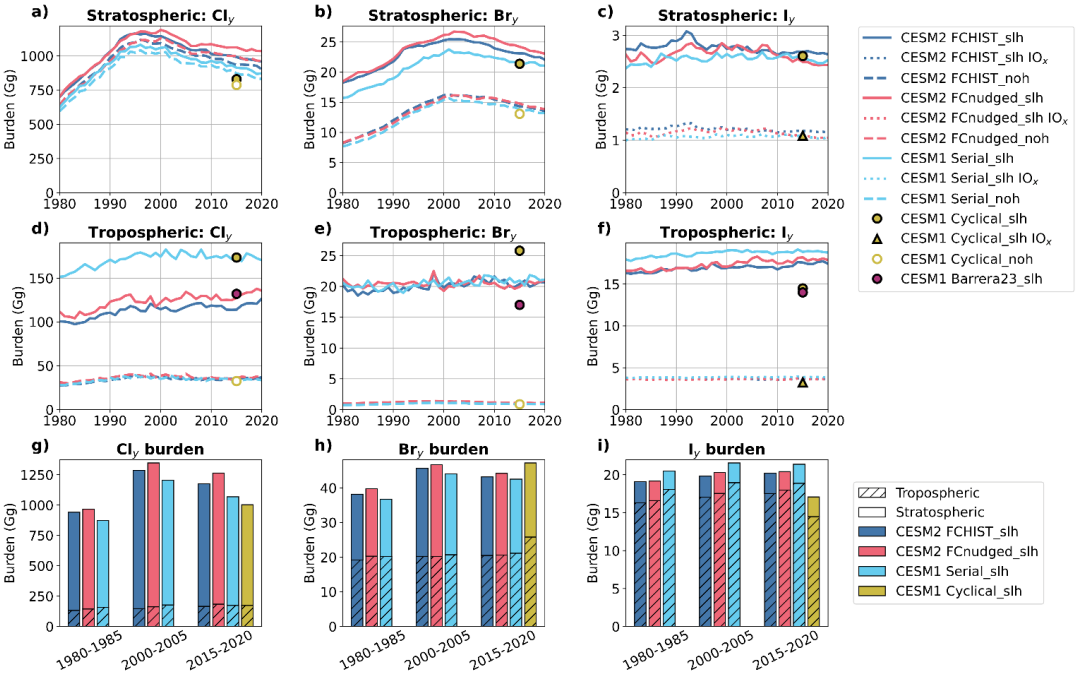

Figure 3: Historical evolution of global mean inorganic halogen burden during 1980-2020. Top-row shows the stratospheric burden for a) Cl_y, b) Br_y and c) I_y, while middle-row shows the corresponding tropospheric burden for d) Cl_y, e) Br_y and f) I_y for different model configurations including (*compset_slh*, solid lines) and neglecting (*compset_noh*, dashed lines) the contribution of SLH sources and chemistry. Note that as *compset_non* configurations do not consider iodine chemistry, panels c) and f) shows the reactive iodine fraction (IO_x = I + IO) for the *compset_slh* using dotted lines to avoid confusion with Iy. Results for the main *FCnudged_slh* (pink) and *FCHIST_slh* (blue) compsets obtained with the CESM2-SLH release are compared with those obtained in previous CESM1 studies: *Serial_slh* (cyan line) setup from (Li et al., 2022) **as well as *Cyclical_slh* configurations from** (Saiz-Lopez et al., 2023) **(yellow circle) and** (Barrera et al., 2023) **(red circle). IO_x results are shown with yellow triangles. Bottom-row shows the mean total inorganic halogen burden for the 1980-1985, 2000-2005 and 2015-2020 periods using stacked columns distinguishing the tropospheric (striped) and stratospheric (empty) contributions for g) chlorine, h) bromine and i) iodine.**

Second, although the global mean tropospheric halogen burden for *FCnudged_slh* and *FCHIST_slh* are not identical, the spread between the different CESM2-SLH compsets is smaller than that obtained with the different CESM1 configurations used in previous studies. Indeed, for the case of bromine, the tropospheric Br_y burden for both *FCnudged_slh* and *FCHIST_slh* compsets are equivalent to those obtained for the CESM1 *Serial_slh* setup, although they lie in between the CESM1 *Cyclical_slh* simulations from (Saiz-Lopez et al., 2023) and (Barrera et al., 2023). Here we note that the tropospheric Br_y burden of the former is larger as that setup considered the original sea-salt aerosol logical mask typically applied to the SSA-dehalogenation (Fernandez et al., 2014, 2021), while the later (*Barrera23_slh* in Fig. 3) imposed a latitudinal dependent sea-salt mask that resulted in significantly lower bromine recycling (Barrera et al., 2023), highlighting the large sensitivity of the SSA-dehalogenation source to the modelled changes in SSA abundance and distribution (see Fig. S1). Most notably, both CESM2-SLH *FCnudged_slh* and *FCHIST_slh* configurations now result in a global tropospheric Br_y burden that lies in between those obtained in previous CESM1 studies (Fig. 3e). In addition, the tropospheric Cl_y burden for any CESM2-SLH (2°×2°) setup is lower than in any of the CESM1 configurations, which ensures that in any case the impact of chlorine chemistry on tropospheric composition (e.g., the degradation of VOCs and CH_4 by Cl atoms) is, in any case, in the lower edge of previously published studies (Li et al., 2022; Bossolasco et al., 2025).

Third, it is worth highlighting that despite the tropospheric I_y trend for all timeline simulations follows the oceanic iodine flux increase due to the enhanced ozone levels between 1980 and 2020 (Fig. 2f), the overall stratospheric burden remains constant with time (Fig. 3c). This implies that most of the inorganic iodine enhancement occurring in the MBL and close to

https://doi.org/10.5194/egusphere-2025-3250
Preprint. Discussion started: 13 October 2025

the surface is washed out in the free troposphere before reaching the tropopause. The larger tropospheric I_y burden between current *FCHIST_slh* and *FCnudged_slh* compsets (17.2-17.7 Tg I) and the recent estimations from (Saiz-Lopez et al., 2023) and (Barrera et al., 2023) using CESM1 (14-14.5 Tg I) for present-day conditions are explained by the significant changes in reactive (IO_x) vs. reservoir iodine partitioning (IO_x / I_y) between CESM1 and CESM2. Despite the differences in I_y burdens, the tropospheric IO_x burden for all CESM1 and CESM2 configurations are equivalent (see dotted lines in Fig. 2f), and therefore the influence of iodine on atmospheric composition shown in Section 3.3.3 remains consistent with previous CESM1 studies.

3.2 SLH Abundance During Present-Day

Table 8 summarizes the global halogen sources, LBCs, tropospheric abundances and sinks during present-day for the *FCnudged_slh* and *FCHIST_slh* (2º×2º) compsets. These global-mean reference values should be taken as guideline for any other CESM2-SLH configuration and/or resolution considered. Equivalent results highlighting the main similarities and differences with respect to the remaining CESM2-SLH compsets are shown in Section 3.4.

The global annual emission flux for VSL halogens in both CESM2-SLH compsets during present-day is 65.3 Gg Cl yr^{-1}, 721.3 Gg Br yr^{-1}, and 599.7 Gg I yr^{-1}. Here, we recall that due to changes in transport and OH abundance within the MBL between CESM1 and CESM2 (see Section 2.2.1), we increased the flux strength of the original VSL inventory (Ordóñez et al., 2012) by 15% for all VSL bromo- and chloro-carbon but retained the magnitudes of iodo-carbon species, including mixed species (CH_2ICl, CH_2IBr). Thus, VSL iodine mean global emissions are the same between CESM1 and CESM2, while the Cl and Br emissions are ~14% and 6% larger in CESM2 compared to CESM1. The higher (lower) percentage change for bromine (chlorine) arises due to the minor CH_2IBr (predominant CH_2ICl) relative contribution of iodo-carbons to the total VSL bromocarbon (chlorocarbon) flux (Ordóñez et al., 2012). We highlight that the contribution of anthropogenic VSLs (1265.5 Gg Cl yr^{-1}) has also been increased by 15% and results in surface fluxes up to 20 times larger than the natural oceanic source from VSL chlorocarbons (65.3 Gg Cl yr^{-1}), in agreement with previous estimates (Villamayor et al., 2023). Here, it should be noted that the additional contribution from other anthropogenic VSL chlorocarbons ($CHCl_3$ and $C_2H_4Cl_2$) are also included at the model surface as LBCs instead of considering offline emissions, reaching a total of ~48 pptv at the model surface.

The largest variability among all online sources arises from the uptake and release of bromine and chlorine from sea-salt aerosol. In absolute terms, the global annual mean SSA-dehalogenation source for the *FCHIST_slh* compset is 877.3 Gg Cl yr^{-1} (26%) and 1616.7 Gg Br yr^{-1} (58%) larger than for the *FCnudged_slh* setup (see Table 8). This is explained by the large non-linear response of the heterogeneous recycling process implemented in Eq. (3) to the large variability in the parameterized fields of SAD_{SSA} (Fig. S1), as well as to the change in partitioning between inorganic halogen reservoirs (Fig. 7). Similarly, the chlorine source from the acid-displacement for the *FCnudged_slh* compsets is larger by ~1700 Gg Cl yr^{-1}, which in relative terms represents only ~8% variability but in absolute terms surpasses the total contribution from VSL chlorine sources. Despite the variability in modelled online sources, the estimated global fluxes are in line with previous estimations obtained with different models. For example, our present-day global chlorine source is equivalent to CESM1 (21.5 Gg Cl yr^{-1}) and around 4 times smaller than an equivalent implementation of acid displacement dehalogenation in the TOMCAT model (~90 Tg Cl yr^{-1}; (Hossaini et al., 2016) and between 1.5 and 3 times lower than the range of values estimated by (Graedel and Keene, 1995) (~37−73 Tg Cl yr^{-1}). For the case of bromine, which presents the largest variability between CESM2-SLH compsets, our global annual flux remains lower than the recent estimates obtained with GEOS-Chem when the reactivity of bromine with tropospheric aerosols is considered (3.5−6.4 Tg yr^{-1}) (Chen et al., 2018; Zhu et al., 2018), highlighting that in any case the influence of SLH chlorine and bromine in the troposphere represents a lower limit compared to other models.

Regardless of the large variability on the online computation of inorganic halogen sources, we highlight that CESM2-SLH considers a species-independent removal of inorganic halogens from the atmosphere, and consequently, the larger the

https://doi.org/10.5194/egusphere-2025-3250
Preprint. Discussion started: 13 October 2025

emission flux for any specific configuration, the larger the corresponding global sink. Indeed, inspection of Table 8 shows that absolute and percentage changes in both dry and wet deposition between *FCnudged_slh* and *FCHIST_slh* are of equivalent magnitude to their corresponding sources. Here, it should be noted that the surface dry deposition occurring only at the model surface accounts for almost half of the total halogen sink, representing ~45%, ~40% and ~50% for chlorine, bromine and iodine, respectively. For the case of wet deposition tendencies, the NEU scheme represents the largest individual sink for bromine and chlorine, while for iodine, the NEU scheme accounts only for approximately half of the total wet deposition, with a substantial contribution from the FRA removal of HOI in liquid clouds. In contrast, the FRA only represents a small fraction (< 5-7%) of the total bromine wet deposition compared to the NEU scheme, as only ice_uptake of $BrONO_2$ is considered to occur through FRA (see Section 2.4). Finally, it is worth noting that despite dry and wet deposition are computed for all individual species compiled in Table 4, the net sink of each halogen family is typically dominated by a single or a couple of species that dominates the halogen partitioning in different layers of the troposphere (e.g., HCl for chlorine, HOBr and HBr for bromine and HOI for iodine, see (Fernandez et al., 2014; Saiz-Lopez et al., 2014)).

Table 8 also quantifies the mean surface abundance and global tropospheric burdens for both organic VSL and inorganic SLH during present-day. Despite minor differences between the two compsets that in general remain below ~10%, the surface abundance and tropospheric burden for all halogen species are slightly larger for the *FCnudged_slh* configuration. The exception is surface Br_y, which is ~44% larger in *FCHIST_slh* due to its larger SSA-dehalogenation source. However, note that the tropospheric Br_y burden between both CESM2 configurations is almost identical (20.1 Gg Br for *FCnudged_slh* vs. 20.0 Gg Br for *FCHIST_slh*). Surface chlorine abundance is dominated by anthropogenic VSL reaching 135-139 pptv that largely surpass the contribution from oceanic VSL (less than 1 pptv), while surface inorganic Cl_y reaches approximately 40 pptv. The corresponding values for brominated compounds reach 7.8-8.4 pptv for VSL bromine and 2.5-3.6 pptv Br_y, while for the case of iodine global mean values are 1.1-1.2 pptv and 2.9-3.3 pptv, respectively. Here we highlight that for the particular case of inorganic chlorine and bromine, current results for *FCHIST_slh* and *FCnudged_slh* configurations in CESM2-SLH have been adjusted to achieve global annual surface values and tropospheric burdens that lie in between previous CESM1 studies (Li et al., 2022; Barrera et al., 2023; Saiz-Lopez et al., 2023). Regarding the partitioning between reactive and reservoir halogen species for the different compsets, our model results show that surface and tropospheric XO_x / X_y ratio for chlorine, bromine and iodine ranges between 0.2-1.5%, 6-12% and 10-20%, respectively, with general larger values for *FCHIST_slh* compared to *FCnudged_slh*.

In contrast to bromine and chlorine, surface I_y abundance in CESM2-SLH is ~25-40% higher compared to CESM1 (2.3 pptv I_y), which is mainly due to the different IO_x/I_y and OH/HO_2 ratios between CESM versions (see Fig. 2i,k): the larger OH abundance and lower HO_2/OH ratio in CESM2-SLH compared to CESM1 increases the contribution of HOI to the total I_y loading, and therefore, there is a major shift on the partitioning from reactive to reservoir species for iodine (see Table 8). Therefore, the reactive IO_x abundance between the different compsets remains similar compared to (Saiz-Lopez et al., 2023) and (Li et al., 2022) both at the surface as well as integrated in the whole troposphere. Indeed, Table 8 and Fig. 3 show that despite the large surface I_y differences, the IO_x burden change between CESM2 (3.5-3.6 Gg I) and CESM1 (3.2 Gg I) remains close to ~10%.

Finally, we highlight the different contributions of inorganic chlorine, bromine and iodine to the total (tropospheric + stratospheric) burden when SLH are considered (Fig. 3 bottom-row). We found that for present-day conditions, the contribution of tropospheric Cl_y, Br_y and I_y to the total halogen loading represents ~14%, ~47% and ~87%, respectively. This increasing contribution of tropospheric X_y content going from chlorine to bromine to iodine is in line with the enhanced efficiency/reactivity of each halogen species in reacting with tropospheric ozone ($X + O_3 \rightarrow XO + O_2$, see R2), and result in tropospheric iodine to be the dominant species affecting the tropospheric oxidative capacity and ozone abundance (see Section 3.3.2). Given the turnover in stratospheric halogen loading from anthropogenic ODSs around year 2000, we note that the percentage contributions change for the different time periods.

https://doi.org/10.5194/egusphere-2025-3250
Preprint. Discussion started: 13 October 2025

962

963 **Table 8: Quantitative values for global annual SLH burdens during present-day conditions**

Species		Chlorine		Bromine		Iodine	
Simulation		Fcnudged_slh	FCHIST_slh	Fcnudged_slh	FCHIST_slh	Fcnudged_slh	FCHIST_slh
Offline Sources							
Natural VSL	Surface (Gg yr^{-1})	65.3	65.3	721.3	721.3	599.7	599.7
Anthro VSL	Surface (Gg yr^{-1})	1265.5	1265.5	-	-	-	-
Anthro VSL (LBCs)	Surface (pptv)	48.1	48.1	-	-	-	-
Online Sources							
SSA-dehalogenation	Tropo (Gg yr^{-1})	3365.3	4242.6	2764.3	4381.1	-	-
HNO_3	Tropo (Gg yr^{-1})	20844.4	19257.8	-	-	-	-
N_2O_5	Tropo (Gg yr^{-1})	1235.0	1123.9	-	-	-	-
Oceanic Iodine	Surface (Gg yr^{-1})	-	-	-	-	2540.3	2387.6
Abundance							
Long-Lived Halogens	Surface	3139.9	3139.9	14.2	14.2	-	-
	Tropo	15970.3	15987.3	161.1	161.5	-	-
Short-Lived Halogens							
Natural VSL	Surface (pptv)	0.8	0.7	8.4	7.8	1.2	1.1
	Tropo (Gg)	2.5	2.4	55.1	53.8	4.8	4.7
Anthro VSL	Surface (pptv)	138.7	135.1	-	-	-	-
	Tropo (Gg)	574.2	571.8	-	-	-	-
Inorganic Halogens (X_y)	Surface (pptv)	41.0	38.7	2.5	3.6	3.3	2.9
	Tropo (Gg)	177.4	159.4	20.1	20.0	17.7	17.2
Reactive Halogens (XO_x)	Surface (pptv)	0.1	0.1	0.2	0.3	0.4	0.3
	Tropo (Gg)	2.1	2.9	2.1	2.4	3.5	3.6
Sinks							
Dry deposition	Surface (Gg yr^{-1})	14102.1	13066.9	1484.76	2168.33	1680.93	1483.13
Wet deposition (NEU)	Tropo (Gg yr^{-1})	16057.9	16481.4	1952.3	2808.8	836.711	941.331
Wet deposition (FRA)	Surface (Gg yr^{-1})	-	-	106.148	188.316	634.221	574.448

964
965

https://doi.org/10.5194/egusphere-2025-3250
Preprint. Discussion started: 13 October 2025

3.2.1 Latitudinal and Vertical Distribution of SLH

Figure 4 shows the zonal average latitudinal-height distribution of total organic long-lived (top row) and short-lived (bottom row) halogens for the *FCnudged_slh* configuration during present-day. Here it is evident that while long-lived halogenated ODSs remain unreactive throughout the troposphere and are converted to inorganic Cl_y and Br_y only after crossing the tropopause, VSL halocarbons photolyze at much lower heights in the atmosphere. Consequently, iodine VSL is nearly completely decomposed in the lower troposphere (Fig. 4f), whereas only a small fraction of the emitted VSL bromine and chlorine SGs is transported unaltered to the stratosphere (Fig. 4d,e). In contrast to the naturally emitted bromine and iodine VSLs, the modelled VSL chlorine abundances show a remarkable inter-hemispheric difference with larger values over the NH, due to its dominant anthropogenic sources (Fig. 4d).

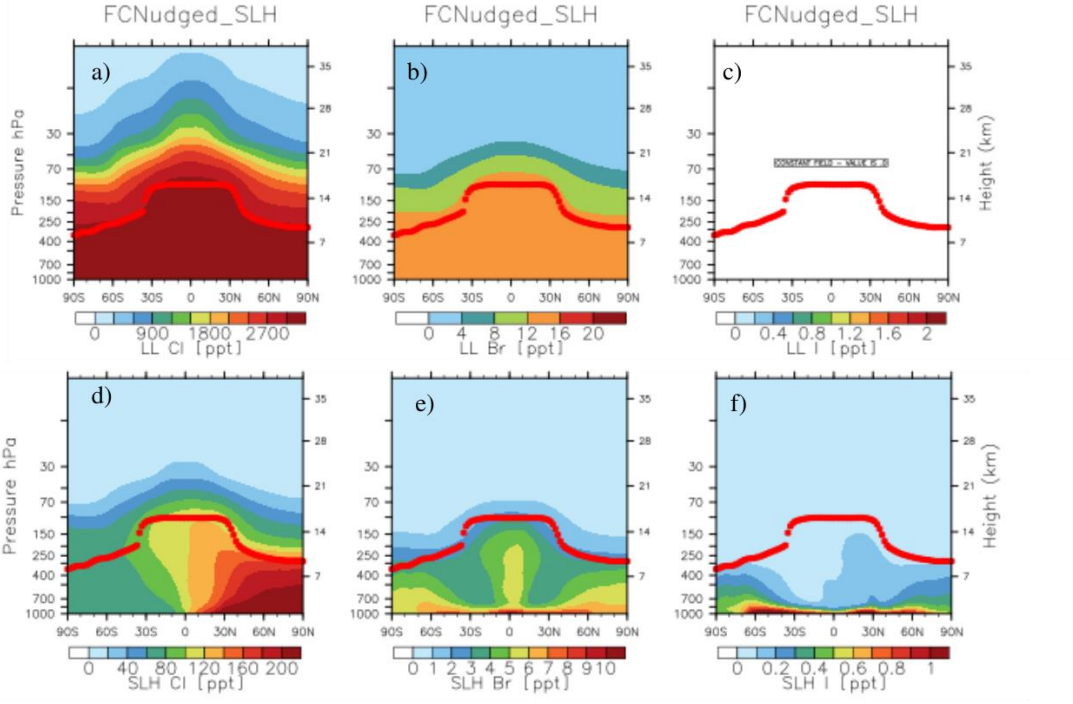

Figure 4: Zonal Average distribution of the organic (carbon bonded) halogen fraction during present-day (2015-2020) for the *FCnudged_slh* compset. Top row shows the long-lived (LL) distribution for a) chlorine (LL_{Cl}) and b) bromine (LL_{Br}). Note that CESM2-SLH does not include long-lived iodine species (empty panel c). Bottom row shows the very short-lived (VSL) distribution for d) chlorine (VSL_{Cl}), e) bromine (VSL_{Br}) and f) iodine (VSL_I). The red-dotted line shows the mean model tropopause.

In addition, Figure 5 shows the corresponding zonal average distribution of inorganic halogens (Cl_y, Br_y and I_y) from the model surface up to the middle stratosphere for the *FCnudged_slh* (top row) and *FCnudged_noh* (middle-row), as well as the difference between both configurations (bottom row). Note that the *FCnudged_slh* configuration does not consider any long-lived iodine source (Fig. 4c) while the *FCnudged_noh* configuration does not include iodine chemistry at all (Fig. 5f). Notably, not only the total X_y abundance at the model top, but also the conversion from organic SGs to inorganic halogen (PGs) shown in Figure 5 occurs at lower heights for the *FCnudged_slh* (top panels) than for the *FCnudged_noh* (bottom panels), following the different ODS and VSL photodecomposition shown in Fig. 4. Given the typically longer photochemical lifetimes of both long-lived chlorinated compounds compared to brominated halons (see for example Table A-1 in the Annex of (WMO, 2022) and elsewhere), the conversion from unreactive organic to reactive inorganic species occurs faster for bromine

https://doi.org/10.5194/egusphere-2025-3250
Preprint. Discussion started: 13 October 2025

than for chlorine, which results in a steeper gradient for the former in the lower stratosphere, and an almost complete conversion to inorganic bromine in the upper stratosphere (see also Fig. 6).

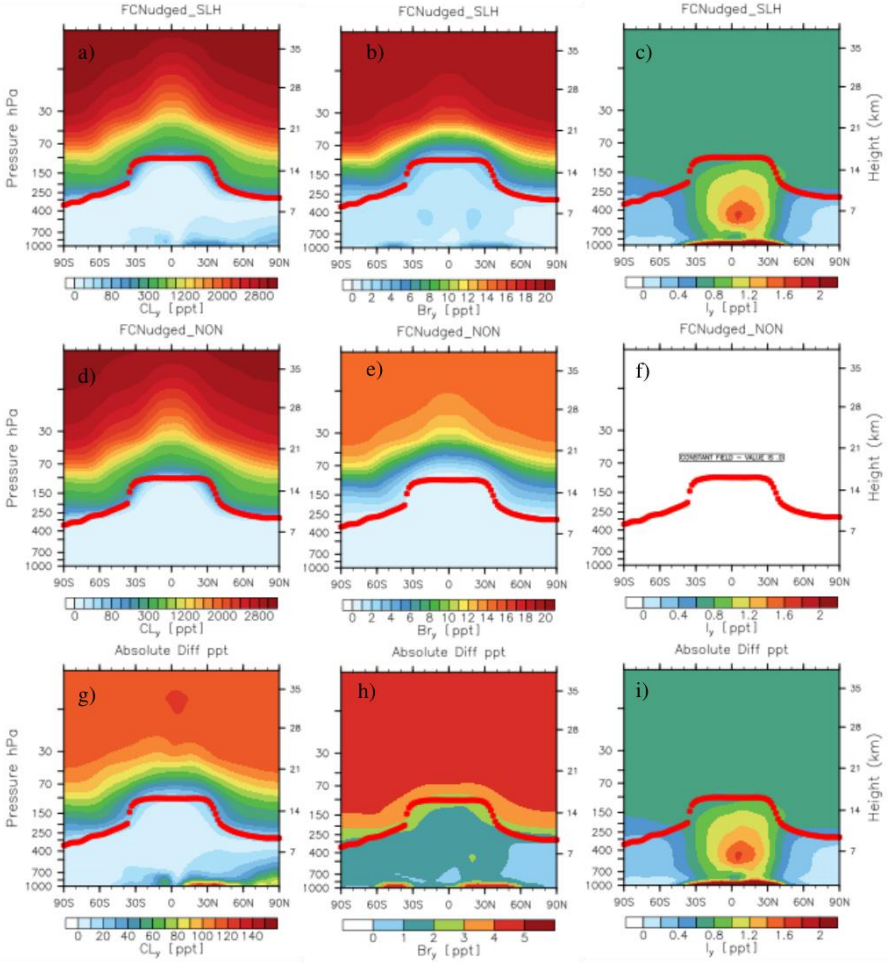

Figure 5: Zonal Average distribution of total inorganic halogen (X_y) during present-day (2015-2020) for different model configurations including (top-row; *FCnudged_slh*) and neglecting (middle-row; *FCnudged_noh*) the contribution of SLH sources and chemistry. The bottom-row show the absolute difference between both compsets (*FCnudged_slh* − *FCnudged_noh*). Left column (a, d, g) show the distribution for chlorine (Cl_y), while the middle (b, e, h) and right (c, f, i) columns show the distribution of bromine (Br_y) and iodine (I_y), respectively. The red-dotted line shows the mean model tropopause.

The change in inorganic halogen abundance X_y due to SLH (Figure 5, bottom panels) highlights the different behaviour for each individual halogen family in different regions of the atmosphere. For example, within the troposphere, both Cl_y and Br_y show a pronounced enhancement in the MBL and close to the surface mostly in the NH mid-latitude regions that is rapidly reduced in the free-troposphere, which is driven by the efficient SSA-dehalogenation source and acid displacement that presents a sharp vertical profile (see Fig. 7). For the case of iodine, the largest abundances at the surface are driven by the strong I_2/HOI emission occurring in the tropical regions (Fig. 1f). In this region, up to 1 pptv of I_y is transported to the tropical free troposphere where, due the local changes in ozone abundance and temperature, a pronounced partitioning shift lead to the formation of the tropical rings of atomic halogens (Saiz-Lopez and Fernandez, 2016). A fraction of this tropospheric inorganic iodine is washed out below the tropopause, and the remaining fraction is injected to the stratosphere as inorganic PGs

https://doi.org/10.5194/egusphere-2025-3250
Preprint. Discussion started: 13 October 2025

throughout tropical injection with an almost negligible contribution from VSL SGs (see Section 3.2.2). In contrast, Fig. 5g shows a gradual enhancement in Cl_y occurs in the middle stratosphere, which arises due to the longer photochemical lifetime of chlorinated VSLs which are mostly transported unaltered to the lower stratosphere (Fig. 4a). For bromine, Fig. 4e and Fig. 5h highlights that both organic VSL SGs and inorganic Br_y PGs contribute to the total stratospheric bromine loading due to SLH.

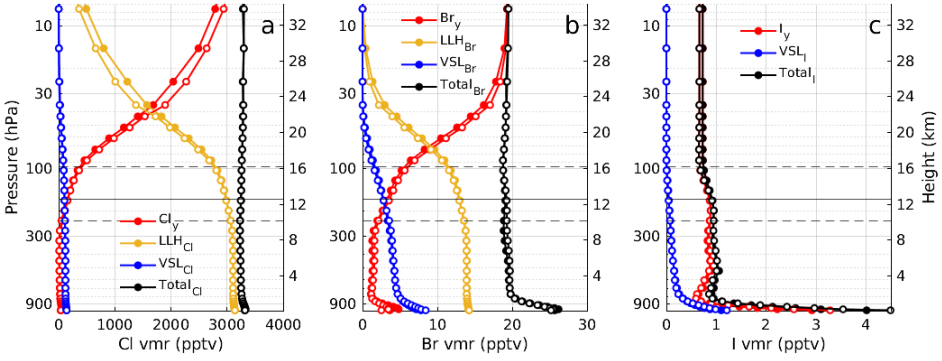

Figure 6: Global mean vertical profile of organic and inorganic halogens during present-day (2015-2020) for a) chlorine, b) bromine and c) iodine. Each coloured line shows individual contributions from organic long-lived (LLH_X, yellow) and very short-lived (VSL_X, blue) halogens, as well as for the total inorganic halogen fraction (X_y, red) for the *FCnudged_slh* (empty symbols) and *FCHIST_slh* (filled symbols) compsets. The total sum of all three contributions for each individual halogen species (X = Cl, Br, I) is shown in black. The solid and dashed horizontal line shows the mean height ± standard deviation of the global tropopause.

Figure 6 summarizes the global mean (90ºN – 90ºS) vertical profiles of the sum of all organic and inorganic halogen species from the surface to the middle stratosphere for the *FCnudged_slh* and *FCHIST_slh* configurations. The figure distinguishes the contributions from long-lived chlorine and bromine species, as well as the total halogen fraction transported as VSL SGs and inorganic PGs, consistent with the separate depictions presented in Figures 4 and 5. The conversion of unreactive organic SGs to reactive PGs is found to be very similar between the two model compsets. However, minor differences, primarily within the MBL and the Upper Troposphere/Lower Stratosphere (UTLS), appear due to the differing meteorological representations (free-running vs. nudged dynamics) between the *FCHIST_slh* and *FCnudged_slh*. Three main differences characterize the vertical distribution between unreactive organic and reactive inorganic species for each halogen family. First, the tropospheric chlorine abundance is dominated by long-lived species, with minor contributions from VSL chlorine and Cl_y. Due to the long lifetimes of CFCs and CH_3Cl, the crossing point between LLH_{Cl} and Cl_y representing the photochemical conversion from the organic to the inorganic fractions occurs in the middle stratosphere (~40 hPa). Second, the VSL bromine contribution is comparable (although smaller) to the contribution from long-lived halons and CH_3Br, and therefore the initial enhancement in Br_y abundance, as well as the crossing point with LLH_{Br}, occurs at lower heights in the stratosphere (~75 hPa). Third, given that there are no long-lived iodine species and the short photochemical lifetimes of VSL_I (particularly CH_3I), both the tropospheric and stratospheric abundance is dominated by inorganic I_y. This is in line with the tropospheric and stratospheric mean burdens shown in the stacked bars of Fig. 3g-i.

https://doi.org/10.5194/egusphere-2025-3250
Preprint. Discussion started: 13 October 2025

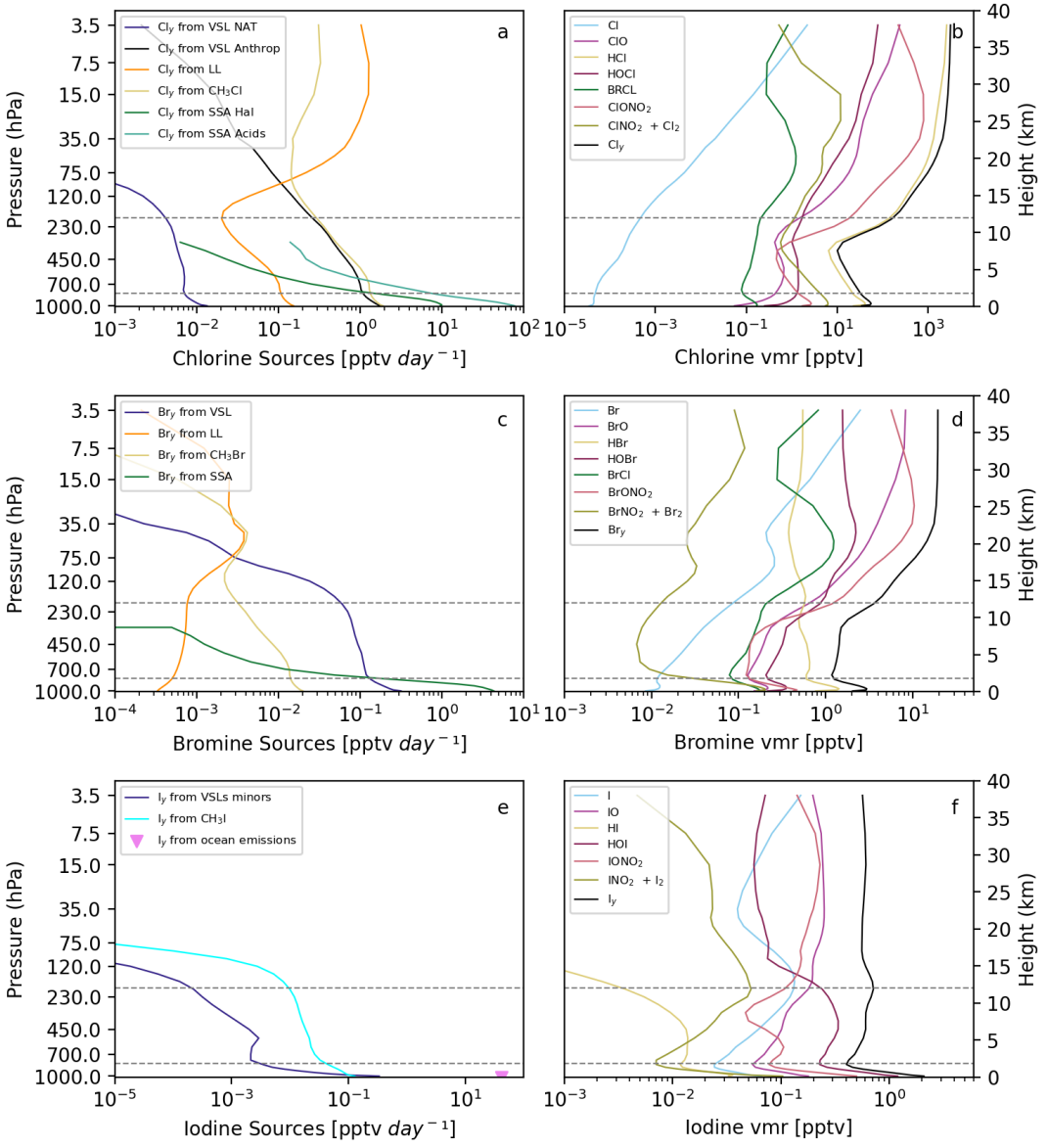

Figure 7: Global mean vertical profile of inorganic halogen release from different types of sources (left column) and the corresponding abundance for the different species conforming each halogen family (right column) during present-day (2015-2020). Individual panel show results for (a, b) chlorine, (c, d) bromine and (e, f) iodine for the *FCnudged_slh* configuration. The halogen atom release arising from the photochemical (Oh + hv) degradation of organic very short-lived (VSL, blue) and long-lived (LLH, yellow) halogens, including the independent contribution from CH_3Cl and CH_3Br (orange) are distinguished on the left panels. The vertically-resolved inorganic halogen source arising from SSA-dehalogenation and acid-displacement processes is shown in green, while the surface oceanic iodine emission is indicated by a pink triangle. Right panels show the contribution of each individual halogen species to the total inorganic halogen loading (X_y, black), where red and blue lines highlight the abundance of the dominant reactive halogen species (X and XO) for each family (X = Cl, Br, I). The dashed lines shows the global mean height of the global boundary layer and the tropopause.

Given that the atmospheric impact of SLH over different atmospheric components depend on the overall abundance of reactive halogens, whose initial step is the release of a halogen atom Cl, Br and I through reactions R1a,b, left panels in Figure 7 shows the halogen atom release from the different organic and inorganic sources as a function of height. Here note

https://doi.org/10.5194/egusphere-2025-3250
Preprint. Discussion started: 13 October 2025

that only emissions or processes that lead to net inorganic halogen production are considered. In addition, right panels in Figure 7 show the chemical partitioning between all halogen species constituting each inorganic halogen family (X_y) which interconvert between one and the other following gas-phase and heterogeneous phase reactions involving other atmospheric components such as O_3, OH and NO_2 (see summarized R1-R13 scheme in Section 1 and Tables S1-S3 in the Supplementary Material).

As summarized in Table 8, SSA-dehalogenation is the dominant source of bromine and the second largest source for chlorine. However, Figure 7c highlights that these sources are primarily confined to the MBL. For chlorine, the contribution of the acid-displacement HCl release dominates, particularly in the NH mid-latitudes and coastal locations. Above the boundary layer, the photochemical degradation of both VSL_{Cl} and VSL_{Br} dominates the release of Br and Cl atoms throughout the free troposphere, although a particular difference becomes evident: the biogenic ocean flux is the sole source of bromine, while for the case of chlorine the contribution from anthropogenic VSL_{Cl} sources are at least two orders of magnitude larger than the natural oceanic source. In addition, the release of Cl atoms from long-lived CH_3Cl accounts for an equivalent source as that arising from anthropogenic VSL_{Cl} even below the tropopause (Fig. 7a). In contrast, bromine release from long-lived CH_3Br only surpass that arising from VSL_{Br} in the lower stratosphere (Fig. 7c). For iodine, ocean HOI/I_2 release dominates the surface emissions, while the photochemical degradation of CH_3I alone controls the organic to inorganic iodine conversion throughout the free troposphere.

Figure 7b shows that the dominant inorganic chlorine species throughout the troposphere is HCl, which represents between 63% and 85% of the total Cl_y partitioning. The Cl atom and ClO partitioning are generally 4 and 1-2 orders of magnitude smaller than the global mean Cl_y, respectively, although due to rapid heterogeneous recycling their contributions on the regional scale can increase, particularly in coastal locations (see Fig. 10). For bromine (Fig. 7d), the dominant species in the lower troposphere is HBr both during day and night (Fernandez et al., 2014). However, as it is transported to the upper troposphere and reacts heterogeneously on tropospheric ice-crystals (see Table 2), HBr is converted at first to HOBr and finally to the dominant $BrONO_2$ fraction in the lower stratosphere. The vertical profile of iodine partitioning in Fig. 7f shows that HOI is the dominant iodine species throughout the troposphere and therefore its washout controls the transport and abundance of inorganic iodine from their dominant surface sources to the stratosphere. It should be noted that the chemical partitioning from reservoir to reactive halogen species is the largest for iodine, followed by bromine and last by chlorine (i.e., IO_x/I_y > BrO_x/Br_y > ClO_x/Cl_y). This is associated with the much faster photochemistry of iodine compared to bromine and, to a larger extent, chlorine, which in turn controls the efficiency of each halogen family in altering the composition and oxidative capacity of the troposphere (see Section 3.3.2).

3.2.2 Validation of SLH Abundance with Observations

This section presents a general validation of the model performance by comparing CESM2-SLH results with observations. In doing so, we highlight that all SLH developments were implemented over the well validated CESM2 chemistry-climate model that has been widely used for climate projections and air-quality studies (Danabasoglu et al., 2020; Emmons et al., 2020; Jo et al., 2023; Tilmes et al., 2023), and consequently we do not evaluate all aspects of the model's chemistry and dynamics. For this exercise, we perform standardized evaluations against mean SLH observations and distributions compiled in international assessments.

Several studies highlight the importance of properly distinguishing between the contribution of Source Gas Injection (SGI) and Product Gas Injection (PGI) to the stratosphere when representing the contribution of SLH to stratospheric ozone depletion (Fernandez et al., 2014, 2021; WMO, 2018, 2022). This is mainly because the ozone destruction efficiency of SLH in the lowermost stratosphere depends on the net fraction of the emitted VSLs that has already been converted to the reactive inorganic form (Fernandez et al., 2021). In order to quantify the total contribution of SLH to the net SGI + PGI of each halogen

https://doi.org/10.5194/egusphere-2025-3250
Preprint. Discussion started: 13 October 2025

species during stratospheric injection, we computed the tropical mean (20ºN – 20ºS) vertical profiles of all VSL source gases (VSL_X) as well as the change in inorganic halogen product gases (ΔX_y) from the Earth's surface to the stratosphere (Fig. 8). Here, the ΔCl_y, ΔBr_y and ΔI_y profiles are computed as the difference between the *FCnudged_slh* − *FCnudged_noh* as well as for the *FCHIST_slh* − *FCHIST_noh* configurations. Therefore, they only account for the additional contribution of SLH to the total inorganic halogen loading at any given height, without considering the small (but not negligible) contribution from long-lived chlorine and bromine photodecomposition close to the tropopause (see Figs. 4d,e and 7a,c). In addition, Fig. 8 shows the sum of SG + PG for each halogen family (i.e., $VSL_{Cl}+\Delta Cl_y$, $VSL_{Br}+\Delta Br_y$ and $VSL_I+\Delta I_y$) accounting for the total additional chlorine, bromine and iodine due to SLH transported from the model surface to the stratosphere. Given that for bromine the contribution of SGs and PGs are of similar magnitude, we first provide a brief description of the individual VSL_{Br} and ΔBr_y vertical profiles, and then describe the more extreme contributions for chlorine and iodine below.

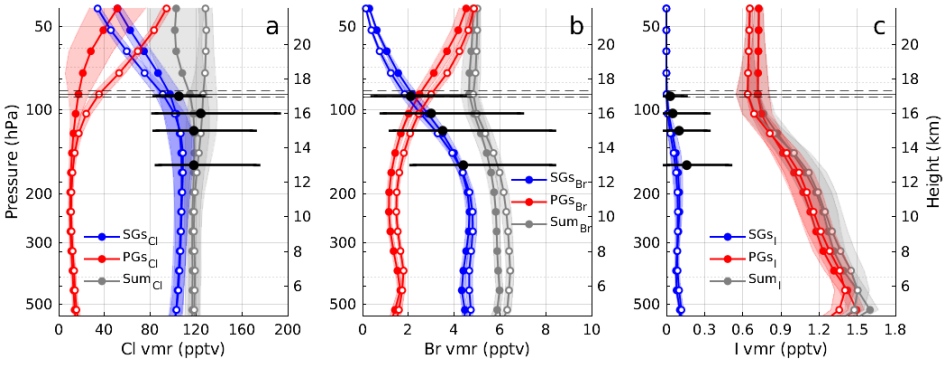

Figure 8: Tropical vertical profile of organic very short-lived (VSL_X) source gases (SGs) and change in inorganic halogens (ΔX_y) product gases (PGs) during present-day (2015-2020) for a) chlorine, b) bromine and c) iodine. The VSL_{Cl}, VSL_{Br} and VSL_I vertical profile (blue lines) correspond to the *FCnudged_slh* (empty symbols) and *FCHIST_slh* (filled symbols) compsets, while ΔX_{Cl}, ΔX_{Br}, and ΔX_I (red lines) show the corresponding difference with respect to the configuration neglecting SLH sources and chemistry (i.e., *compset_slh – compset_noh*). The total additional halogen abundance due to SLH (SGs + PGs)$_X$ is shown in grey (Sum_x). The tropical (20°N – 20°S) mean ± range (computed as the standard deviation for the 2015-2020 period) is shown by the solid-symbol lines and coloured shading, respectively. The observed mean ± range mole fractions within the tropical tropopause layer compiled in Table 1-5 of (WMO, 2022) **are shown by black symbols and solid-thick horizontal lines at 13, 15, 16 and 17 km, respectively. The solid and dashed horizontal line shows the mean height ± standard deviation of the tropical tropopause.**

Based on a mean modelled tropical tropopause at approximately 85 hPa (17 km), we found that the modelled CESM2-SLH contribution of SGI and PGI to the total bromine injection reaches 1.8-2.2 pptv + 2.5-3.0 = 4.3-5.2 pptv during present-day, where the modelled range indicate the variability between compsets. Notably, both *FCHIST_slh* and *FCnudged_slh* configurations simulate SGs values that are within the accepted range reported in the last Ozone Assessment Report (WMO, 2022) throughout the tropical troposphere. Indeed, our model results show a continuous conversion from SGs into PGs just below the tropopause that results in a larger fraction of inorganic bromine (PGI) compared to the organic halocarbon fraction (SGI). We highlight that once all organic VSL_{Br} has been converted to reactive Br_y, the total contribution of SLH to the stratospheric bromine loading remains at ~5 pptv roughly from the tropopause to the model top (grey line in Fig. 8b). Finally, note that the dominant contribution of VSLs to the total SGI arises from the major CH_2Br_2 and $CHBr_3$ emissions, with minor contributions from the remaining VSL bromocarbons (Fernandez et al., 2014). In contrast, CH_2IBr emissions, which constitute the largest source of bromine mass to the atmosphere (Ordóñez et al., 2012), barely contributes with a negligible fraction to the stratospheric SGI due to its particularly short lifetime.

Differing to bromine and due to the larger lifetime of chlorinated VSLs, the contribution to the total chlorine injection (114-126 pptv) arising from SGI (91-97 pptv) is notably larger than that from PGI (17-35 pptv), in agreement with reported

https://doi.org/10.5194/egusphere-2025-3250
Preprint. Discussion started: 13 October 2025

ranges (WMO, 2022). Here note that due to the large anthropogenic contribution from developed regions over US, Europe and Asia (Hossaini et al., 2019; Claxton et al., 2020), the VSL_{Cl} distribution for the Northern and Southern mid-latitudes shown in Fig. 4 shows a clear hemispheric asymmetry just below the tropopause. This asymmetry on VSL distributions have already been described in the literature for chlorine (Roozitalab et al., 2024) as well as bromine (Keber et al., 2020; Jesswein et al., 2022), although note that anthropogenic VSL_{Br} sources are not considered in this work (see Section 2.2.2). For the case of iodine, we highlight that due to the faster photochemistry compared to chlorine and bromine, almost the complete injection occurs through PGI = I_y (Fig. 8c), with a total injection of approximately 0.65-0.72 pptv, in agreement with observations and previous estimations using CESM1 (Saiz-Lopez et al., 2015; Koenig et al., 2020).

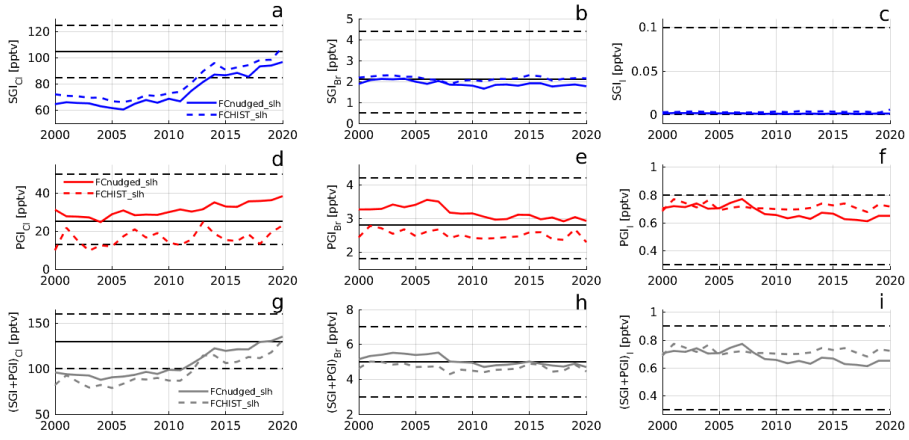

Figure 9: Temporal evolution of source gas injection (SGI_X, top-row), product gas injection (PGI_X, middle-row) and total SLH injection (SGI_X + PGI_X. bottom-row) between year 2000 and 2020 for the *FCnudged_slh* (solid lines) and *FCHIST_slh* (dashed lines) compsets. Individual results for (a, d, g) chlorine, (b, e, h) bromine and (c, f, i) iodine are shown on the left, center and right columns, respectively. Stratospheric injection values have been computed as the sum of the halogen mixing ratio of all species at the model tropical tropopause, considering the *compset_slh* output for organic VSL SGI_X and the difference between *compset_slh* – *compset_noh* for PGI_X (see text for details). The best estimation of the SLH contribution to the total halogen stratospheric injection for each individual family compiled in Table 1-6 of (WMO, 2022) **is shown by the horizontal solid and dashed lines on each panel. Note the intermediate species $COCl_2$, $CHCl_2O_2$ and COFCl (see Fig. S3) has been considered to contribute to PGI_{Cl} following** (WMO, 2022)**.**

Figure 9 shows the temporal evolution of SGI = VSL_X and PGI = ΔX_y occurring at the model tropical tropopause for chlorine, bromine and iodine for the *FCnudged_slh* and *FCHIST_slh* compsets, where the modelled values are compared with the latest assessed values of SLH injection to the stratosphere (i.e., see Table 1-6 in (WMO, 2022)), which are assumed constant along the recent past. Most notably, the contribution of SLH to PGI for all three halogens does not show a significant trend and lies within the range of WMO-estimated values throughout the entire modelling period. For the particular case of bromine and chlorine, note that the *FCnudged_slh* results show slightly larger values than the *FCHIST_slh* compset, which are coherent with the changes in the representation of convective transport within the tropics and the nudging to observed trends in the Brewer-Dobson circulation. Regarding SGI_{Cl}, note that model simulations before 2010 show a negative bias in comparison with the observational mean within the tropics, presenting an increasing trend after 2010 which is in agreement with previous reports (Hossaini et al., 2019; WMO, 2022). Here we recall that in CESM2-SLH we applied a 15% enhancement to the natural oceanic bromine source as well as to the anthropogenic chlorine emissions in comparison to CESM1 (see Section 2.2.2). Based on Fig. 9a, we recognize that current CESM2-SLH configuration lies at the low edge of the estimated VSL_{Cl} contribution, and therefore the original emissions and LBCs for anthropogenic chlorinated halocarbons from (Hossaini et al., 2019; Claxton et al., 2020) could be increased by a factor larger than 15% to reproduce previous stratospheric chlorine SGI results with CESM1 and other models (Li et al., 2022; Saiz-Lopez et al., 2023; Hossaini et al., 2024). Having said this, we acknowledge that the

https://doi.org/10.5194/egusphere-2025-3250
Preprint. Discussion started: 13 October 2025

model underestimation of SGI_{Cl} to the stratosphere should not represent a significant bias in our model implications on other atmospheric components. This is because chlorine influence on stratospheric ozone is dominated by long-lived CFCs and HCFCs, while in the troposphere VSL_{Cl} photodegradation represent only a minor contribution to atomic Cl release, which is largely dominated by the acid-displacement online sources (see Fig. 7 and Section 3.1). In quantitative terms, we highlight that for bromine, SLH contributes to a significant enhancement on present-day stratospheric halogen loading which represents approximately 25-26% in all the different configurations, while for chlorine, given the larger contributions of CFCs and HCFCs to the total stratospheric chlorine loading, the contribution of SLH represents only an increase 3.7-3.8%, in agreement with the latest estimation from (WMO, 2022). Finally, the iodine SGI contribution is almost zero and all the iodine injection to the stratosphere occurs as PGI (Fig. 9c).

3.2.3 Geographical Heterogeneity and Seasonality of SLH

To highlight the geographical heterogeneity of SLH abundances, Figure 10 shows the spatial distribution of carbon-bonded VSLs (top row), total inorganic halogens (middle-row) and the most relevant reactive fraction (bottom-row) of each halogen family over the boundary layer (i.e., mean modelled value from the surface up to ~850 hPa). Note that depending on the halogen family considered, the bottom row presents the most relevant reactive species for each family; namely Cl atom for chlorine, BrO for bromine and the sum of I + IO = IO_x for iodine. Several distinctive features are observed for each individual family as detailed below:

Chlorine: Figure 10a shows a pronounced North-South latitudinal gradient for VSL_{Cl} between 250 and 200 pptv, driven by the major anthropogenic emissions arising from the NH, particularly over China where maximum values exceed 500 pptv. The inorganic Cl_y abundance also maximizes over the NH, with hot-spots over coastal oceanic and continental locations where the mixing of SSA-halogen rich and enriched-nitrogen plumes (with high levels of HNO_3 and N_2O_5) results in an enhanced acid-displacement source (see section 2.2.3). Maximum Cl atom values are found over the coastal regions of Europe, US and East Asia, with maximum values smaller than 0.4×10^{-3} pptv and a global mean average of 4×10^{-5} pptv, which are consistent with maximum and mean Cl_y levels of ~640 pptv and ~47 pptv, respectively.

Bromine: This species presents a more homogeneous VSL_{Br} distribution with the largest abundances found over the equatorial regions due to the dominant oceanic sources arising from the tropical oceans (Ordóñez et al., 2012). Minimum, maximum and mean global VSL_{Br} mixing ratios reach 2.9 pptv, 12.9 pptv and 6.8 pptv, respectively. In line with chlorine, modelled Br_y also maximizes over coastal regions co-located with high SSA abundance (Fig. S1). However, the inter-hemispheric bromine enhancement is less pronounced than for chlorine because SSA-debromination does not directly depend on HNO_3 and N_2O_5 abundance, but rather on the partitioning shift of Br_y to $BrONO_2$, $BrNO_2$ and HOBr. Indeed, despite maximum Br_y peaks in the NH are up to 2 times larger than in the SH, the corresponding maximum BrO abundances are of equivalent magnitude (between 1.1 and 1.2 pptv, respectively) compared to the NH, highlighting the strong dependence of halogen partitioning on the background atmospheric composition of NO_x and HO_x.

Iodine: Despite high local emissions of CH_3I, primarily from rice paddies over east Asia (Fig. 10c; see (Ordóñez et al., 2012)), the main near-surface VSL_I and I_y distributions depends on HOI/I_2 oceanic emissions that peak within the tropics. The mean modelled I_y and I+IO values reach ~1.25 pptv and ~0.15 pptv, respectively, with corresponding (minimum – maximum) mixing ratios ranging between (0.05 - 21) pptv and (0.008 - 0.90) pptv over the boundary layer. Notably, the mean IO_x / I_y partitioning for the global mean average reaches ~0.12, while at locations with the highest values of I_y, the IO_x / I_y ratio remains below ~0.04.

https://doi.org/10.5194/egusphere-2025-3250
Preprint. Discussion started: 13 October 2025

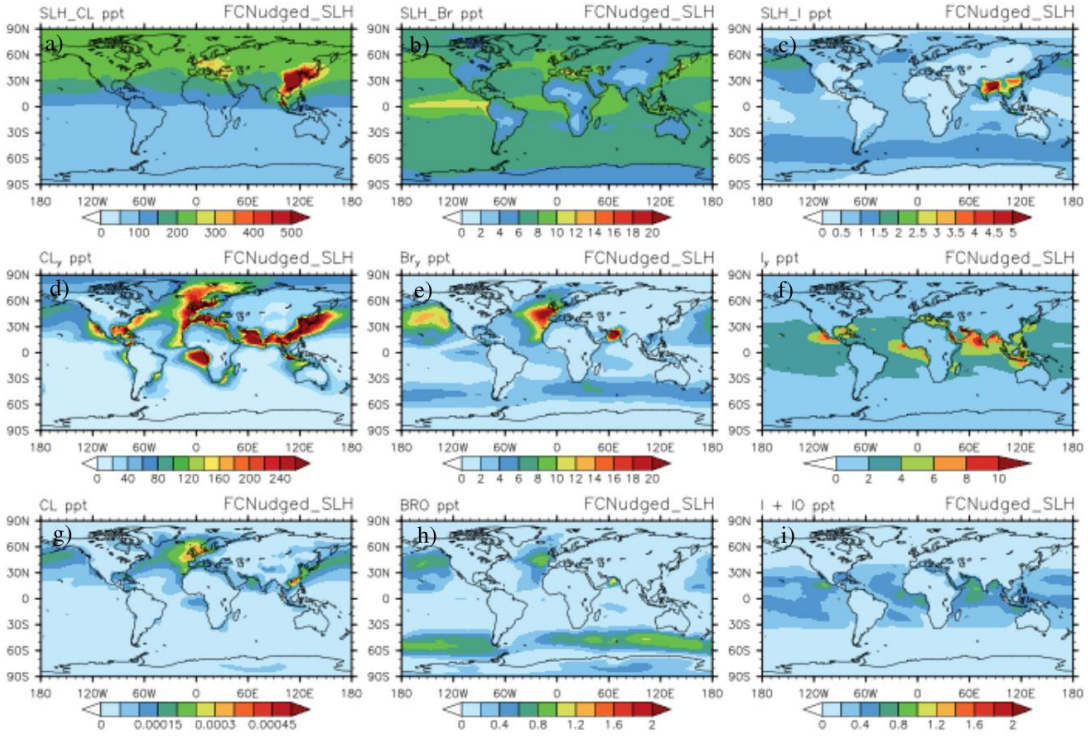

Figure 10: Annual mean geographical distribution of organic and inorganic halogens during present-day (2015-2020) for the *FCnudged_slh* compset. Top row shows the very short-lived (VSL) distribution for a) chlorine (VSL_{Cl}), b) bromine (VSL_{Br}) and c) iodine (VSL_I), while middle-row show the distribution of the total inorganic halogen content for d) chlorine (Cl_y), e) bromine (Br_y) and f) iodine (I_y). The bottom-row show the corresponding distribution for the most important reactive halogen species for each family: g) Cl atom, h) bromine monoxide (BrO) and i) reactive iodine (IOx = I + IO). All magnitudes have been averaged within the boundary layer (from the model surface up to ~850 hPa).

Figure 11 presents the seasonal variation of surface organic and inorganic halogen species averaged within different latitudinal bands. To highlight the distinctive behaviour between the northern (NH) and southern (SH) hemispheres, we distinguish between the tropics (20ºN-20ºS), and the extratropical domains in the NH (20ºN-90ºN) and the SH (20ºS-90ºS). The stacked bars shown in Fig. 11 represent the total halogen abundance decomposed into the reactive (XO_x), reservoir (X_y) and organic (VSL_X) species for each of the the *FCnudged_slh* and *FCHIST_slh* compsets. The corresponding zonal average seasonality of VSL_X halocarbons, as well as the geographical X_y seasonal cycle over the boundary layer are shown in Figures S4 and S5, respectively. We first describe the seasonality in the NH extratropics and then highlight the main similarities and differences with the SH extratropics and the tropical mean.

The NH extratropical Cl_y presents a pronounced seasonal cycle with approximately doubled values during the boreal winter (~90-100 pptv) compared to the summertime (~45-50 pptv). This is coherent with the seasonal variation of the heterogeneous recycling efficiency that reduces the conversion of both chlorinated (e.g., $ClONO_2$) and nitrogen (e.g., N_2O_5 and HNO_3) reservoirs to more reactive species. For the same reason, the organic VSL_{Cl} and VSL_{Br} abundances also peak during the winter when the photochemical decomposition is smallest (see Fig. S4). In contrast, the iodine seasonal cycle shows maximum abundances during the summertime, both for I_y and VSL_I. This is explained by the dominant contribution of oceanic sources for iodine, which increase associated with the largest fraction of ice-free ocean in winter and the enhanced tropospheric ozone levels in winter promoting deposition over the ocean. The inorganic Br_y abundance is lower and maximizes during the spring for *FCnudged_slh* in comparison with *FCHIST_slh*, which shows larger values and a maximum peak during the

https://doi.org/10.5194/egusphere-2025-3250
Preprint. Discussion started: 13 October 2025

summer, due to the larger efficiency of SSA-dehalogenation recycling in *FCHIST_slh*. Here we recall that sea-ice polar halogen emissions are not yet considered in CESM2-SLH, and therefore, the modelled seasonal cycle observed for the different halogen species differs from those described in the NH high- and mid-latitudes as well as near Antarctica in previous work (Fernandez et al., 2019, 2024).

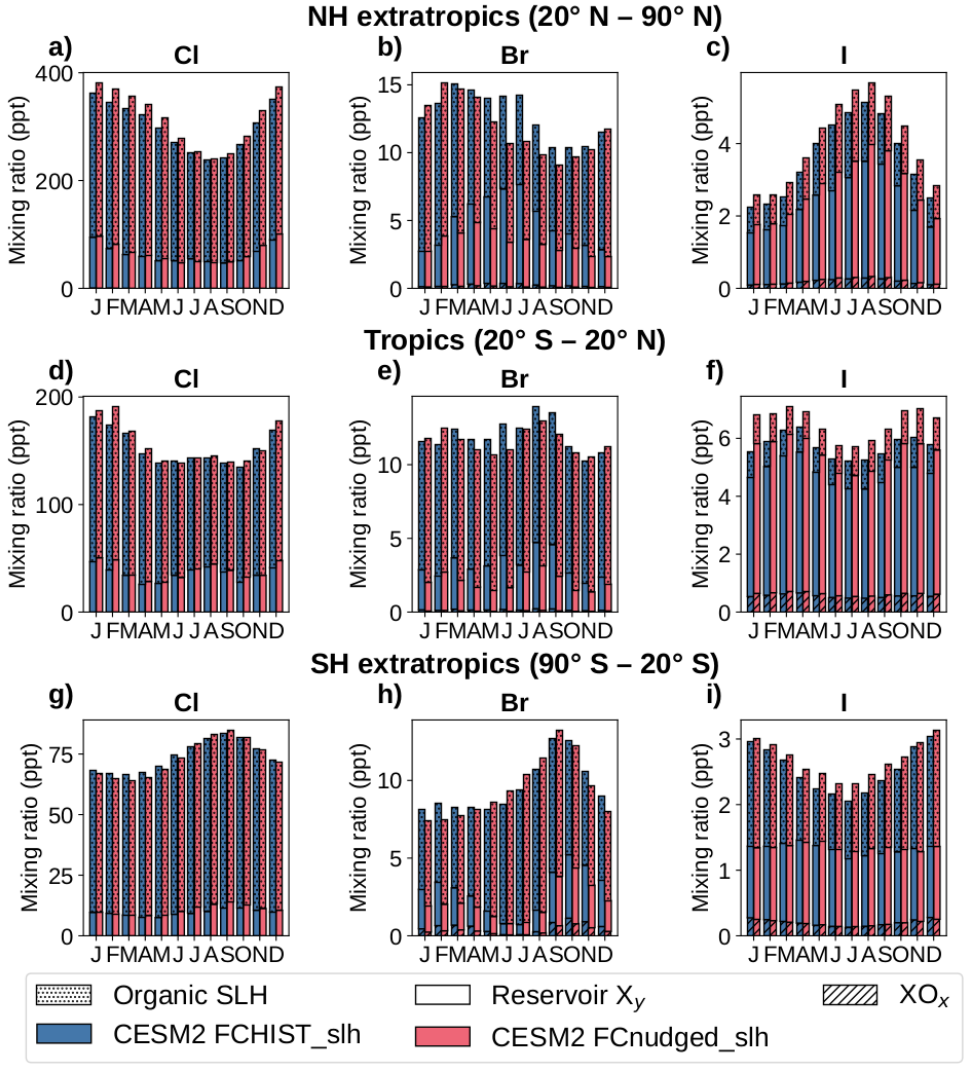

Figure 11: Seasonal distribution of total SLH abundance during present-day (2015-2020) for (left column) chlorine, (center column) bromine, and (right column) iodine. Model results for the Northern Hemisphere (NH = 20°N - 90°N) and Southern Hemisphere (SH = 20°S - 90°S) extra-tropical regions are shown in the top and bottom rows, respectively, while Tropical (20°N – 20°S) mean values are shown in the middle-row. Each panel distinguish the contribution from reactive (XO_x, striped bars), reservoir (X_y, empty bars) and organic VSL_X (stippled bars) halogens using coloured stacked bars for the *FCnudged_slh* (pink) and *FCHIST_slh* (blue) compsets.

The predicted seasonal cycle of iodine over the SH extratropical regions presents a similar pattern to that in the NH, although with a 6-months shift, mostly for VSL_I. However, and due to the much lower influence of anthropogenic ozone pollution over the SH, the I_y abundance remains less variable throughout the entire year. In contrast, VSL_{Br} show larger abundances during the austral winter due to the reduced photodecomposition. The same seasonal pattern is also observed for

https://doi.org/10.5194/egusphere-2025-3250
Preprint. Discussion started: 13 October 2025

VSL_{Cl}, although we note that total mixing ratio are remarkably lower in the SH compared to the NH extratropics. Larger Br_y abundance is predicted during austral spring and summer following the seasonal changes in sea-salt distributions particularly over the Southern Ocean, resulting in higher Br_y enhancement for *FCHIST_slh* than for *FCnudged_slh* (see Fig. 11h). Is worth noting that over the SH extratropical latitudes, the Cl_y seasonality follows that of Br_y, which is explained by the fact that within this region, the SSA-dehalogenation flux for chlorine (which is linked to that for bromine, see Table 1) dominates over the acid-displacement reaction controlling the total chlorine flux over the NH.

Finally, the tropical VSL_I abundance is the lowest compared to the NH and SH extratropics due to the higher photochemical decomposition close to the Equator. In contrast, I_y abundance is the largest due to the dominant I_2/HOI source (Fig. 1f). On the other side, and driven by the much larger lifetimes of VSL_{Br} and VSL_{Cl} compared to iodine, the tropical abundances of VSL_{Br} are larger than over the extratropical regions (Fig. 11e), while VSL_{Cl} show intermediate abundances between the NH and SH extratropics. In both cases, surface VSL_{Cl} and VSL_{Br} tropical surface abundances lack of a pronounced seasonal cycle, although a regional seasonality is predicted in their contribution to the SGI due to the changes in their convective transport to the tropical tropopause layer (Fernandez et al., 2014, 2021). The double peak annual cycle in reservoir X_y observed within the tropics is attributed the seasonal changes in atmospheric rainout during the wet and dry seasons that affect the washout of inorganic halogens.

3.3 Influence of SLH on Atmospheric Composition

This section describes how the changes in SLH influence the baseline abundance and distribution of other atmospheric components (O_3, OH and NO_2), which in turn determine the oxidative capacity of the atmosphere. We begin quantifying the global mean surface and tropospheric responses to SLH, then address the zonal, latitudinal and vertical distribution of the halogen-driven chemical changes, and finalize with a comprehensive description of the SLH-induced perturbations on the modelled ozone and OH budgets and burdens for the different *FCnudged_slh* an *FCHIST_slh* compsets in 2º×2º resolution. A comparison with previous work using CESM1 is also included to facilitate the interpretation and contextualization of CESM2-SLH results, pointing at specific references where additional details have been provided for individual processes and/or locations.

Table 9 presents the global mean O_3, OH and NO_2 abundance represented by the main CESM2-SLH compsets during the 2015-2020 period, distinguishing the absolute and percentage differences between equivalent simulations including (*compset_slh*) and neglecting (*compset_noh*) SLH within the surface and for the entire troposphere. Including SLH chemistry in the model results in a significant (16.9-17.3%) reduction in the tropospheric ozone burden, decreasing from 336-345 Tg O_3 for the *FCnudged_noh* and *FCHIST_noh* configurations to 278-287 Tg O_3 for the *FCnudged_slh* and *FCHIST_slh*, respectively. The negative O_3 response is more remarkable at the surface with a reduction of 21.4-22.5%. Given the general higher ozone abundance in CESM2-SLH compared to CESM1 (Emmons et al., 2020), the absolute SLH-driven tropospheric and surface ozone reductions are larger for *FCnudged_slh* and *FCHIST_slh* compared with *Cyclical_slh* and *Serial_slh*, although we highlight that the corresponding percentage decreases of global mean ozone at the surface (~24.4%) and the troposphere (~16.9%) are in very good agreement with previous CESM1 studies, ranging from −13% to −24% at the surface and from −16% to −20% in the troposphere (Iglesias-Suarez et al., 2020; Badia et al., 2021; Barrera et al., 2023; Saiz-Lopez et al., 2023). In addition, previous CESM1 estimations of stratospheric ozone depletion due to SLH were –5.2 DU (−2.0%) (Saiz-Lopez et al., 2023), which falls within our CESM2-SLH simulated values of ozone depletion between −6.4 DU and −4.0 DU (−2.5% and −1.6%), respectively obtained with the *FCnudged_slh* and *FCHIST_slh* configurations (see Section 3.3.4).

https://doi.org/10.5194/egusphere-2025-3250
Preprint. Discussion started: 13 October 2025

Table 9: Quantitative changes in atmospheric composition between SLH and NoSLH sensitivities.

Species Abunance		O_3			OH		NO_2	
Compset	Sensitivity	Surface	Tropo[&]	Strat[$]	Surface	Tropo[&]	Surface	Tropo[&]
		ppbv	Tg	DU	ppqv	Mg	pptv	Gg
FCnudged_slh	NOH	29.2	336.0	254.6	67.1	236.2	673.2	383.0
	SLH	22.9	277.9	248.2	65.2	222.8	669.2	355.4
	Absolute Change	-6.2	-58.1	-6.4	-1.8	-13.4	-4.0	-27.6
	Percentage Change (%)	-21.4	-17.3	-2.5	-2.7	-5.7	-0.6	-7.2
FCHIST_slh	NOH	31.1	345.6	251.8	70.4	240.2	639.7	381.8
	SLH	24.1	287.1	247.8	67.6	226.2	635.3	349.1
	Absolute Change	-7.0	-58.5	-4.0	-2.8	-14.0	-4.4	-32.7
	Percentage Change (%)	-22.5	-16.9	-1.6	-3.9	-5.8	-0.7	-8.6
CESM1 (Cyclical_slh)	NOH	27.8	317.1	264.4	53.0	209.2	313.3	266.0
	SLH	21.0	263.5	259.2	48.3	188.6	317.1	251.8
	Absolute Change	-6.8	-53.7	-5.2	-4.7	-20.6	3.8	-14.2
	Percentage Change (%)	-24.4	-16.9	-2.0	-8.8	-9.8	1.2	-5.4
CESM1 (Serial_slh)	NOH	28.3	326.0	259.8	48.4	212.7	320.5	263.3
	SLH	22.6	277.5	255.2	45.5	198.6	326.6	256.6
	Absolute Change	-5.7	-48.5	-4.6	-2.8	-14.0	6.0	-6.8
	Percentage Change (%)	-20.1	-14.9	-1.8	-5.9	-6.6	1.9	-2.6

[&]All tropospheric magnitudes have been computed considering the chemical tropopause (O_3 < 150 ppbv).

Similar to ozone, SLH sources and chemistry globally reduce OH and NO_2. Regardless of the compset, this reduction ranges between −2.7% and −3.9% at the surface and approximately −6% integrated in the troposphere for OH, while for NO_2 differences remain below −1% at the surface and ranging between −7.2% and −8.6% in the troposphere. In comparison with CESM1, the percentage change induced by SLH in CESM2-SLH is smaller for OH and larger for NO_2 (see Table 9). Note that not only the absolute abundance but also the HO_2/OH and NO_2/NO ratio are significantly different between CESM1 and CESM2 (see Fig. 2k,l), which also impact on the estimated global mean values. Given the large number of factors influencing the rapid interconversion between HO_x and NO_x species, such as the strength and spatial distribution of sources and the changes in chemical schemes between CESM versions, a deeper analysis of the dominant processes controlling these changes is encouraged for future studies.

Figures 12 and 13 show the absolute and percentage change, respectively, induced by SLH over the atmospheric abundance of O_3, OH and NO_2 between the *FCnudged_slh* and *FCnudged_noh* compsets. The changes are shown for the zonal average (top), within the boundary layer (middle) and integrated in the troposphere (bottom row). Despite distinctive features for each individual compound, SLH globally reduce the abundance of all species, particularly over the ocean and at high latitudes, with exception of some continental regions where the model shows an enhancement in OH and NO_2 abundance. The largest reductions in ozone mixing ratios occur in the lower stratosphere, although due to the high O_3 levels within the ozone layer, the tropospheric percentage changes are larger than in the stratosphere. Similarly, the larger background ozone abundance over the NH results in larger absolute changes north of the Equator, although in percentage terms, the largest changes are observed in the SH, with minimum ozone changes occurring over the tropical regions.

https://doi.org/10.5194/egusphere-2025-3250
Preprint. Discussion started: 13 October 2025

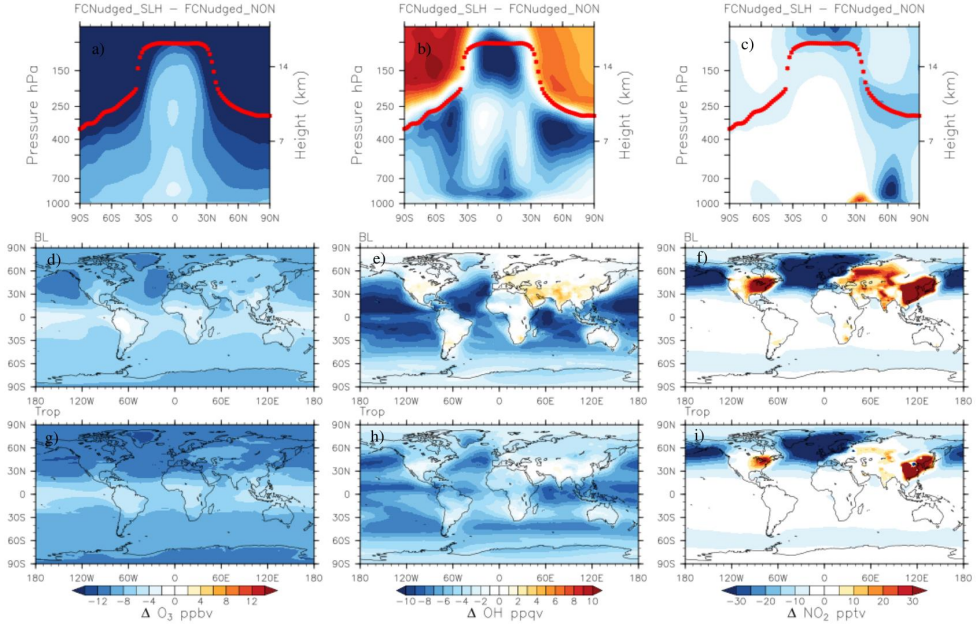

Figure 12: Geographical distribution of the SLH effect on the O_3, OH and NO_2 abundances during present-day (2015-2020). First row: zonal average vertical distribution of a) O_3, b) OH and c) NO_2. Second row: boundary layer mean (below 850 hPa) for d) O_3, e) OH and f) NO_2. Third row: tropospheric mean (surface up to the tropopause) for g) O_3, h) OH and i) NO_2. The absolute difference computed as (*FCnudged_slh* − *FCnudged_noh*) is shown in all panels. Equivalent results with the percentage change are shown in Fig. 13.

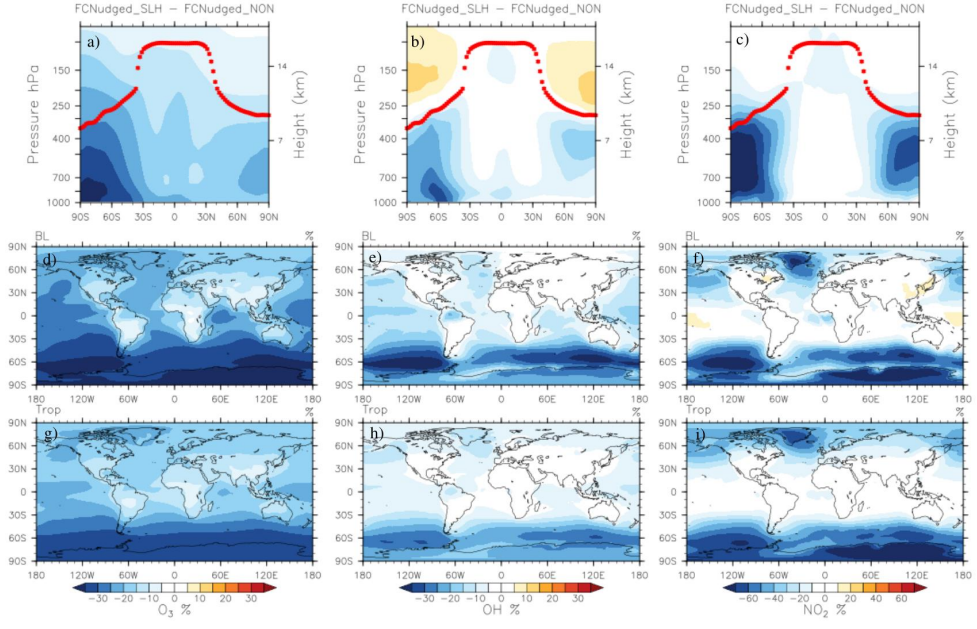

Figure 13: Geographical distribution of the SLH effect on the O_3, OH and NO_2 abundances during present-day (2015-2020). First row: zonal average vertical distribution of a) O_3, b) OH and c) NO_2. Second row: boundary layer mean (below 850 hPa) for d) O_3, e) OH and f) NO_2. Third row: tropospheric mean (surface up to the tropopause) for g) O_3, h) OH and i) NO_2. The percentage difference computed as (*FCnudged_slh* − *FCnudged_noh*) / *FCnudged_noh* × 100% is shown in all panels. Equivalent results with the absolute difference are shown in Fig. 12.

https://doi.org/10.5194/egusphere-2025-3250
Preprint. Discussion started: 13 October 2025

Given the dominant role of O_3 as the primary source of OH in the troposphere, the spatial distribution of OH changes is similar to the analogous pattern of O_3. However, and driven by its higher reactivity, OH changes are more pronounced than for O_3, with the largest reductions over the ocean as well as some continental enhancements (Bossolasco et al., 2025). In percentage terms, OH reduction due to SLH is lower over tropical regions, where most of the global tropospheric oxidation takes place. Maximum percentage differences are found over the pristine southern ocean due to the smaller contribution of the dominant secondary OH source driven by NO_x (see Section 3.3.2) compared with the north Atlantic and Pacific oceans, which presents the larger absolute differences. Similarly, the large NO_2 changes exceeding 50 pptv over continental regions barely represent a small percentage. Indeed, and despite the large heterogeneity, the global mean change of surface NO_2 remains below ~1% (see Table 9).

3.3.1 Evaluation of Model Performance with Air-Pollutants

To evaluate the performance of CESM2-SLH, surface ozone abundance from the compsets *FCnudged_noh* and *FCnudged_slh* was compared with observations reported in the first phase of Tropospheric Ozone Assessment Report (TOAR-I) (https://igacproject.org/activities/TOAR/TOAR-I) (Schultz et al., 2017). The central panel in Figure 14 shows the geographical distribution of annual mean surface ozone for the *FCnudged_slh* compset during year 2015, along with 12 surrounding panels showing the seasonal comparison with observational sites at coastal or close-to-coastal locations (red points). The central panel shows that the model reproduces the hemispheric asymmetry in surface ozone, with background levels below 40 ppbv in the pristine SH, contrasting with peak concentrations (60–75 ppbv) over continental and coastal Asia. Moreover, the ozone peak on the African continent is mainly linked to biomass burning. These maxima values are consistent with those reported by previous studies using CESM2 (Emmons et al., 2020). Moreover, Fig. 14 also shows a visual comparison of the monthly (lines) and annual mean (markers) surface ozone concentrations between the *FCnudged_slh* (red) and *FCnudged_noh* (blue) simulations and TOAR-I observations (black) across multiple stations located between latitudes 60N-60S. Overall, the model captures the observed seasonal ozone cycles across most stations. This agreement is particularly strong at northern mid-latitude stations (>30°N), where the model reproduces both the magnitude and seasonality of ozone, with peaks in spring-summer driven by enhanced photochemical production. Similarly, good representation of ozone seasonality is observed at station 7, located in central Chile as well as in Station 8 east of Madagascar. The inclusion of SLH sources and chemistry in the *FCnudged_slh* simulation improves the agreement with observations in terms of both monthly variability and annual mean, particularly at coastal-stations. However, discrepancies emerge at some stations like 11 and 12, where the model successfully reproduces the observed ozone magnitude but fails to capture their seasonal cycle. This divergence likely stems from incomplete representation of ozone sources and sinks in this pristine region. Finally, note that the coarse resolution of the model is a factor that certainly impact in the comparison with in-situ observations, as the local ozone values in some observational sites do not necessarily represent the mean background levels predicted by a $1.9^o \times 2.5^o$ pixel size in the model. Nevertheless, Fig. 14 clearly shows that the model values are in the same range as observations, reproduce the monthly variability, and demonstrate that the inclusion of SLH chemistry in the model helps to close the gap with observations.

https://doi.org/10.5194/egusphere-2025-3250
Preprint. Discussion started: 13 October 2025

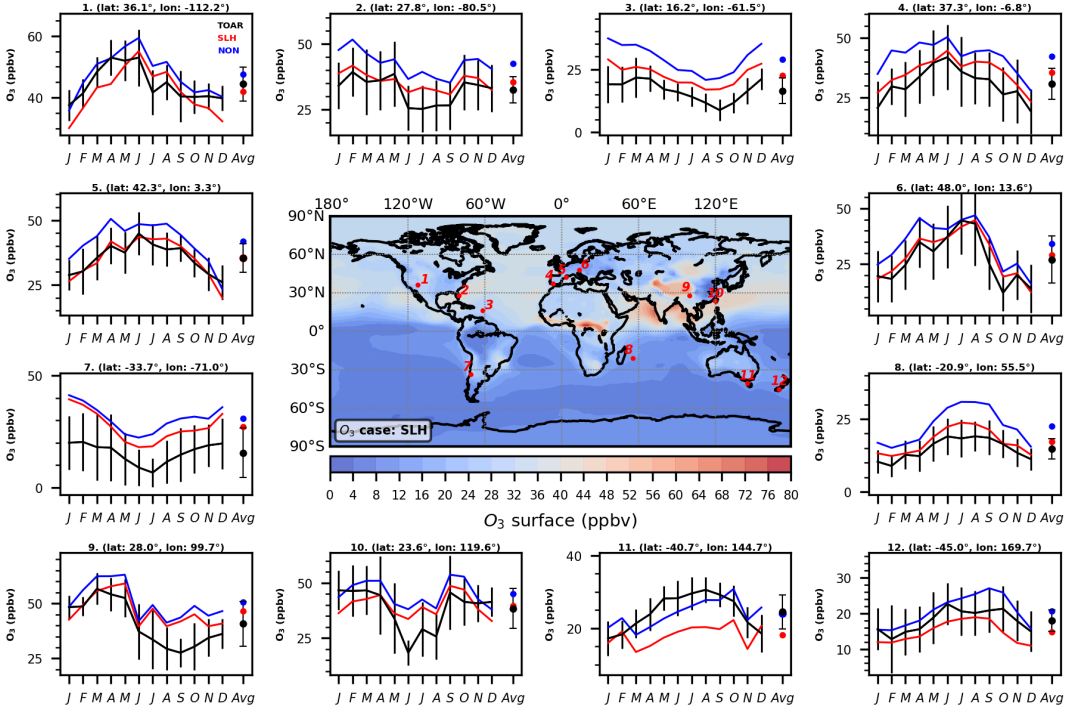

Figure 14: Comparison of CESM2-SLH *FCnudged_slh* and *FCnudged_noh* compset with TOAR-I observations. The center panel shows the geographical distribution of surface ozone on *FCnudged_slh* compset and the observational sites location corresponding to the side panels (red points). The side panels show the comparison of the seasonal distribution and the annual average (marker) of surface ozone between *FCnudged_slh* (red) and *FCnudged_noh* (blue) simulations/compsets with respect to surface observations (black) reported in the first phase of Tropospheric Ozone Assessment Report (TOAR-I) (Schultz et al., 2017) **(https://igacproject.org/activities/TOAR/TOAR-I). Both simulations and observations correspond to the year 2015.**

3.3.2 SLH Enhanced Ozone Chemical Loss

This section highlights the effect of SLH on ozone destruction by means of computing the odd-oxygen chemical loss (*OddOx_Loss*) as performed in previous studies, following the definitions presented in Table 5 of (Saiz-Lopez et al., 2014) (see Chart S2 in the Supplementary Material). Figure 15 shows the annual mean *OddOx_Loss* as a function of latitude and height for the *FCnudged_slh* compset, where the individual contribution of the different families contributing to ozone depletion are distinguished. Going from top to bottom, in the upper stratosphere, *OddOx_Loss* is dominated by NO_x cycles (Fig. 15c), while from the middle and lower stratosphere down to the free-troposphere, the dominant *OddOx_Loss* family is HO_x (Fig. 15b) until O_x becomes the dominant ozone loss channel over the boundary layer (Fig. 15a). Note the halogen-driven *OddOx_Loss* shown in Fig. 15d-f maximize in the tropical upper troposphere (dominated by IO_x) and global lower stratosphere (both BrO_x and IO_x increase, with a minor role of ClO_x), where they significantly contribute to additional ozone destruction. Most of this halogen-driven ozone loss results from: *i)* faster recycling and gas-phase iodine chemistry compared to bromine and chlorine; and *ii)* the larger conversion of iodine to reactive product gases occurring in the lower troposphere. In addition, note the important contribution of BrO_x and ClO_x cycles on ozone depletion over the Antarctic lower stratosphere of the southern hemisphere high latitudes (Fig. 15e,f), which maximizes during spring and is responsible for the formation of the Antarctic ozone hole (see Section 3.3.4).

https://doi.org/10.5194/egusphere-2025-3250
Preprint. Discussion started: 13 October 2025

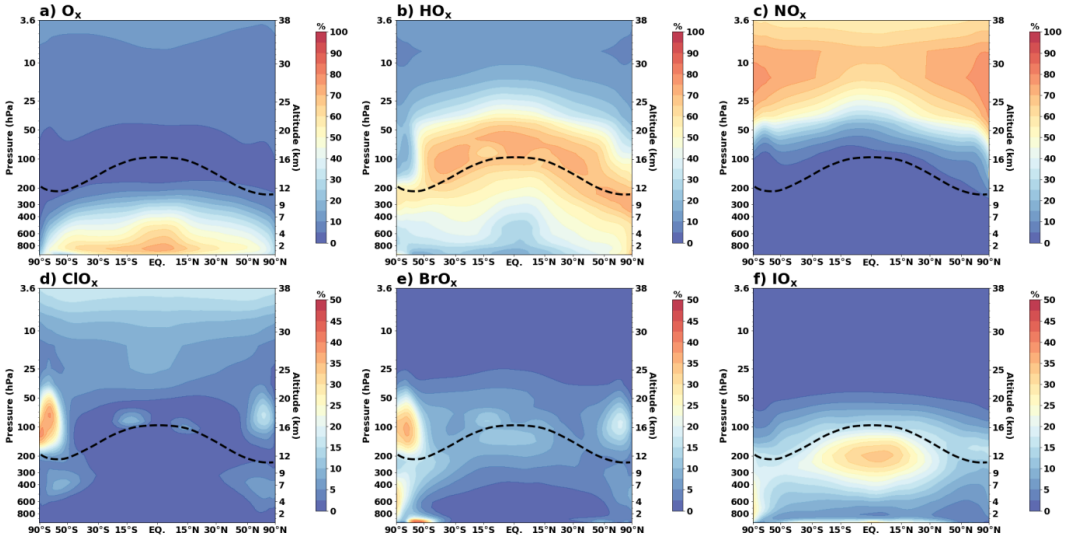

Figure 15: Zonal average distribution of Odd-oxygen loss rates (*OddOx_Loss*) for different ozone depleting families during present-day (2015-2020). Each panel presents the percentage contribution of each *OddOx_Loss* family to the total ozone loss for the *FCnudged_slh* compset. The top-row show results for the main *OddOx_Loss* channels when SLH are not considered: a) O_x, b) HO_x and c) NO_x loss cycles, while the bottom-row shows the percentage contribution from the individual halogen-driven *OddOx_Loss* cycles: d) ClO_x, e) BrO_x and f) IO_x. The black-dashed line indicates the model mean tropopause.

Figure 16 shows the mean vertical distribution of the dominant *OddOx_Loss* channels averaged globally (top row) and within the tropical regions (bottom row). To highlight the influence of SLH on tropospheric chemistry, we quantify in absolute terms the contribution from each family for the *FCnudged_noh* and *FCnudged_slh* simulations, as well as the differences between them in a separate panel. The dominant ozone losses in the troposphere for the *FCnudged_noh* compset (Fig. 16a) are due to direct O_x photolysis, followed by HO_x cycles, both of which are significantly reduced when SLH are included, particularly in the lower and free troposphere (note NO_x only contribute significantly to *OddOx_Loss* in the middle and upper stratosphere). Indeed, for the *FCnudged_slh* setup (Fig. 16b), the total contribution of halogens increases significantly and represents between 10% and 30% globally (Fig. 16c), with a variable vertical profile that is dominated by IO_x cycles in the troposphere, and an increasing contribution mostly from BrO_x close to the tropopause. To compensate the increase in the halogen contribution to total *OddOx_Loss*, Fig. 16c,f shows a proportional decrease in the *OddOx_Loss* destruction by HO_x and O_x in comparison with the *FCnudged_noh* sensitivity (negative change). Most notably, the largest halogen-driven contribution to total ozone loss is due to iodine chemistry, which represents up to 30% within the tropical free troposphere in agreement with previous estimates (Saiz-Lopez et al., 2012, 2014), followed by bromine and with a minor contribution by chlorine. Given that only the reactive fraction of inorganic Br_y is capable of participate in ozone destruction, and most of its contribution occurs in the lower stratosphere (see Fig. 15e), an adequate representation of the SGI and PGI from bromine occurring over the tropical regions (Figs. 8 and 9) is of major importance to properly quantify the impact of SLH bromine and iodine on lowermost stratospheric ozone (see Section 3.3.4).

https://doi.org/10.5194/egusphere-2025-3250
Preprint. Discussion started: 13 October 2025

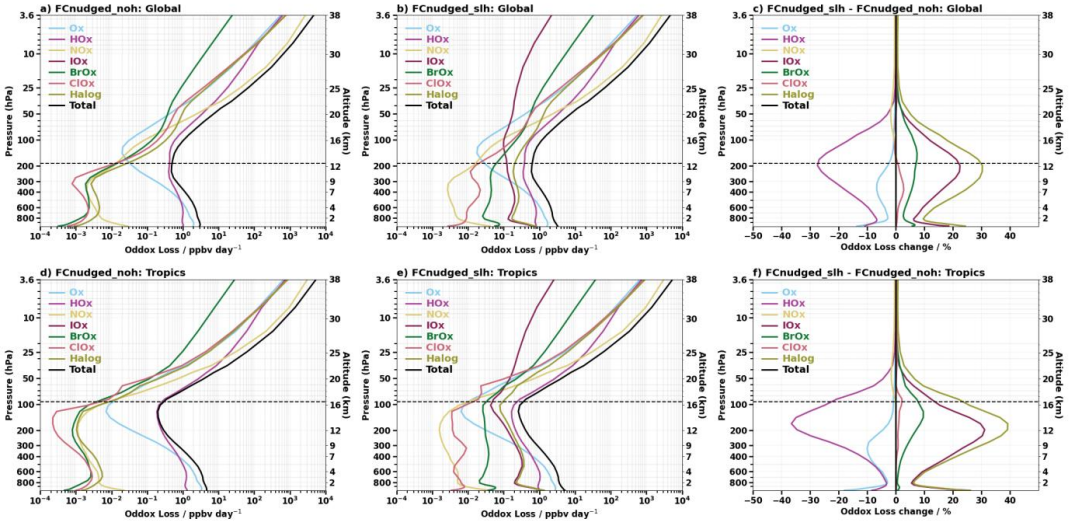

Figure 16: Vertical profile distribution of Odd-oxygen loss rates (*OddOx_Loss*) cycles during present-day (2015-2020) for different model configurations neglecting (left-column; *FCnudged_noh*) and including (center column; *FCnudged_slh*) the contribution of SLH sources and chemistry. The right-column show the percentage difference between both compsets computed as (*FCnudged_slh* − *FCnudged_noh*) / *FCnudged_noh* × 100%. Results for the global mean (90°N – 90°S) are shown in the top row while tropical mean (20°N – 20°S) vertical profiles are shown in the bottom-row. The horizontal dashed line on each panel shows the mean model tropopause.

3.3.3 Impact of SLH in the Troposphere

Table 10 summarized the annual mean odd-oxygen loss channels, as well as the net chemical ozone production and net chemical change for the different simulations considered. Globally, of the total halogen driven tropospheric ozone destruction (505 Tg yr^{-1} for the *FCHIST_slh* and 522 Tg yr^{-1} for the *FCnudged_slh*), IO_x-induced *OddOx_Loss* represents the dominant family, accounting for 76-79%, with minor contributions for bromine and chlorine that represents, respectively, 16-18% and 5%. These values show excellent agreement with previously reported halogen influences obtained with CESM1 (Badia et al., 2021; Barrera et al., 2023). Table 10 also shows the ozone photochemical production, which remains almost unaltered (with minor changes below 2%) regardless of the consideration or not of SLH sources and chemistry, consistent with previous studies. In contrast, and driven mainly by the larger ozone destruction when SLH are considered, the estimated O_3 dry deposition, typically considered in tropospheric budget analysis, is reduced by approximately 16% for *FCnudged_slh* and *FCHIST_slh* compared to their corresponding *FCnudged_noh* and *FCHIST_noh* configurations, which is in line with the 11% reduction previously estimated in CESM1. Finally, the net stratospheric to tropospheric exchange (STE) for *FCnudged_slh* and *FCHIST_slh* reaches 164 and 261 Tg yr^{-1}, respectively. Even though in absolute terms the contribution of STE to the tropospheric ozone budget in CESM2-SLH is smaller than for CESM1 (e.g., STE accounts for 341 Tg yr^{-1} for the *Cyclical_slh* (Saiz-Lopez et al., 2023)), the inclusion of SLH compared to the no-halogen setup results in an equivalent halogen-driven reduction in the contribution of STE of approximately 20%, particularly for the nudging setup (Barrera et al., 2023). This highlights that, despite the dynamical changes in the representation of air subsidence and downward ozone transport across the tropopause between the old nudging over model layers or interfaces used in CESM1 (SD, specified dynamics) and the most recent nudging approach on model levels implemented in CESM2 (Davis et al., 2022), the chemical influence of SLH on tropospheric and stratospheric transport is of equivalent magnitude.

Table 11 shows the most important chemical pathways contributing to the formation of OH, where the individual contributions have been separated between the dominant primary production (*P*), which is the production of O^1D by ozone

https://doi.org/10.5194/egusphere-2025-3250
Preprint. Discussion started: 13 October 2025

photolysis at hν < 330 nm followed by reaction with tropospheric water vapour; and secondary production (*S*), which accounts for all the remaining processes involving VOCs, NO_x and O_x (Lelieveld et al., 2016), as well as the reactions of hydrogen peroxide and halogenated hypohalous acids (see (Bossolasco et al., 2025)). Due to the larger O_3 burden in CESM2-SLH compared with CESM1, we note that the changes in OH production are also expected to differ between the different model versions.

Table 10: Tropospheric ozone budget with and without SLH

Simulation	FCHIST_slh	FCHIST_noh	FCnudged_slh	FCnudged_noh
O_3 photochemical production (P_{O3}; Tg yr^{-1})	5317.0	5490.0	5409.0	5580.0
O_3 chemical Sinks (Tg yr^{-1})				
O_x-Loss	2379.0	2713.0	2387.0	2734.0
NO_x-Loss	16.0	13.6	16.3	13.6
HO_x-Loss	1670.0	2061.0	1677.0	2097.0
ClO_x-Loss	34.0	4.0	30.0	3.9
BrO_x-Los	123.0	4.0	107.4	4.7
IO_x-Loss	505.0	0.0	522.0	0.0
$Halog_x$-Loss	662.0	8.0	659.4	8.6
Other O_x-Loss	73.8	78.4	101.8	104.1
O_3 gross chemical loss (L_{O3}; Tg yr^{-1})	4800.8	4874.0	4841.5	4957.3
P_{O3} - L_{O3}	516.2	616.0	567.5	622.7
O_3 dry depostion (*DryDep*)	777.0	928.0	731.0	872.0
O_3 STE (P_{O3} - L_{O3} - *DryDep*)	-261.0	-314.0	-164.0	-251.0
O_3 Burden (Tg)	311.1	370.0	297.5	360.0
O_3 Lifetime (days)	23.6	27.7	22.4	26.5

All tropospheric magnitudes have been computed considering the internal model tropopause (TROP_P, hPa), defined as the level where the minimum lapse rate pressure is derived.

The tropospheric ozone depletion induced by SLH result in a reduction of *P* from approximately 116 Tg yr^{-1} for the *FCHIST_noh* and *FCnudged_noh* sensitivities (which represent approximately 47-48% of the total OH source) to approximately 101 Tg yr^{-1} (44-45%) for the *FCHIST_slh* and *FCnudged_slh* compsets. Similarly, the secondary ozone-driven pathway (O_3 + HO_2) reduces from approximately 12% to 10% due to the inclusion of SLH, inducing minor alterations in the other secondary channels that remain below a few percent (see Table 11). These reductions in *P* and *S* are compensated by ~5% increase in the contribution from the photolysis of HOCl, HOBr and HOI, which accounts for more than 11 Tg yr^{-1} of the global annual production. We note that the largest percentage contribution is observed within the free troposphere. Consequently, there is a continuous shift in the chemical OH production from primary to secondary sources, which implies that once formed, OH has an increased capability of being chemically re-generated in the atmosphere when SLH are considered. Therefore, and despite SLH result in a net reduction of OH abundance, the tropospheric oxidation capacity of OH on a per atom basis increases. This is typically measured by computing the OH recycling probability, $r = 1 - P / (P + S)$ (Lelieveld et al., 2016), which represents the capability of OH to be regenerated from secondary sources. Most notably, considering SLH in CESM2 increases *r* from approximately 52-53% to 55-56% (see Table 11). Despite percentage values for *r* being lower in CESM2-SLH than in CESM1, the overall global *P* and *S* terms are in line with previous studies using other

https://doi.org/10.5194/egusphere-2025-3250
Preprint. Discussion started: 13 October 2025

models (Lelieveld et al., 2002), while we also acknowledge that several anthropogenic halogen sources considered in the work of (Bossolasco et al., 2025) have not been implemented in CESM2 (see Section 2.5.2).

Table 11: Global OH production with and without SLH

Sources (Tmol yr^{-1})	FCHIST_slh	FCHIST_noh	*FCnudged_slh*	*FCnudged_noh*
Primary (*P*)				
$O^1D + H_2O$	100.7 (44.5%)	115 (48%)	101.2 (44%)	115.7 (47%)
Secondary				
$NO_x + HO_2$	71.7 (31.7%)	75.1 (31.4%)	72.9 (31.5%)	75.8 (31%)
$O_3 + HO_2$	23.1 (10.2%)	28.7 (12%)	24 (10.4%)	30 (12%)
$H_2O_2 + hu$	13 (5.7%)	14 (5.8%)	15 (6.5%)	16 (6.5%)
VOCs, ROOH +hu	5.8 (2.6%)	6 (2.5%)	6.6 (2.8%)	6.8 (2.8%)
HOX + hu	11.1(4.9%)	-	11.6 (5%)	-
Others	0.26 (0.11%)	0.28 (0.12%)	0.26 (0.11%)	0.28 (0.11%)
Total Secondary (*S*)	125 (55.6%)	124 (52%)	130 (56%)	129 (53%)
Net				
Gross (*P* + *S*)	226	239	231.6	245
Recycling probability, r (%)	55.6	52	56	53

The recycling probability (r) in percentage (%) is calculated as $1 - (P/G) \times 100\%$, where P is the primary OH production channel, S is the net sum of secondary production sources and $G = P + S$ is the gross OH production.

3.3.4 Impact of SLH in the Stratosphere

Finally, in this section we evaluate the combined role of SLH chlorine, bromine and iodine over stratospheric ozone using CESM2-SLH, distinguishing the impact over the lowermost global stratosphere as well as its influence over the Antarctic ozone hole as performed in previous studies (Saiz-Lopez et al., 2015; Fernandez et al., 2017; Cuevas et al., 2022; Barrera et al., 2023; Villamayor et al., 2023). Figure 17a shows the change in O_3 partial column densities (DU) as a function of latitude and height for *FCnudged_slh* − *FCnudged_noh*, where it is evident that SLH influence on stratospheric ozone maximizes in the lowermost stratosphere just above the tropopause, which is of major importance as the radiative perturbations in this region of the atmosphere are most sensitive to small changes in ozone abundance (Riese et al., 2012; Saiz-Lopez et al., 2012, 2023). Most notably, the SLH influence on lowermost stratospheric ozone presents a significant latitudinal variation, with increasing reductions moving from the Equator and tropical regions to the mid-to-high latitudes (Fig. 17b,c). This is due to the larger conversion from SGI to PGI as air is transported from the tropical regions towards the poles through Brewer-Dobson circulation, as well as due to the lower temperatures prevailing at high latitudes that accelerate the halogen chemical cycles. Here is worth noting that, despite the SLH influence in lower stratospheric ozone is dominated by bromine and iodine chemistry (see Figs. 15-16), the net effect of the additional halogen injection due to SLH is particularly sensitive to the background inorganic chlorine (Cl_y) levels in the stratosphere (Barrera et al., 2020; Villamayor et al., 2023), and therefore the total SLH impact will change for different periods of time following the overall stratospheric chlorine loading before and after the turnover in the concentration peaks of ODS in the stratosphere following the Montreal protocol.

https://doi.org/10.5194/egusphere-2025-3250
Preprint. Discussion started: 13 October 2025

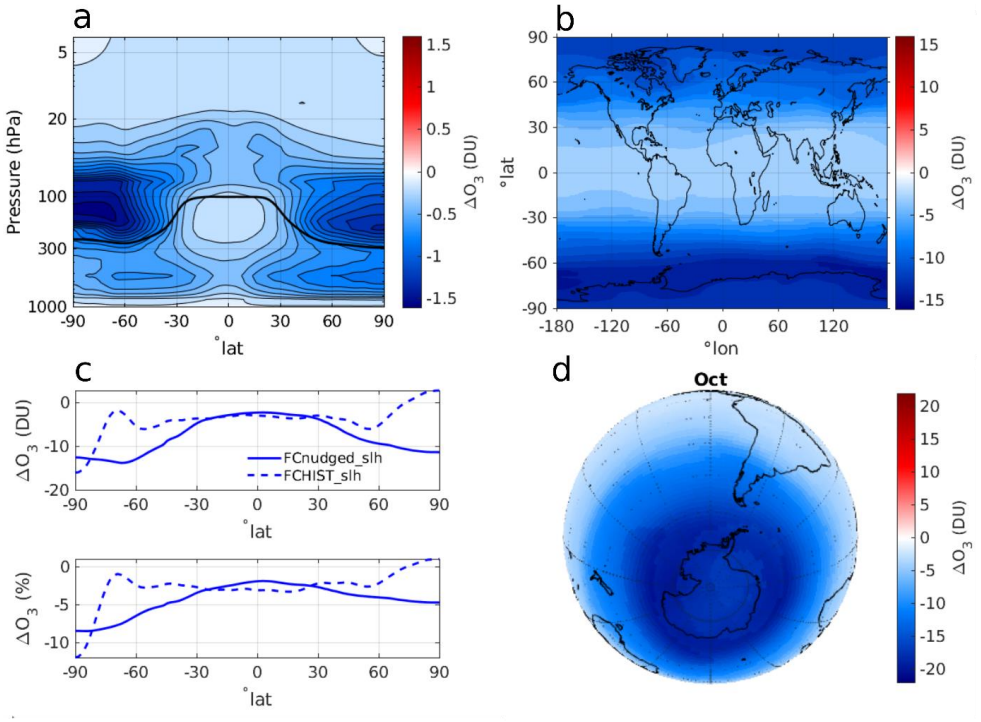

Figure 17: Column integrated ozone change (ΔO_3) in Dobson units (DU) due to SLH during present-day (2015-2020) for the (*FCnudged_slh* − *FCnudged_noh*) compset: a) Annual mean zonal average of partial columns. The solid black-line shows the tropopause height (TROP_P). b) Annual mean geographical distribution of ΔO_3 in the lower stratosphere integrated between the tropopause and the 20 hPa model level. c) Absolute (top) and percentage (bottom) latitudinal distribution of ΔO_3 for the *FCnudged_slh* (solid) and *FCHIST_slh* (dashed) compsets with respect to their corresponding *compset_noh*. d) South-polar view of stratospheric ΔO_3 for the October mean integrated between the tropopause and ~20 hPa.

Figures 17b and 17c shows the net O_3 change in the lowermost stratosphere integrated from the model tropopause up to ~20 hPa, where most of the SLH influence occurs. The ΔO_3 ranges from −2.2-3.3 DU within the tropics (20ºN – 20ºS) up to −9.5-13.8 DU over the high-latitudes (poleward of 60º). These values are larger than those described in previous CESM1 works (Barrera et al., 2020; Fernandez et al., 2021) because those studies only considered SLH bromine, while the CESM2-SLH configuration used here includes SLH iodine as well as the anthropogenic contribution of anthropogenic VSL chlorine. These ozone changes represent, respectively, −1.8-2.7% and −4.0-8.5% of the lower stratospheric ozone for the annual mean, depending on latitude. Due to the efficient chemical coupling of SLH with the large levels of inorganic bromine and chlorine from long-lived CFCs and halons, the net influence of SLH on stratospheric ozone maximizes during austral spring over the South Polar Vortex, where SLH bromine and iodine increased the ozone hole destruction by more than −20 DU and −14%, in agreement with previous reports performed with CESM1 (Fernandez et al., 2017; Cuevas et al., 2022).

3.4 Comparison Between Different Model Resolutions and Configurations

All results using CESM2-SLH presented in this works have been performed using the *FCnudged_slh* and *FCHIST_slh* compsets with (2º×2º) resolution. We recommend selecting this coarse resolution configuration because, as highlighted above, several on-line halogen sources, heterogeneous recycling reactions and washout rates depend on the abundance, extent and distribution of CAM6-Chem atmospheric fields such as sea-salt aerosols, liquid-clouds and ice-crystals, which are well known to differ between CESM2 configurations. Specifically, for studies comparing SLH vs. noSLH, we recommend starting with

https://doi.org/10.5194/egusphere-2025-3250
Preprint. Discussion started: 13 October 2025

the *FCnudged_slh* compset. This ensures that dynamical transport is consistently represented across simulations, which is crucial for isolating and quantifying chemical changes between sensitivities. Depending on the specific applications, many users may need to develop other CESM2-SLH configurations differing from the ones considered in this work, and therefore here we provide a basic guideline of model resolution and configuration inter-comparison that, at minimum, should be performed to validate the SLH model performance. We emphasize that it is the final user's responsibility to properly evaluate that the halogen abundance and distribution in any new user-defined configuration remain consistent with the results provided in this work for the standard *FCnudged_slh* and *FCHIST_slh* (2°×2°) compsets. Below we provide a first-order general inter-comparison of organic VSL and inorganic halogen distributions that is recommended to execute to validate model performance. Given the large spatio-temporal heterogeneity of short-lived species, particularly Cl_y, Br_y and I_y (as well as their reactive fractions ClO_x, BrO_x and IO_x), additional validation for region- and period- specific output should be performed against local observations to avoid obtaining unrealistic or biased results of the influence of SLH on atmospheric composition.

Figure 18 shows a comparison of the VSL zonal average for the 6 (six) different SLH compsets and resolutions defined in Table 6 (see Section 2.5.1), where all distributions have been averaged for the 2000-2005 period. Most notably, all configurations show an equivalent distribution for all halocarbons and families, with slightly lower values occurring at the surface for the finer resolution (1°×1°) grids (*f09_f09_mg17*), particularly for VSL_{Cl} (see Table 12). Figure 19 shows a comparison of the tropical (20°N – 20°S) and global (90°N – 90°S) mean vertical profiles of Cl_y, Br_y and I_y for the same set of simulations. In particular, for the *FWnudged_slh* and *BWHIST_slh* compset using WACCM 70L, a bi-linear interpolation of model output to the default CAM6-Chem 32L vertical grid has been performed using the NCAR-provided *interpic* routine. Despite minor discrepancies in the vertical distribution for the different halogen species, we highlight that all model configurations result in a very similar profile all the way from the surface to the upper stratosphere. Indeed, the corresponding tropospheric percentage variability ranges from −0.4% to +20 % for bromine and −24% to −0.2% for iodine (see Fig. S6), where as expected, the largest percentage differences appear at those heights where the X_y abundance is small. Note that for the particular case of Br_y within the boundary layer, the largest differences appear for the *FCHIST_slh* and *FCnudged_slh* (2×2) configurations, due to the very different representation of sea-salt abundance and distribution, particularly over the Southern Ocean (see Fig. 20). However, when integrated over the troposphere, note that the *FCnudged_slh* (1×1) and *BWHIST_slh* configurations present a larger Br_y burden (see Table 12). For the particular case of chlorine, which of all halogen species show the largest range in Cl_y abundance from the surface to the top of the model, tropospheric changes between the different compsets remain below ~7.5% and maximize close to the tropopause. Here, we highlight that most of the modelled Cl_y change is not driven by the inclusion of SLH sources, but mostly due to the contribution of long-lived CFCs and HCFCs that dominates the transport and distribution of inorganic chlorine in the stratosphere species within each independent case. Indeed, equivalent Cl_y changes for the different *compset_noh* are also predicted. With exception of the *BWHIST_slh* configuration which results in an approximately 1 pptv Br_y larger abundance at the model top, all sensitivities show an equivalent stratospheric bromine and iodine loading regardless of the compset considered. Most notably, within the model top level where most of the long-lived and short-lived halogens have been converted to inorganic chlorine, bromine and iodine, the ΔCl_y, ΔBr_y and ΔI_y, between the different compsets remain below ~5%.

https://doi.org/10.5194/egusphere-2025-3250
Preprint. Discussion started: 13 October 2025

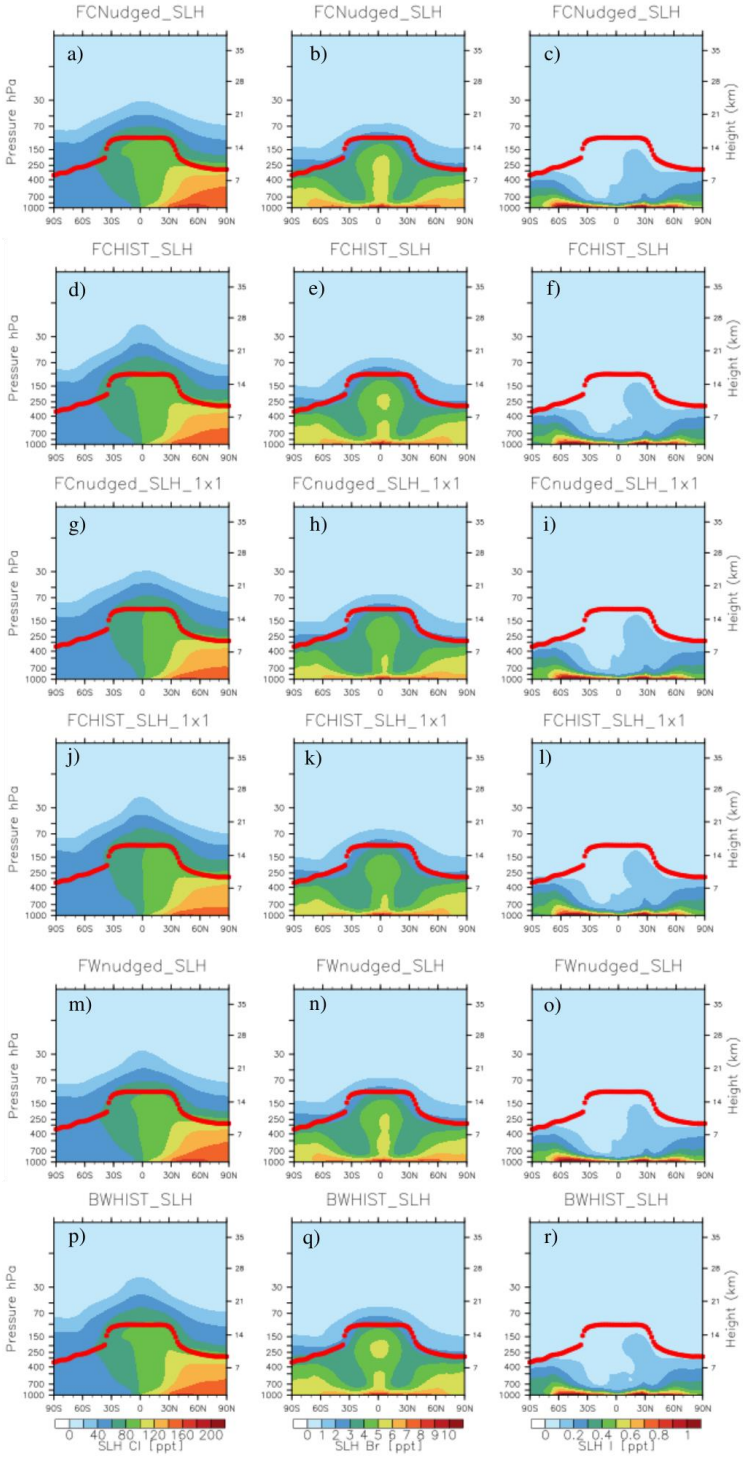

Figure 18: Comparison of VSL abundance between different CESM2-SLH compsets and resolutions. Left, middle and right columns show the zonal average distribution for chlorine (VSL_{Cl}), bromine (VSL_{Br}) and iodine (VSL_{I}), respectively. Each row presents results for an individual CESM2-SLH configuration: FCnudged_slh 2×2 (1st row), FCHIST_slh 2×2 (2nd row), FCnudged_slh 1×1 (3rd row), FCHIST_slh 1×1 (4th row), FWnudged_slh 2×2 (5th row) and BWHIT_slh 2×2 (6th row). All output correspond to the annual mean for the 2000-2005 period. The red-dotted line shows the mean model tropopause.

https://doi.org/10.5194/egusphere-2025-3250
Preprint. Discussion started: 13 October 2025

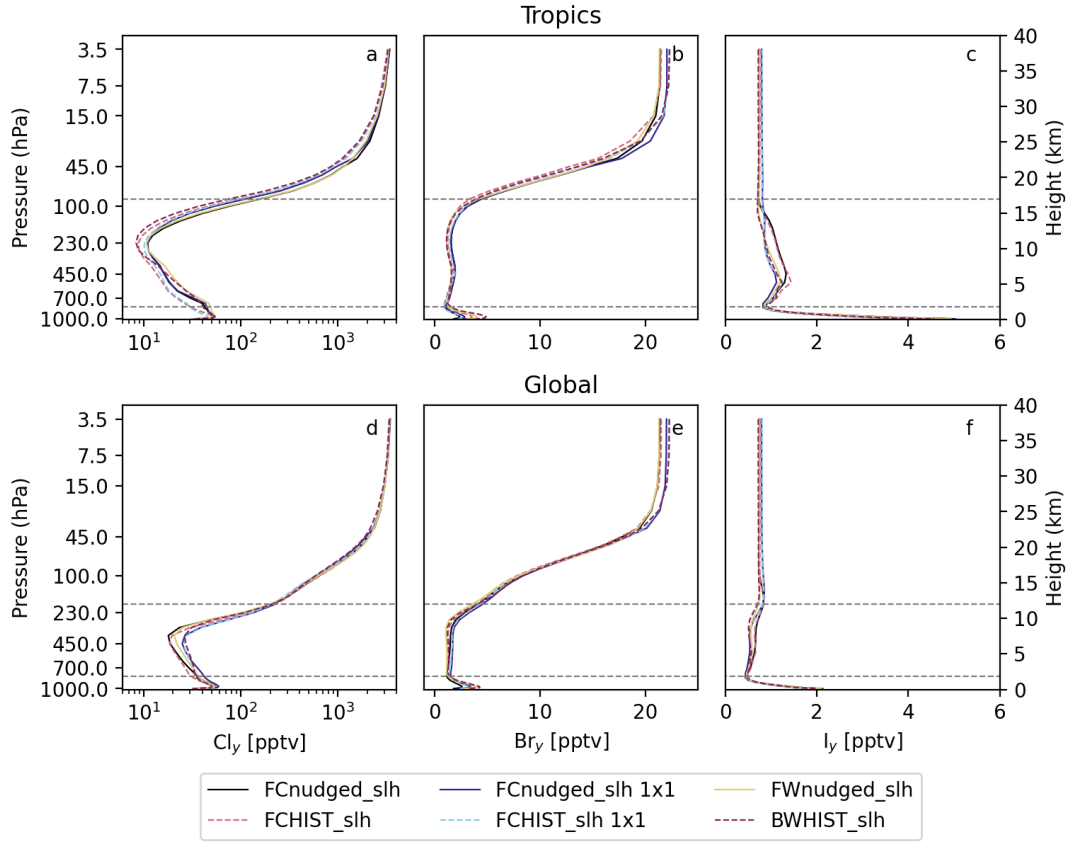

Figure 19: Comparison of the Tropical (top-row) and global (bottom-row) vertical profile distribution of total inorganic halogen abundance (X_y) between the 5 different CESM2-SLH compsets and resolutions. Left, middle and right columns show results for (a, d) chlorine, (b, e) bromine and (c, f) iodine. The dashed lines shows the global mean height of the global tropopause and boundary layer.

Figure 20 shows the geographical distribution of Cl_y, Br_y and I_y abundance averaged within the boundary layer for the different model configurations. Although all compsets show comparable global distributions and mean values (see Table 12), we highlight that the maximum abundance and partitioning between reactive and reservoir species within regional hot-spots present significant differences. Particularly remarkable are the Br_y differences between the *FCHIST_slh* and *BWHIST_slh* compsets over the North Atlantic and North Pacific oceans, as well as over the Southern ocean. This is coherent with the larger SSA-dehalogenation sources simulated in these regions, which affect the BrO/Br_y partitioning. Similarly, the higher (1×1) resolution for *FCHIST_slh* and *FCnudged_slh* display greater Cl_y abundances over the oceanic outflow of polluted air masses from Europe, Eastern US and East Asia. This is associated with to the enhancement of the acid-displacement reaction occurring when HNO_3 air-masses are mixed with halogen rich SSA-oceanic fresh air.

https://doi.org/10.5194/egusphere-2025-3250
Preprint. Discussion started: 13 October 2025

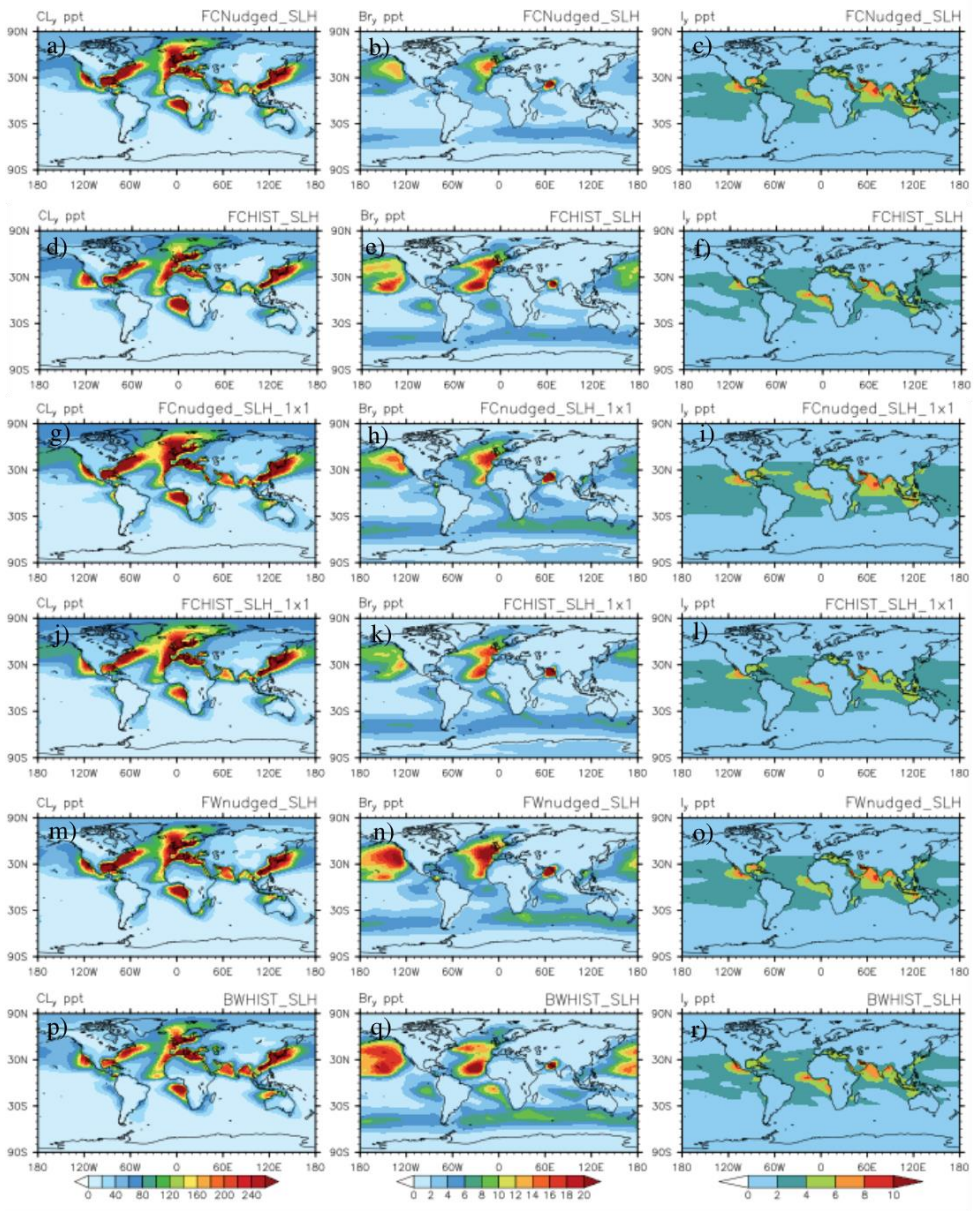

Figure 20: Comparison of the geographical distributions between different CESM2-SLH compsets and resolutions. Left, middle and right columns show the 2000-2005 annual mean distribution over the boundary layer for inorganic chlorine (Cl_y), bromine (Br_y) and iodine (I_y), respectively. (VSL_{Cl}), Each row presents results for an individual CESM2-SLH configuration: FCnudged_slh 2×2 (1st row), FCHIST_slh 2×2 (2nd row), FCnudged_slh 1×1 (3rd row), FCHIST_slh 1×1 (4th row), FWnudged_slh (5th row), and BWHIT_slh 2×2 (6th row).

Finally, Table 12 summarize a comparison of the global mean surface and tropospheric halogen abundance of halogenated VSLs and inorganic halogens across the different model configurations assessed, as well as the changes in O_3, OH and NO_2 abundance between *compset_slh* and *compset_noh* sensitivities. We highlight that all values and results presented in Section 3.4 were obtained considering the compset-individual *&slh_nl* scaling factors compiled in Table 7, which should be taken as the starting point to adjust SLH and X_y abundance in CESM2-SLH for any other model configuration besides those that have been addressed here.

https://doi.org/10.5194/egusphere-2025-3250
Preprint. Discussion started: 13 October 2025

Table 12: Global annual mean surface and tropospheric SLH loading and the corresponding changes in O_3, OH, and NO_2 abundance for different model compsets and resolutions.

Species							
Simulation	Units	FCnudged_slh	FCHIST_slh	FCnudged_slh_1x1	FCHIST_slh_1x1	FWnudged_slh	BWHIST_slh
Offline Sources							
VSL_{Cl}	Tropo (Gg yr^{-1})	1624.0	1658.8	1587.3	1603.7	1644.1	1652.9
VSL_{Br}	Tropo (Gg yr^{-1})	715.5	715.4	715.3	715.2	717.7	716.7
VSL_{I}	Tropo (Gg yr^{-1})	602.6	601.6	602.0	601.3	602.8	602.3
Online Sources							
Acid-displacement	Tropo (Gg yr^{-1})	20488.2	19036.5	20926.6	19212.2	20906.2	20936.3
SSA-dehal. Cl	Tropo (Gg yr^{-1})	3212.0	4051.7	4024.5	3730.4	4054.2	4686.6
SSA-dehal. Br	Tropo (Gg yr^{-1})	2323.7	3886.1	2961.4	2840.7	4224.9	5208.5
Oceanic Iodine	Surface (Gg yr^{-1})	2391.4	2189.0	2234.4	2143.6	2258.4	2321.3
Abundance							
Short-Lived Halogens							
VSL_{Cl}	Surface (pptv)	101.6	98.4	103.0	101.3	100.3	98.3
	Tropo (Gg)	419.1	415.2	437.2	433.6	413.0	418.6
VSL_{Br}	Surface (pptv)	8.5	7.9	8.6	8.2	8.4	7.7
	Tropo (Gg)	56.7	55.2	59.3	58.5	55.2	55.4
VSL_{I}	Surface (pptv)	1.2	1.1	1.2	1.1	1.2	1.0
	Tropo (Gg)	4.8	4.7	4.9	4.8	4.7	4.6
Inorganic Halogens							
Cl_y	Surface (pptv)	37.4	36.0	40.8	37.5	38.3	36.8
	Tropo (Gg)	155.9	140.7	176.5	161.9	171.3	165.6
Br_y	Surface (pptv)	2.2	3.3	2.7	2.7	3.5	4.1
	Tropo (Gg)	19.8	19.8	22.7	20.9	20.5	22.1
I_y	Surface (pptv)	3.1	2.7	3.0	2.7	3.0	2.9
	Tropo (Gg)	17.3	16.8	15.3	15.5	16.0	15.7

Continue next page

Simulation FCnudged_slh FCHIST_slh FCnudged_slh_1x1 FCHIST_slh_1x1 FWnudged_slh BWHIST_slh

https://doi.org/10.5194/egusphere-2025-3250
Preprint. Discussion started: 13 October 2025

1588

Species		FCnudged_slh		FCHIST_slh		FCnudged_slh_1x1		FCHIST_slh_1x1		FWnudged_slh		BWHIST_slh	
Simulation													
Atmospheric Implications		Abs.	Perc. (%)	Abs.	Perc. (%)	Abs.	Perc. (%)	Abs.	Perc. (%)	Abs.	Perc. (%)	Abs.	Perc. (%)
ΔO_3	Surface (ppbv)	-6.2	-21.8	-7.0	-23.4	-8.1	-27.5	-8.5	-28.2	-6.3	-22.8	-7.7	26.2
	Tropo (Gg)	-58.9	-18.0	59.6	-18.3	-69.6	-21.3	-73.0	-22.1	-57.2	-17.7	-64.0	19.6
ΔOH	Surface (ppqv)	-1.9	-3.0	-3.1	-4.6	-3.4	-5.4	-3.7	-5.7	-2.4	-3.7	-3.8	-5.7
	Tropo (Mg)	-13.0	-5.7	14.6	-6.4	-20.8	-9.6	-21.0	-9.5	-14.8	-6.2	-15.3	-6.7
ΔNO_2	Surface (pptv)	-0.7	-0.1	-3.7	-0.6	1.0	0.2	-0.2	0.0	-1.8	-0.3	-5.2	-0.9
	Tropo (Gg)	-23.0	-6.5	28.9	-8.3	-31.8	-8.9	-35.3	-9.7	-30.5	-8.6	-33.5	-9.5

1589

1590

https://doi.org/10.5194/egusphere-2025-3250
Preprint. Discussion started: 13 October 2025

4 Final Remarks

In this work, we provide a comprehensive description of the technical implementation and operational configuration of a complete set of CESM compsets conceived to represent the baseline influence of SLH emissions and chemistry on the global atmosphere. The new CESM2-SLH version includes a detailed representation of the main organic halocarbon and natural inorganic sources, as well as the gas-phase and heterogeneous chemistry of chlorine, bromine and iodine in the marine boundary layer, free troposphere and lowermost stratosphere, highlighting the dominant processes determining the role played by SLH on atmospheric composition. In doing so, we evaluate their global budgets, chemical partitioning and spatio-temporal distributions, with a special focus on the regional and global implications of SLH on atmospheric oxidizing capacity and atmospheric chemistry. Despite during the past 15 years most of the SLH developments have already been reported using different CESM1 versions, there was still missing a complete description integrated in the context of the latest model developments made within the Community Earth System Model framework, i.e., CESM2.

The released CESM2-SLH version comprises six new model compsets and includes a complete set of configuration files and namelist updated that must be properly setup with user-defined namelist options. This include increasing the number of default emission sources and prescribed LBCs, as well as expanding the list of species that suffer dry- and wet-deposition, including the ice-uptake list. Similarly, a new set of initialization and absorption cross-section files including updated data for VSL halocarbon and inorganic halogen species are now available. Most notably, and with the intention of avoid unintended misevaluation of SLH influence on atmospheric composition for users familiarized with current CESM2 configurations typically used for climate and air quality studies on the global scale, this work provides a general but complete inter-comparison of organic VSL and inorganic halogen distributions obtained for the different model compsets. Given the large spatio-temporal variability of Cl_y, Br_y and I_y within different regions of the atmosphere, as well as its strong dependence with several model variables and parameters such as the abundance and distribution of sea-salt aerosols and other substrate surfaces where inorganic halogens recycle, we recommend new-users not familiarized with SLH chemistry to initially select the coarse ($2^o \times 2^o$) resolution, particularly with the *FCnudged_slh* compset. This ensures that dynamical transport is consistently represented across simulations, which is crucial for isolating and quantifying chemical changes between different model sensitivities. In case other model configuration is preferred, we strongly recommend performing an equivalent model intercomparison as the one provided here to ensure that the global halogen sources and budgets are within the ranges of the many model configurations compiled in this work.

Given the important role played by SLH in tropospheric and stratospheric chemitry, as well as their changing influence depending on many Earth's system components which in turn depends on background atmospheric composition and climate, we call the wider CESM community to consider the CESM2-SLH release to obtain a realistic representation of the background influence of natural and anthropogenic short-lived halogen sources and chemistry in air quality and Earth's climate studies. Similarly, we encourage other global chemistry-climate models and regional chemistry-transport models to implement equivalent representations of SLH sources and chemistry to improve their representation of the natural halogen baseline in the atmosphere.

Author contributions

A.S.-L. deigned research and lead the development of SLH chemistry in CESM. R.P.F. with the help of C.A.C., D.K. and F.V. implemented the porting of the code. R.P.F., C.A.C. and J.V. run the simulations. R.P.F., C.A.C., J.V., A.F., A.B., J.A.B., A.R., O.T. and Q.L. performed the data curation, processed the output and validated the model results. All co-authors contributed to investigation, discussion and visualization. R.P.F., C.A.C. and A.S.-L. wrote the original draft, with further review and editing from all co-authors.

https://doi.org/10.5194/egusphere-2025-3250
Preprint. Discussion started: 13 October 2025

Acknowledgements

This study has been funded by the European Research Council Executive Agency under the European Union´s Horizon 2020 Research and Innovation programme (Project "ERC-- 2016-- COG 726349 CLIMAHAL"), and supported by the Consejo Superior de Investigaciones Científicas (CSIC) of Spain. R.P.F. would like to thank financial support from ANPCyT (PICT 2019-2187 & 2022-0474) and MinCyT (REMATE IF-2023-85161983-APN). The National Center for Atmospheric Research (NCAR) is sponsored by NSF under grant number 1852977. Computing resources, support, and data storage are provided and maintained by the Computational and Information System Laboratory from NCAR (https://doi.org/10.5065/D6RX99HX). A.F. acknowledges support from Horizon Europe through a Marie Skłodowska-Curie Actions Postdoctoral Fellowship (grant agreement 101103544, SUMAC). Q.L. is supported by National Natural Science Foundation of China (W2411028). We would like to thanks to an endless list of scientists, postdocs. technical personnel and PhD students from many groups around the world that contributed to the development and evaluation of SLH sources and chemistry in CESM1 and CESM2.

Code and Data Availability

The Community Earth System Model (CESM) code is maintained by the NSF National Center for Atmospheric Research (NCAR). The benchmark version of CESM2 is distributed via GitHub (https://github.com/ESCOMP/CESM) and available at the NCAR's official site (https://www.cesm.ucar.edu/models/cesm2). The complete CESM2-SLH branch used in this work (*cesm2.2-asdbranch_slh*) can be downloaded from GitHub (https://github.com/RafaPedroFernandez/CESM/tree/cesm2.2-asdbranch_slh), which is a fork version of the official CESM2 repository (https://github.com/ESCOMP/CESM/tree/cesm2.2-asdbranch). NCAR recommends citing the CESM2 model as (Danabasoglu et al., 2020). All SLH code and data supporting this work, including the complete set of building scripts, Fortran routines, individual namelist templates for *compset_slh* and *compset_noh* configurations with the necessary input files, as well as the annual mean output used to generate all Figures and Tables, can be obtained from Mendeley Datasets at https://doi.org/10.17632/f87hvrv25v.1 (Fernandez et al., 2025).

References

Abrahamsson, K., Granfors, A., Ahnoff, M., Cuevas, C. A. and Saiz-Lopez, A.: Organic bromine compounds produced in sea ice in Antarctic winter, Nat. Commun., 9(1), doi:10.1038/s41467-018-07062-8, 2018.

Alicke, B., Hebestreit, K., Stutz, J. and Platt, U.: Iodine oxide in the marine boundary layer, Nature, 397(6720), 572–573, doi:10.1038/17508, 1999.

Aschmann, J. and Sinnhuber, B.-M.: Contribution of very short-lived substances to stratospheric bromine loading: uncertainties and constraints, Atmos. Chem. Phys., 13(3), 1203–1219, doi:10.5194/acp-13-1203-2013, 2013.

Aschmann, J., Sinnhuber, B.-M., Chipperfield, M. P. and Hossaini, R.: Impact of deep convection and dehydration on bromine loading in the upper troposphere and lower stratosphere, Atmos. Chem. Phys., 11(6), 2671–2687, doi:10.5194/acp-11-2671-2011, 2011.

Atkinson, R., Baulch, D. L., Cox, R. A., Crowley, J. N., Hampson, R. F., Hynes, R. G., Jenkin, M. E., Rossi, M. J. and Troe, J.: Evaluated kinetic and photochemical data for atmospheric chemistry: Volume III – gas phase reactions of inorganic halogens, Atmos. Chem. Phys., 7(4), 981–1191, doi:10.5194/acp-7-981-2007, 2007.

Atkinson, R., Baulch, D. L., Cox, R. A., Crowley, J. N., Hampson, R. F., Hynes, R. G., Jenkin, M. E., Rossi, M. J., Troe, J.

https://doi.org/10.5194/egusphere-2025-3250
Preprint. Discussion started: 13 October 2025

and Wallington, T. J.: Evaluated kinetic and photochemical data for atmospheric chemistry: Volume IV – gas phase reactions of organic halogen species, Atmos. Chem. Phys., 8(15), 4141–4496, doi:10.5194/acp-8-4141-2008, 2008.

Badia, A., Iglesias-Suarez, F., Fernandez, R. P., Cuevas, C. A., Kinnison, D. E., Lamarque, J.-F., Griffiths, P. T., Tarasick, D. W., Liu, J. and Saiz-Lopez, A.: The Role of Natural Halogens in Global Tropospheric Ozone Chemistry and Budget Under Different 21st Century Climate Scenarios, J. Geophys. Res. Atmos., 126(20), e2021JD034859, doi:https://doi.org/10.1029/2021JD034859, 2021.

Badia, A., Reeves, C. E., Baker, A. R., Saiz-Lopez, A., Volkamer, R., Koenig, T. K., Apel, E. C., Hornbrook, R. S., Carpenter, L. J., Andrews, S. J., Sherwen, T. and Von Glasow, R.: Importance of reactive halogens in the tropical marine atmosphere: A regional modelling study using WRF-Chem, Atmos. Chem. Phys., 19(5), 3161–3189, doi:10.5194/acp-19-3161-2019, 2019.

Barrera, J. A., Kinnison, D. E., Fernandez, R. P., Lamarque, J., Cuevas, C. A., Tilmes, S. and Saiz-Lopez, A.: Comparing the Effect of Anthropogenically Amplified Halogen Natural Emissions on Tropospheric Ozone Chemistry Between Pre-Industrial and Present-Day, J. Geophys. Res. Atmos., 128(14), e2022JD038283, doi:10.1029/2022JD038283, 2023.

Barrera, J., Fernandez, R., Iglesias-Suarez, F., Cuevas, C., Lamarque, J.-F. and Saiz-Lopez, A.: Seasonal impact of biogenic VSL bromine on the evolution of mid-latitude lowermost stratospheric ozone during the 21st century, Atmos. Chem. Phys. Discuss., (January), 1–31, doi:10.5194/acp-2019-1091, 2020.

Benavent, N., Mahajan, A. S., Li, Q., Cuevas, C. A., Schmale, J., Angot, H., Jokinen, T., Quéléver, L. L. J., Blechschmidt, A. M., Zilker, B., Richter, A., Serna, J. A., Garcia-Nieto, D., Fernandez, R. P., Skov, H., Dumitrascu, A., Simões Pereira, P., Abrahamsson, K., Bucci, S., Duetsch, M., Stohl, A., Beck, I., Laurila, T., Blomquist, B., Howard, D., Archer, S. D., Bariteau, L., Helmig, D., Hueber, J., Jacobi, H. W., Posman, K., Dada, L., Daellenbach, K. R. and Saiz-Lopez, A.: Substantial contribution of iodine to Arctic ozone destruction, Nat. Geosci., 15(10), 770–773, doi:10.1038/s41561-022-01018-w, 2022.

Bossolasco, A., Fernandez, R., Li, Q., Mahajan, A., Villamayor, J., Barrera, J., Heard, D. E., Cuevas, C., Caram, C., Szopa, S. and Saiz-Lopez, A.: Key role of short-lived halogens on global atmospheric oxidation during historical periods, Environ. Sci. Atmos., doi:10.1039/D4EA00141A, 2025.

Burkholder, J. B., Sander, S. P., Abbatt, J. P. D., Barker, J. R., Cappa, C., Crounse, J. D., Dibble, T. S., Huie, R. E., Kolb, C. E., Kurylo, M., Orkin, V., Percival, C., Wilmouth, D. and PH, W.: Chemical Kinetics and Photochemical Data for Use in Atmospheric Studies Evaluation Number 19 - Publication 19-5, JPL_NASA, 32(15–10), 170 [online] Available from: https://jpldataeval.jpl.nasa.gov/, 2019.

Butler, J. H., King, D. B., Lobert, J. M., Montzka, S. a., Yvon-Lewis, S. a., Hall, B. D., Warwick, N. J., Mondeel, D. J., Aydin, M. and Elkins, J. W.: Oceanic distributions and emissions of short-lived halocarbons, Global Biogeochem. Cycles, 21(1), n/a-n/a, doi:10.1029/2006GB002732, 2007.

Caram, C., Szopa, S., Cozic, A., Bekki, S., Cuevas, C. A. and Saiz-Lopez, A.: Sensitivity of tropospheric ozone to halogen chemistry in the chemistry-climate model LMDZ-INCA vNMHC, Geosci. Model Dev., 16(14), 4041–4062, doi:10.5194/gmd-16-4041-2023, 2023.

Carpenter, L. J. and Liss, P. S.: On temperate sources of bromoform and other reactive organic bromine gases, J. Geophys. Res., 105(D16), 20539–20547, doi:10.1029/2000JD900242, 2000.

Carpenter, L. J., Liss, P. S. and Penkett, S. A.: Marine organohalogens in the atmosphere over the Atlantic and Southern Oceans, J. Geophys. Res. Atmos., 108(D9), doi:10.1029/2002JD002769, 2003.

Carpenter, L. J., MacDonald, S. M., Shaw, M. D., Kumar, R., Saunders, R. W., Parthipan, R., Wilson, J. and Plane, J. M. C.: Atmospheric iodine levels influenced by sea surface emissions of inorganic iodine, Nat. Geosci., 6(2), 108–111, doi:10.1038/ngeo1687, 2013.

Carpenter, L. J., Malin, G., Liss, P. S. and Küpper, F. C.: Novel biogenic iodine-containing trihalomethanes and other short-

https://doi.org/10.5194/egusphere-2025-3250
Preprint. Discussion started: 13 October 2025

lived halocarbons in the coastal East Atlantic, Global Biogeochem. Cycles, 14(4), 1191–1204, doi:10.1029/2000GB001257, 2000.

Chance, K.: Analysis of BrO measurements from the Global Ozone Monitoring Experiment, Geophys. Res. Lett., 25(17), 3335–3338, doi:10.1029/98GL52359, 1998.

Chang, D., Li, Q., Wang, Z., Dai, J., Fu, X., Guo, J., Zhu, L., Pu, D., Cuevas, C. A., Fernandez, R. P., Wang, W., Ge, M., Fung, J. C. H., Lau, A. K. H., Granier, C., Brasseur, G., Pozzer, A., Saiz-Lopez, A., Song, Y. and Wang, T.: Significant chlorine emissions from biomass burning affect the long-term atmospheric chemistry in Asia, Natl. Sci. Rev., 11(9), doi:10.1093/nsr/nwae285, 2024.

Chen, Q., Sherwen, T., Evans, M. and Alexander, B.: DMS oxidation and sulfur aerosol formation in the marine troposphere: A focus on reactive halogen and multiphase chemistry, Atmos. Chem. Phys., 18(18), 13617–13637, doi:10.5194/acp-18-13617-2018, 2018.

Claxton, T., Hossaini, R., Wilson, C., Montzka, S. A., Chipperfield, M. P., Wild, O., Bednarz, E. M., Carpenter, L. J., Andrews, S. J., Hackenberg, S. C., Mühle, J., Oram, D., Park, S., Park, M., Atlas, E., Navarro, M., Schauffler, S., Sherry, D., Vollmer, M., Schuck, T., Engel, A., Krummel, P. B., Maione, M., Arduini, J., Saito, T., Yokouchi, Y., O'Doherty, S., Young, D. and Lunder, C.: A Synthesis Inversion to Constrain Global Emissions of Two Very Short Lived Chlorocarbons: Dichloromethane, and Perchloroethylene, J. Geophys. Res. Atmos., 125(12), e2019JD031818, doi:10.1029/2019JD031818, 2020.

Cuevas, C. A., Fernandez, R. P., Kinnison, D. E., Li, Q., Lamarque, J. F., Trabelsi, T., Francisco, J. S., Solomon, S. and Saiz-Lopez, A.: The influence of iodine on the Antarctic stratospheric ozone hole, Proc. Natl. Acad. Sci. U. S. A., 119(7), e2110864119, doi:10.1073/pnas.2110864119, 2022.

Cuevas, C. A., Maffezzoli, N., Corella, J. P., Spolaor, A., Vallelonga, P., Kjær, H. A., Simonsen, M., Winstrup, M., Vinther, B., Horvat, C., Fernandez, R. P., Kinnison, D., Lamarque, J., Barbante, C. and Saiz-lopez, A.: Rapid increase in atmospheric iodine levels in the North Atlantic since the mid-20th century, Nat. Commun., 1–6, doi:10.1038/s41467-018-03756-1, 2018.

Danabasoglu, G., Lamarque, J. F., Bacmeister, J., Bailey, D. A., DuVivier, A. K., Edwards, J., Emmons, L. K., Fasullo, J., Garcia, R., Gettelman, A., Hannay, C., Holland, M. M., Large, W. G., Lauritzen, P. H., Lawrence, D. M., Lenaerts, J. T. M., Lindsay, K., Lipscomb, W. H., Mills, M. J., Neale, R., Oleson, K. W., Otto-Bliesner, B., Phillips, A. S., Sacks, W., Tilmes, S., van Kampenhout, L., Vertenstein, M., Bertini, A., Dennis, J., Deser, C., Fischer, C., Fox-Kemper, B., Kay, J. E., Kinnison, D., Kushner, P. J., Larson, V. E., Long, M. C., Mickelson, S., Moore, J. K., Nienhouse, E., Polvani, L., Rasch, P. J. and Strand, W. G.: The Community Earth System Model Version 2 (CESM2), J. Adv. Model. Earth Syst., 12(2), 1–35, doi:10.1029/2019MS001916, 2020.

Davis, N. A., Callaghan, P., Simpson, I. R. and Tilmes, S.: Specified dynamics scheme impacts on wave-mean flow dynamics, convection, and tracer transport in CESM2 (WACCM6), Atmos. Chem. Phys., 22(1), 197–214, doi:10.5194/acp-22-197-2022, 2022.

Emmons, L. K., Schwantes, R. H., Orlando, J. J., Tyndall, G., Kinnison, D., Lamarque, J. F., Marsh, D., Mills, M. J., Tilmes, S., Bardeen, C., Buchholz, R. R., Conley, A., Gettelman, A., Garcia, R., Simpson, I., Blake, D. R., Meinardi, S. and Pétron, G.: The Chemistry Mechanism in the Community Earth System Model Version 2 (CESM2), J. Adv. Model. Earth Syst., 12(4), 1–21, doi:10.1029/2019MS001882, 2020.

Eyring, V., Lamarque, J.-F., Hess, P., Arfeuille, F., Bowman, K., Chipperfield, M. P., Duncan, B., Fiore, A., Gettelman, A., Giorgetta, M. A., Granier, C., Hegglin, M., Kinnison, D., Kunze, M., Langematz, U., Luo, B., Martin, R., Matthes, K., Newman, P. A., Peter, T., Robock, A., Ryerson, T., Saiz-Lopez, A., Salawitch, R., Schultz, M., Shepherd, T. G., Shindell, D., Stähelin, J., Tegtmeier, S., Thomason, L., Tilmes, S., Vernier, J.-P., Waugh, D. W. and Young, P. J.: Overview of IGAC/SPARC Chemistry-Climate Model Initiative (CCMI) Community Simulations in Support of Upcoming Ozone and

https://doi.org/10.5194/egusphere-2025-3250
Preprint. Discussion started: 13 October 2025

Climate Assessments, SPARC Newsl., 40(January), 48–66 [online] Available from: http://www.met.reading.ac.uk/ccmi/?page_id=15, 2013.

Fernandez, R. P., Barrera, J. A., López-Noreña, A. I., Kinnison, D. E., Nicely, J., Salawitch, R. J., Wales, P. A., Toselli, B. M., Tilmes, S., Lamarque, J. F., Cuevas, C. A. and Saiz-Lopez, A.: Intercomparison Between Surrogate, Explicit, and Full Treatments of VSL Bromine Chemistry Within the CAM-Chem Chemistry-Climate Model, Geophys. Res. Lett., 48(4), 1–10, doi:10.1029/2020GL091125, 2021.

Fernandez, R. P., Berná, L., Tomazzeli, O. G., Mahajan, A. S., Li, Q., Kinnison, D. E., Wang, S., Lamarque, J.-F., Tilmes, S., Skov, H., Cuevas, C. A. and Saiz-Lopez, A.: Arctic halogens reduce ozone in the northern mid-latitudes, Proc. Natl. Acad. Sci., 121(39), 2017, doi:10.1073/pnas.2401975121, 2024.

Fernandez, R. P., Carmona-Balea, A., Cuevas, C. A., Barrera, J. A., Kinnison, D. E., Lamarque, J., Blaszczak-Boxe, C., Kim, K., Choi, W., Hay, T., Blechschmidt, A., Schönhardt, A., Burrows, J. P. and Saiz-Lopez, A.: Modeling the Sources and Chemistry of Polar Tropospheric Halogens (Cl, Br, and I) Using the CAM-Chem Global Chemistry-Climate Model, J. Adv. Model. Earth Syst., 11(7), 2259–2289, doi:10.1029/2019ms001655, 2019.

Fernandez, R. P., Cuevas, C., Villamayor, J., Feinberg, A., Kinnison, D., Vitt, F., Bossolasco, A., Barrera, J. A., Reynoso, A., Tomazzeli, O., Li, Q. and Saiz-Lopez, A.: Dataset for the CESM2-SLH Description Paper, , v1, doi:10.17632/f87hvrv25v.1, 2025.

Fernandez, R. P., Kinnison, D. E., Lamarque, J. F., Tilmes, S. and Saiz-Lopez, A.: Impact of biogenic very short-lived bromine on the Antarctic ozone hole during the 21st century, Atmos. Chem. Phys., 17(3), 1673–1688, doi:10.5194/acp-17-1673-2017, 2017.

Fernandez, R. P., Salawitch, R. J. J., Kinnison, D. E. E., Lamarque, J.-F. and Saiz-Lopez, A.: Bromine partitioning in the tropical tropopause layer: implications for stratospheric injection, Atmos. Chem. Phys., 14(24), 13391–13410, doi:10.5194/acp-14-13391-2014, 2014.

Fu, X., Sun, X., Travnikov, O., Li, Q., Qin, C., Cuevas, C. A., Fernandez, R. P., Mahajan, A. S., Wang, S., Wang, T. and Saiz-Lopez, A.: Anthropogenic short-lived halogens increase human exposure to mercury contamination due to enhanced mercury oxidation over continents, Proc. Natl. Acad. Sci. U. S. A., 121(12), e2315058121, doi:10.1073/pnas.2315058121, 2024.

Ge, W., Liu, J., Xiang, S., Zhou, Y., Zhou, J., Hu, X., Ma, J., Wang, X., Wan, Y., Hu, J., Zhang, Z., Wang, X. and Tao, S.: Improvement and Uncertainties of Global Simulation of Sulfate Concentration and Radiative Forcing in CESM2, J. Geophys. Res. Atmos., 127(20), e2022JD037623, doi:10.1029/2022JD037623, 2022.

Gettelman, A., Hannay, C., Bacmeister, J. T., Neale, R. B., Pendergrass, A. G., Danabasoglu, G., Lamarque, J. -F., Fasullo, J. T., Bailey, D. A., Lawrence, D. M. and Mills, M. J.: High Climate Sensitivity in the Community Earth System Model Version 2 (CESM2), Geophys. Res. Lett., 46(14), 8329–8337, doi:10.1029/2019GL083978, 2019a.

Gettelman, A., Mills, M. J., Kinnison, D. E., Garcia, R. R., Smith, A. K., Marsh, D. R., Tilmes, S., Vitt, F., Bardeen, C. G., McInerny, J., Liu, H. L., Solomon, S. C., Polvani, L. M., Emmons, L. K., Lamarque, J. F., Richter, J. H., Glanville, A. S., Bacmeister, J. T., Phillips, A. S., Neale, R. B., Simpson, I. R., DuVivier, A. K., Hodzic, A. and Randel, W. J.: The Whole Atmosphere Community Climate Model Version 6 (WACCM6), J. Geophys. Res. Atmos., 124(23), 12380–12403, doi:10.1029/2019JD030943, 2019b.

Gómez Martín, J. C., Spietz, P. and Burrows, J. P.: Spectroscopic studies of the I2/O3 photochemistry. Part 1: Determination of the absolute absorption cross sections of iodine oxides of atmospheric relevance, J. Photochem. Photobiol. A Chem., 176(1–3), 15–38, doi:10.1016/j.jphotochem.2005.09.024, 2005.

Graedel, T. E. and Keene, W. C.: Tropospheric budget of reactive chlorine, Global Biogeochem. Cycles, 9(1), 47–77, doi:10.1029/94GB03103, 1995.

Hegglin, M. I., Lamarque, J.-F., Eyring, V., Hess, P., Young, P. J., Fiore, A. M., Myhre, G., Nagashima, T., Ryerson, T.,

https://doi.org/10.5194/egusphere-2025-3250
Preprint. Discussion started: 13 October 2025

Shepherd, T. G. and Waugh, D. W.: IGAC/SPARC Chemistry-Climate Model Initiative (CCMI) 2014 Science Workshop, SPARC Newsl., 43(July), 32–35 [online] Available from: http://www.met.reading.ac.uk/ccmi/?page_id=15, 2014.

van Herpen, M. M. J. W., Li, Q., Saiz-Lopez, A., Liisberg, J. B., Röckmann, T., Cuevas, C. A., Fernandez, R. P., Mak, J. E., Mahowald, N. M., Hess, P., Meidan, D., Stuut, J. B. W. and Johnson, M. S.: Photocatalytic chlorine atom production on mineral dust–sea spray aerosols over the North Atlantic, Proc. Natl. Acad. Sci. U. S. A., 120(31), e2303974120, doi:10.1073/PNAS.2303974120, 2023.

Hossaini, R., Atlas, E., Dhomse, S. S., Chipperfield, M. P., Bernath, P. F., Fernando, A. M., Mühle, J., Leeson, A. A., Montzka, S. A., Feng, W., Harrison, J. J., Krummel, P., Vollmer, M. K., Reimann, S., O'Doherty, S., Young, D., Maione, M., Arduini, J. and Lunder, C. R.: Recent Trends in Stratospheric Chlorine From Very Short-Lived Substances, J. Geophys. Res. Atmos., 124(4), 2318–2335, doi:10.1029/2018JD029400, 2019.

Hossaini, R., Chipperfield, M. P., Saiz-Lopez, A., Fernandez, R., Monks, S., Brauer, P. and von Glasow, R.: A global model of tropospheric chlorine chemistry: organic versus inorganic sources and impact on methane oxidation, J. Geophys. Res. Atmos., 121, 1–27, doi:10.1002/2016JD025756, 2016.

Hossaini, R., Sherry, D., Wang, Z., Chipperfield, M. P., Feng, W., Oram, D. E., Adcock, K. E., Montzka, S. A., Simpson, I. J., Mazzeo, A., Leeson, A. A., Atlas, E. and Chou, C. C. K.: On the atmospheric budget of 1,2-dichloroethane and its impact on stratospheric chlorine and ozone (2002-2020), Atmos. Chem. Phys., 24(23), 13457–13475, doi:10.5194/acp-24-13457-2024, 2024.

Huang, B., Thorne, P. W., Banzon, V. F., Boyer, T., Chepurin, G., Lawrimore, J. H., Menne, M. J., Smith, T. M., Vose, R. S. and Zhang, H. M.: Extended reconstructed Sea surface temperature, Version 5 (ERSSTv5): Upgrades, validations, and intercomparisons, J. Clim., 30(20), 8179–8205, doi:10.1175/JCLI-D-16-0836.1, 2017.

Iglesias-Suarez, F., Badia, A., Fernandez, R. P. R. P., Cuevas, C. A. C. A., Kinnison, D. E. D. E., Tilmes, S., Lamarque, J.-F. J. F., Long, M. C. M. C., Hossaini, R. and Saiz-Lopez, A.: Natural halogens buffer tropospheric ozone in a changing climate, Nat. Clim. Chang., 10(2), 147–154, doi:10.1038/s41558-019-0675-6, 2020.

Inamdar, S., Tinel, L., Chance, R., Carpenter, L. J., Sabu, P., Chacko, R., Tripathy, S. C., Kerkar, A. U., Sinha, A. K., Venkateswaran Bhaskar, P., Sarkar, A., Roy, R., Sherwen, T., Cuevas, C., Saiz-Lopez, A., Ram, K. and Mahajan, A. S.: Estimation of reactive inorganic iodine fluxes in the Indian and Southern Ocean marine boundary layer, Atmos. Chem. Phys., 20(20), 12093–12114, doi:10.5194/acp-20-12093-2020, 2020.

IPCC: Climate Change 2022: Impacts, Adaptation, and Vulnerability. Contribution of Working Group II to the Sixth Assessment Report of the Intergovernmental Panel on Climate Change, edited by B. R. H.-O. Pörtner, D.C. Roberts, M. Tignor, E.S. Poloczanska, K. Mintenbeck, A. Alegría, M. Craig, S. Langsdorf, S. Löschke, V. Möller, A. Okem, Cambridge University Press, Cambridge University Press, Cambridge, UK and New York., 2022.

Jesswein, M., Fernandez, R. P., Berná, L., Saiz-lopez, A., Grooß, J., Hossaini, R., Apel, E. C., Hornbrook, R. S., Atlas, E. L., Blake, D. R., Montzka, S., Keber, T., Schuck, T., Wagenhäuser, T. and Engel, A.: Global seasonal distribution of CH2Br2 and CHBr3 in the upper troposphere and lower stratosphere, Atmos. Chem. Phys. Discuss., (July), 1–36, doi:https://doi.org/10.5194/acp-2022-472, 2022.

Jia, Y., Hahn, J., Quack, B., Jones, E., Brehon, M. and Tegtmeier, S.: Anthropogenic Bromoform at the Extratropical Tropopause, Geophys. Res. Lett., 50(9), e2023GL102894, doi:10.1029/2023GL102894, 2023.

Jo, D. S., Tilmes, S., Emmons, L. K., Wang, S. and Vitt, F.: A new simplified parameterization of secondary organic aerosol in the Community Earth System Model Version 2 (CESM2; CAM6.3), Geosci. Model Dev., 16(13), 3893–3906, doi:10.5194/gmd-16-3893-2023, 2023.

Jones, C. E., Hornsby, K. E., Sommariva, R., Dunk, R. M., von Glasow, R., McFiggans, G. and Carpenter, L. J.: Quantifying the contribution of marine organic gases to atmospheric iodine, Geophys. Res. Lett., 37(18), L18804 (1-6), doi:10.1029/2010GL043990, 2010.

https://doi.org/10.5194/egusphere-2025-3250
Preprint. Discussion started: 13 October 2025

Karagodin-Doyennel, A., Rozanov, E., Sukhodolov, T., Egorova, T., Saiz-Lopez, A., Cuevas, C. A., Fernandez, R. P., Sherwen, T., Volkamer, R., Koenig, T. K., Giroud, T. and Peter, T.: Iodine chemistry in the chemistry-climate model SOCOL-AERv2-I, Geosci. Model Dev., 14(10), 6623–6645, doi:10.5194/gmd-14-6623-2021, 2021.

Keber, T., Bönisch, H., Hartick, C., Hauck, M., Lefrancois, F., Obersteiner, F., Ringsdorf, A., Schohl, N., Schuck, T., Hossaini, R., Graf, P., Jöckel, P. and Engel, A.: Bromine from short-lived source gases in the extratropical northern hemispheric upper troposphere and lower stratosphere (UTLS), Atmos. Chem. Phys., 20(7), 4105–4132, doi:10.5194/acp-20-4105-2020, 2020.

Keller-Rudek, H., Moortgat, G. K., Sander, R. and Sörensen, R.: The MPI-Mainz UV/VIS spectral atlas of gaseous molecules of atmospheric interest, Earth Syst. Sci. Data, 5(2), 365–373, doi:10.5194/essd-5-365-2013, 2013.

Kinnison, D. E., Brasseur, G. P., Walters, S., Garcia, R. R., Marsh, D. R., Sassi, F., Harvey, V. L., Randall, C. E., Emmons, L., Lamarque, J. F., Hess, P., Orlando, J. J., Tie, X. X., Randel, W., Pan, L. L., Gettelman, A., Granier, C., Diehl, T., Niemeier, U. and Simmons, A. J.: Sensitivity of chemical tracers to meteorological parameters in the MOZART-3 chemical transport model, J. Geophys. Res., 112(D20), D20302, doi:10.1029/2006JD007879, 2007.

Knipping, E. M. and Dabdub, D.: Impact of chlorine emissions from sea-salt aerosol on coastal urban ozone, Environ. Sci. Technol., 37(2), 275–284, doi:10.1021/es025793z, 2003.

Koenig, T. K., Baidar, S., Campuzano-Jost, P., Cuevas, C. A., Dix, B., Fernandez, R. P., Guo, H., Hall, S. R., Kinnison, D., Nault, B. A., Ullmann, K., Jimenez, J. L., Saiz-Lopez, A. and Volkamer, R.: Quantitative detection of iodine in the stratosphere, Proc. Natl. Acad. Sci. U. S. A., 117(4), doi:10.1073/pnas.1916828117, 2020.

Koenig, T. K., Volkamer, R., Apel, E. C., Bresch, J. F., Cuevas, C. A., Dix, B., Eloranta, E. W., Fernandez, R. P., Hall, S. R., Hornbrook, R. S., Pierce, R. B., Reeves, J. M., Saiz-Lopez, A. and Ullmann, K.: Ozone depletion due to dust release of iodine in the free troposphere, Sci. Adv., 7(52), 6544, doi:10.1126/sciadv.abj6544, 2021.

Koenig, T. K., Volkamer, R., Baidar, S., Dix, B., Wang, S., Anderson, D. C., Salawitch, R. J., Wales, P. A., Cuevas, C. A., Fernandez, R. P., Saiz-Lopez, A., Evans, M. J., Sherwen, T., Jacob, D. J., Schmidt, J., Kinnison, D., Lamarque, J. F., Apel, E. C., Bresch, J. C., Campos, T., Flocke, F. M., Hall, S. R., Honomichl, S. B., Hornbrook, R., Jensen, J. B., Lueb, R., Montzka, D. D., Pan, L. L., Michael Reeves, J., Schauffler, S. M., Ullmann, K., Weinheimer, A. J., Atlas, E. L., Donets, V., Navarro, M. A., Riemer, D., Blake, N. J., Chen, D., Gregory Huey, L., Tanner, D. J., Hanisco, T. F. and Wolfe, G. M.: BrO and inferred Bryprofiles over the western Pacific: Relevance of inorganic bromine sources and a Bryminimum in the aged tropical tropopause layer, Atmos. Chem. Phys., 17(24), 15245–15270, doi:10.5194/acp-17-15245-2017, 2017.

Lamarque, J.-F., Emmons, L. K., Hess, P. G., Kinnison, D. E., Tilmes, S., Vitt, F., Heald, C. L., Holland, E. A., Lauritzen, P. H., Neu, J., Orlando, J. J., Rasch, P. J. and Tyndall, G. K.: CAM-chem: description and evaluation of interactive atmospheric chemistry in the Community Earth System Model, Geosci. Model Dev., 5(2), 369–411, doi:10.5194/gmd-5-369-2012, 2012.

Leedham, E. C., Hughes, C., Keng, F. S. L., Phang, S.-M., Malin, G. and Sturges, W. T.: Emission of atmospherically significant halocarbons by naturally occurring and farmed tropical macroalgae, Biogeosciences, 10(6), 3615–3633, doi:10.5194/bg-10-3615-2013, 2013.

Lelieveld, J., Gromov, S., Pozzer, A. and Taraborrelli, D.: Global tropospheric hydroxyl distribution, budget and reactivity, Atmos. Chem. Phys., 16(19), 12477–12493, doi:10.5194/acp-16-12477-2016, 2016.

Lelieveld, J., Peters, W., Dentener, F. J. and Krol, M. C.: Stability of tropospheric hydroxyl chemistry, J. Geophys. Res. Atmos., 107(D23), ACH 17-1, doi:10.1029/2002JD002272, 2002.

Lewis, T. R., Martín, J. C. G., Blitz, M. A., Cuevas, C. A., Plane, J. M. C. and Saiz-Lopez, A.: Determination of the absorption cross sections of higher-order iodine oxides at 355 and 532 nm, Atmos. Chem. Phys., 20(18), 10865–10887, doi:10.5194/acp-20-10865-2020, 2020.

Li, Q., Fernandez, R. P., Hossaini, R., Iglesias-Suarez, F., Cuevas, C. A., Apel, E. C., Kinnison, D. E., Lamarque, J. F. and

Saiz-Lopez, A.: Reactive halogens increase the global methane lifetime and radiative forcing in the 21st century, Nat. Commun., 13(1), 1–11, doi:10.1038/s41467-022-30456-8, 2022.

Li, Q., Meidan, D., Hess, P., Añel, J. A., Cuevas, C. A., Doney, S., Fernandez, R. P., van Herpen, M., Höglund-Isaksson, L., Johnson, M. S., Kinnison, D. E., Lamarque, J.-F., Röckmann, T., Mahowald, N. M. and Saiz-Lopez, A.: Global environmental implications of atmospheric methane removal through chlorine-mediated chemistry-climate interactions, Nat. Commun. 2023 141, 14(1), 1–10, doi:10.1038/s41467-023-39794-7, 2023.

Liu, X., Ma, P. L., Wang, H., Tilmes, S., Singh, B., Easter, R. C., Ghan, S. J. and Rasch, P. J.: Description and evaluation of a new four-mode version of the Modal Aerosol Module (MAM4) within version 5.3 of the Community Atmosphere Model, Geosci. Model Dev., 9(2), 505–522, doi:10.5194/gmd-9-505-2016, 2016.

MacDonald, S. M., Gómez Martín, J. C., Chance, R., Warriner, S., Saiz-Lopez, A., Carpenter, L. J. and Plane, J. M. C.: A laboratory characterisation of inorganic iodine emissions from the sea surface: dependence on oceanic variables and parameterisation for global modelling, Atmos. Chem. Phys., 14(11), 5841–5852, doi:10.5194/acp-14-5841-2014, 2014.

Marsh, D. R., Mills, M. J., Kinnison, D. E., Lamarque, J.-F., Calvo, N. and Polvani, L. M.: Climate change from 1850 to 2005 simulated in CESM1(WACCM), J. Clim., 26(19), 7372–7391, doi:10.1175/JCLI-D-12-00558.1, 2013.

McDuffie, E. E., Fibiger, D. L., Dubé, W. P., Lopez Hilfiker, F., Lee, B. H., Jaeglé, L., Guo, H., Weber, R. J., Reeves, J. M., Weinheimer, A. J., Schroder, J. C., Campuzano-Jost, P., Jimenez, J. L., Dibb, J. E., Veres, P., Ebben, C., Sparks, T. L., Wooldridge, P. J., Cohen, R. C., Campos, T., Hall, S. R., Ullmann, K., Roberts, J. M., Thornton, J. A. and Brown, S. S.: $ClNO_2$ Yields From Aircraft Measurements During the 2015 WINTER Campaign and Critical Evaluation of the Current Parameterization, J. Geophys. Res. Atmos., 123(22), 12,994-13,015, doi:10.1029/2018JD029358, 2018.

McDuffie, E. E., Womack, C. C., Fibiger, D. L., Dube, W. P., Franchin, A., Middlebrook, A. M., Goldberger, L., Lee, B. H., Thornton, J. A., Moravek, A., Murphy, J. G., Baasandorj, M. and Brown, S. S.: On the contribution of nocturnal heterogeneous reactive nitrogen chemistry to particulate matter formation during wintertime pollution events in Northern Utah, Atmos. Chem. Phys., 19(14), 9287–9308, doi:10.5194/acp-19-9287-2019, 2019.

McFiggans, G., Plane, J. M. C., Allan, B. J., Carpenter, L. J., Coe, H. and O'Dowd, C.: A modeling study of iodine chemistry in the marine boundary layer, J. Geophys. Res., 105(D11), 14371–14385, doi:10.1029/1999JD901187, 2000.

Meidan, D., Li, Q., Cuevas, C. A., Doney, S. C., Fernandez, R. P., van Herpen, M. M. J. W., Johnson, M. S., Kinnison, D. E., Li, L., Hamilton, D. S., Saiz-Lopez, A., Hess, P. and Mahowald, N. M.: Evaluating the potential of iron-based interventions in methane reduction and climate mitigation, Environ. Res. Lett., 19(5), 54023, doi:10.1088/1748-9326/ad3d72, 2024.

Meinshausen, M., Vogel, E., Nauels, A., Lorbacher, K., Meinshausen, N., Etheridge, D. M., Fraser, P. J., Montzka, S. A., Rayner, P. J., Trudinger, C. M., Krummel, P. B., Beyerle, U., Canadell, J. G., Daniel, J. S., Enting, I. G., Law, R. M., Lunder, C. R., O'Doherty, S., Prinn, R. G., Reimann, S., Rubino, M., Velders, G. J. M., Vollmer, M. K., Wang, R. H. J. and Weiss, R.: Historical greenhouse gas concentrations for climate modelling (CMIP6), Geosci. Model Dev., 10(5), 2057–2116, doi:10.5194/gmd-10-2057-2017, 2017.

Melin, F.: GMIS - SeaWiFS Monthly climatology sea surface Chlorophyll-a concentration (9km) in mg.m^-3, , doi:http://data.europa.eu/89h/d6f9abd9-777c-4a0c-a5f7-669612f83307, 2013.

Mills, M. J., Schmidt, A., Easter, R., Solomon, S., Kinnison, D. E., Ghan, S. J., Neely, R. R., Marsh, D. R., Conley, A., Bardeen, C. G. and Gettelman, A.: Global volcanic aerosol properties derived from emissions, 1990–2014, using CESM1(WACCM), J. Geophys. Res. Atmos., 121(5), 2332–2348, doi:10.1002/2015JD024290, 2016.

Neu, J. L. and Prather, M. J.: Toward a more physical representation of precipitation scavenging in global chemistry models: cloud overlap and ice physics and their impact on tropospheric ozone, Atmos. Chem. Phys., 12(7), 3289–3310, doi:10.5194/acp-12-3289-2012, 2012.

Ordóñez, C., Lamarque, J.-F., Tilmes, S., Kinnison, D. E., Atlas, E. L., Blake, D. R., Sousa Santos, G., Brasseur, G. and Saiz-

https://doi.org/10.5194/egusphere-2025-3250
Preprint. Discussion started: 13 October 2025

Lopez, A.: Bromine and iodine chemistry in a global chemistry-climate model: description and evaluation of very short-lived oceanic sources, Atmos. Chem. Phys., 12(3), 1423–1447, doi:10.5194/acp-12-1423-2012, 2012.

Prados-Roman, C., Cuevas, C. A. a., Hay, T., Fernandez, R. P. P., Mahajan, A. S. S., Royer, S.-J., Galí, M., Simó, R., Dachs, J., Großmann, K., Kinnison, D. E. E., Lamarque, J.-F. and Saiz-Lopez, A.: Iodine oxide in the global marine boundary layer, Atmos. Chem. Phys., 15(2), 583–593, doi:10.5194/acp-15-583-2015, 2015a.

Prados-Roman, C., Cuevas, C. A., Fernandez, R. P., Kinnison, D. E., Lamarque, J.-F. and Saiz-Lopez, A.: A negative feedback between anthropogenic ozone pollution and enhanced ocean emissions of iodine, Atmos. Chem. Phys., 15(4), doi:10.5194/acp-15-2215-2015, 2015b.

Read, K. A., Mahajan, A. S., Carpenter, L. J., Evans, M. J., Faria, B. V. E., Heard, D. E., Hopkins, J. R., Lee, J. D., Moller, S. J., Lewis, A. C., Mendes, L., McQuaid, J. B., Oetjen, H., Saiz-Lopez, A., Pilling, M. J. and Plane, J. M. C.: Extensive halogen-mediated ozone destruction over the tropical Atlantic Ocean., Nature, 453(7199), 1232–5, doi:10.1038/nature07035, 2008.

Rienecker, M. M., Suarez, M. J., Gelaro, R., Todling, R., Bacmeister, J., Liu, E., Bosilovich, M. G., Schubert, S. D., Takacs, L., Kim, G. K., Bloom, S., Chen, J., Collins, D., Conaty, A., Da Silva, A., Gu, W., Joiner, J., Koster, R. D., Lucchesi, R., Molod, A., Owens, T., Pawson, S., Pegion, P., Redder, C. R., Reichle, R., Robertson, F. R., Ruddick, A. G., Sienkiewicz, M. and Woollen, J.: MERRA: NASA's modern-era retrospective analysis for research and applications, J. Clim., 24(14), 3624–3648, doi:10.1175/JCLI-D-11-00015.1, 2011.

Riese, M., Ploeger, F., Rap, A., Vogel, B., Konopka, P., Dameris, M. and Forster, P.: Impact of uncertainties in atmospheric mixing on simulated UTLS composition and related radiative effects, J. Geophys. Res. Atmos., 117(16), 1–10, doi:10.1029/2012JD017751, 2012.

Roozitalab, B., Emmons, L. K., Hornbrook, R. S., Kinnison, D. E., Fernandez, R. P., Li, Q., Saiz-Lopez, A., Hossaini, R., Cuevas, C. A., Hills, A. J., Montzka, S. A., Blake, D. R., Brune, W. H., Veres, P. R. and Apel, E. C.: Measurements and Modeling of the Interhemispheric Differences of Atmospheric Chlorinated Very Short-Lived Substances, J. Geophys. Res. Atmos., 129(2), e2023JD039518, doi:10.1029/2023JD039518, 2024.

Saiz-Lopez, A., Baidar, S., Cuevas, C. A., Koenig, T. K., Fernandez, R. P., Dix, B., Kinnison, D. E., Lamarque, J., Campos, T. L. and Volkamer, R.: Injection of iodine to the stratosphere, Geophys. Res. Lett., 42(16), 6852–6859, doi:doi:10.1002/2015GL064796, 2015.

Saiz-Lopez, A., Cuevas, C. A., Acuña, A. U., Añel, J. A., Mahajan, A. S., de la Torre, L., Feng, W., Dávalos, J. Z., Roca-Sanjuán, D., Kinnison, D. E., Carmona-García, J., Fernandez, R. P., Li, Q., Sonke, J. E., Feinberg, A., Martín, J. C. G., Villamayor, J., Zhang, P., Zhang, Y., Blaszczak-Boxe, C. S., Travnikov, O., Wang, F., Bieser, J., Francisco, J. S. and Plane, J. M. C.: Role of the stratosphere in the global mercury cycle, Sci. Adv., 11(2), 1459, doi:10.1126/sciadv.ads1459, 2025.

Saiz-Lopez, A. and Fernandez, R. P.: On the formation of tropical rings of atomic halogens: Causes and implications, Geophys. Res. Lett., 43(6), doi:10.1002/2015GL067608, 2016.

Saiz-Lopez, A., Fernandez, R. P., Li, Q., Cuevas, C. A., Fu, X., Kinnison, D. E., Tilmes, S., Mahajan, A. S., Gómez Martín, J. C., Iglesias-Suarez, F., Hossaini, R., Plane, J. M. C., Myhre, G. and Lamarque, J.-F.: Natural short-lived halogens exert an indirect cooling effect on climate, Nature, 618(7967), 967–973, doi:10.1038/s41586-023-06119-z, 2023.

Saiz-Lopez, A., Fernandez, R. P., Ordóñez, C., Kinnison, D. E., Martín, J. C. G., Lamarque, J.-F. and Tilmes, S.: Iodine chemistry in the troposphere and its effect on ozone, Atmos. Chem. Phys., 14(23), doi:10.5194/acp-14-13119-2014, 2014.

Saiz-Lopez, A. and von Glasow, R.: Reactive halogen chemistry in the troposphere., Chem. Soc. Rev., 41(19), 6448–6472, doi:10.1039/c2cs35208g, 2012.

Saiz-Lopez, A., Lamarque, J.-F., Kinnison, D. E., Tilmes, S., Ordóñez, C., Orlando, J. J., Conley, A. J., Plane, J. M. C., Mahajan, A. S., Sousa Santos, G., Atlas, E. L., Blake, D. R., Sander, S. P., Schauffler, S., Thompson, A. M. and Brasseur,

https://doi.org/10.5194/egusphere-2025-3250
Preprint. Discussion started: 13 October 2025

G.: Estimating the climate significance of halogen-driven ozone loss in the tropical marine troposphere, Atmos. Chem. Phys., 12(9), 3939–3949, doi:10.5194/acp-12-3939-2012, 2012.

Saiz-Lopez, A., Mahajan, A. S., Salmon, R. A., Bauguitte, S. J.-B., Jones, A. E., Roscoe, H. K. and Plane, J. M. C.: Boundary Layer Halogens in Coastal Antarctica, Science (80-.)., 317(5836), 348–351, doi:10.1126/science.1141408, 2007.

Salawitch, R. J., Weisenstein, D. K., Kovalenko, L. J., Sioris, C. E., Wennberg, P. O., Chance, K., Ko, M. K. W. and McLinden, C. A.: Sensitivity of ozone to bromine in the lower stratosphere, Geophys. Res. Lett., 32(5), L05811, doi:10.1029/2004GL021504, 2005.

Sander, R.: Compilation of Henry's law constants (version 4.0) for water as solvent, Atmos. Chem. Phys., 15(8), 4399–4981, doi:10.5194/acp-15-4399-2015, 2015.

Sarwar, G., Gantt, B., Schwede, D., Foley, K., Mathur, R. and Saiz-Lopez, A.: Impact of Enhanced Ozone Deposition and Halogen Chemistry on Tropospheric Ozone over the Northern Hemisphere, Environ. Sci. Technol., 49(15), 9203–9211, 2015.

Schultz, M. G., Schröder, S., Lyapina, O., Cooper, O. R., Galbally, I., Petropavlovskikh, I., Von Schneidemesser, E., Tanimoto, H., Elshorbany, Y., Naja, M., Seguel, R. J., Dauert, U., Eckhardt, P., Feigenspan, S., Fiebig, M., Hjellbrekke, A. G., Hong, Y. D., Kjeld, P. C., Koide, H., Lear, G., Tarasick, D., Ueno, M., Wallasch, M., Baumgardner, D., Chuang, M. T., Gillett, R., Lee, M., Molloy, S., Moolla, R., Wang, T., Sharps, K., Adame, J. A., Ancellet, G., Apadula, F., Artaxo, P., Barlasina, M. E., Bogucka, M., Bonasoni, P., Chang, L., Colomb, A., Cuevas-Agulló, E., Cupeiro, M., Degorska, A., Ding, A., Fröhlich, M., Frolova, M., Gadhavi, H., Gheusi, F., Gilge, S., Gonzalez, M. Y., Gros, V., Hamad, S. H., Helmig, D., Henriques, D., Hermansen, O., Holla, R., Hueber, J., Im, U., Jaffe, D. A., Komala, N., Kubistin, D., Lam, K. S., Laurila, T., Lee, H., Levy, I., Mazzoleni, C., Mazzoleni, L. R., McClure-Begley, A., Mohamad, M., Murovec, M., Navarro-Comas, M., Nicodim, F., Parrish, D., Read, K. A., Reid, N., Ries, L., Saxena, P., Schwab, J. J., Scorgie, Y., Senik, I., Simmonds, P., Sinha, V., Skorokhod, A. I., Spain, G., Spangl, W., Spoor, R., Springston, S. R., Steer, K., Steinbacher, M., Suharguniyawan, E., Torre, P., Trickl, T., Weili, L., Weller, R., Xiaobin, X., Xue, L. and Zhiqiang, M.: Tropospheric Ozone Assessment Report: Database and metrics data of global surface ozone observations, Elementa, 5, 43, doi:10.1525/elementa.244, 2017.

Sherwen, T., Evans, M. J., Carpenter, L. J., Andrews, S. J., Lidster, R. T., Dix, B., Koenig, T. K., Sinreich, R., Ortega, I., Volkamer, R., Saiz-Lopez, A., Prados-Roman, C., Mahajan, A. S. and Ordóñez, C.: Iodine's impact on tropospheric oxidants: A global model study in GEOS-Chem, Atmos. Chem. Phys., 16(2), 1161–1186, doi:10.5194/acp-16-1161-2016, 2016a.

Sherwen, T., Schmidt, J. A., Evans, M. J., Carpenter, L. J., Gro??mann, K., Eastham, S. D., Jacob, D. J., Dix, B., Koenig, T. K., Sinreich, R., Ortega, I., Volkamer, R., Saiz-Lopez, A., Prados-Roman, C., Mahajan, A. S. and Ord????ez, C.: Global impacts of tropospheric halogens (Cl, Br, I) on oxidants and composition in GEOS-Chem, Atmos. Chem. Phys., 16(18), 12239–12271, doi:10.5194/acp-16-12239-2016, 2016b.

Simpson, I. R., Bacmeister, J., Neale, R. B., Hannay, C., Gettelman, A., Garcia, R. R., Lauritzen, P. H., Marsh, D. R., Mills, M. J., Medeiros, B. and Richter, J. H.: An Evaluation of the Large-Scale Atmospheric Circulation and Its Variability in CESM2 and Other CMIP Models, J. Geophys. Res. Atmos., 125(13), e2020JD032835, doi:10.1029/2020JD032835, 2020.

Simpson, I. R., Rosenbloom, N., Danabasoglu, G., Deser, C., Yeager, S. G., McCluskey, C. S., Yamaguchi, R., Lamarque, J. F., Tilmes, S., Mills, M. J. and Rodgers, K. B.: The CESM2 Single-Forcing Large Ensemble and Comparison to CESM1: Implications for Experimental Design, J. Clim., 36(17), 5687–5711, doi:10.1175/JCLI-D-22-0666.1, 2023.

Simpson, W. R., Brown, S. S., Saiz-Lopez, A., Thornton, J. A. and Glasow, R. Von: Tropospheric Halogen Chemistry: Sources, Cycling, and Impacts., Chem. Rev., doi:10.1021/cr5006638, 2015.

Sinnhuber, B.-M., Sheode, N., Sinnhuber, M., Chipperfield, M. P. and Feng, W.: The contribution of anthropogenic bromine emissions to past stratospheric ozone trends: a modelling study, Atmos. Chem. Phys., 9(8), 2863–2871, doi:10.5194/acp-

https://doi.org/10.5194/egusphere-2025-3250
Preprint. Discussion started: 13 October 2025

9-2863-2009, 2009.

Solomon, S., Garcia, R. R. and Ravishankara, a. R.: On the role of iodine in ozone depletion, J. Geophys. Res., 99(D10), 20491, doi:10.1029/94JD02028, 1994.

Solomon, S., Kinnison, D., Bandoro, J. and Garcia, R.: Simulation of polar ozone depletion : An update, J. Geophys. Res. Atmos., 120(15), 7958–7974, doi:10.1002/2015JD023365.Received, 2015.

Thornton, J. A., Kercher, J. P., Riedel, T. P., Wagner, N. L., Cozic, J., Holloway, J. S., Dub́, W. P., Wolfe, G. M., Quinn, P. K., Middlebrook, A. M., Alexander, B. and Brown, S. S.: A large atomic chlorine source inferred from mid-continental reactive nitrogen chemistry, Nature, 464(7286), 271–274, doi:10.1038/nature08905, 2010.

Tilmes, S., Hodzic, A., Emmons, L. K., Mills, M. J., Gettelman, A., Kinnison, D. E., Park, M., Lamarque, J. -F., Vitt, F., Shrivastava, M., Campuzano-Jost, P., Jimenez, J. L. and Liu, X.: Climate Forcing and Trends of Organic Aerosols in the Community Earth System Model (CESM2), J. Adv. Model. Earth Syst., 11(12), 4323–4351, doi:10.1029/2019MS001827, 2019.

Tilmes, S., Mills, M. J., Zhu, Y., Bardeen, C. G., Vitt, F., Yu, P., Fillmore, D., Liu, X., Toon, B. and Deshler, T.: Description and performance of a sectional aerosol microphysical model in the Community Earth System Model (CESM2), Geosci. Model Dev., 16(21), 6087–6125, doi:10.5194/gmd-16-6087-2023, 2023.

Veres, P. R., Andrew Neuman, J., Bertram, T. H., Assaf, E., Wolfe, G. M., Williamson, C. J., Weinzierl, B., Tilmes, S., Thompson, C. R., Thames, A. B., Schroder, J. C., Saiz-Lopez, A., Rollins, A. W., Roberts, J. M., Price, D., Peischl, J., Nault, B. A., Møller, K. H., Miller, D. O., Meinardi, S., Li, Q., Lamarque, J. F., Kupc, A., Kjaergaard, H. G., Kinnison, D., Jimenez, J. L., Jernigan, C. M., Hornbrook, R. S., Hills, A., Dollner, M., Day, D. A., Cuevas, C. A., Campuzano-Jost, P., Burkholder, J., Paul Bui, T., Brune, W. H., Brown, S. S., Brock, C. A., Bourgeois, I., Blake, D. R., Apel, E. C. and Ryerson, T. B.: Global airborne sampling reveals a previously unobserved dimethyl sulfide oxidation mechanism in the marine atmosphere, Proc. Natl. Acad. Sci. U. S. A., 117(9), 4505–4510, doi:10.1073/pnas.1919344117, 2020.

Villamayor, J., Iglesias-Suarez, F., Cuevas, C. A., Fernandez, R. P., Li, Q., Abalos, M., Hossaini, R., Chipperfield, M. P., Kinnison, D. E., Tilmes, S., Lamarque, J. F. and Saiz-Lopez, A.: Very short-lived halogens amplify ozone depletion trends in the tropical lower stratosphere, Nat. Clim. Chang., 13(6), 554–560, doi:10.1038/s41558-023-01671-y, 2023.

Warwick, N. J., Pyle, J. A., Carver, G. D., Yang, X., Savage, N. H., O'Connor, F. M. and Cox, R. A.: Global modeling of biogenic bromocarbons, J. Geophys. Res., 111(D24), D24305, doi:10.1029/2006JD007264, 2006a.

Warwick, N. J., Pyle, J. a. and Shallcross, D. E.: Global Modelling of the Atmospheric Methyl Bromide Budget, J. Atmos. Chem., 54(2), 133–159, doi:10.1007/s10874-006-9020-3, 2006b.

Wild, O., Voulgarakis, A., O'Connor, F., Lamarque, J. F., Ryan, E. M. and Lee, L.: Global sensitivity analysis of chemistry-climate model budgets of tropospheric ozone and OH: Exploring model diversity, Atmos. Chem. Phys., 20(7), 4047–4058, doi:10.5194/acp-20-4047-2020, 2020.

WMO: Scientific Assessment of Ozone Depletion: 2018, Global Ozone Research and Monitoring Project-Report Nº 58, Geneva, Switzerland., 2018.

WMO: Scientific Assessment of Ozone Depletion: 2022, Global Atmospheric Watch Report No. 278, Geneva, Switzerland., 2022.

Wohl, C., Villamayor, J., Galí, M., Mahajan, A. S., Fernández, R. P., Cuevas, C. A., Bossolasco, A., Li, Q., Kettle, A. J., Williams, T., Sarda-Esteve, R., Gros, V., Simó, R. and Saiz-Lopez, A.: Marine emissions of methanethiol increase aerosol cooling in the Southern Ocean, Sci. Adv., 10(48), 2465, doi:10.1126/sciadv.adq2465, 2024.

Zhu, L., Jacob, D. J., Eastham, S. D., Sulprizio, M. P., Wang, X., Sherwen, T., Evans, M. J., Chen, Q., Alexander, B., Koenig, T. K., Volkamer, R., Huey, L. G., Le Breton, M., Bannan, T. J. and Percival, C. J.: Effect of sea-salt aerosol on tropospheric bromine chemistry, Atmos. Chem. Phys. Discuss., 1–17, doi:10.5194/acp-2018-1239, 2018.